Neural Correlates of Learning in Brain Machine Interface Controlled Tasks

by

Michelle Armenta Salas

A Dissertation Presented in Partial Fulfillment
of the Requirements for the Degree
Doctor of Philosophy

Approved November 2015 by the
Graduate Supervisory Committee:

Stephen Helms Tillery, Chair
Christopher Buneo
Marco Santello
Jennie Si
Jeffrey Kleim

ARIZONA STATE UNIVERSITY

December 2015

ABSTRACT

Brain-machine interfaces (BMIs) were first imagined as a technology that would allow subjects to have direct communication with prosthetics and external devices (e.g. control over a computer cursor or robotic arm movement). Operation of these devices was not automatic, and subjects needed calibration and training in order to master this control. In short, learning became a key component in controlling these systems. As a result, BMIs have become ideal tools to probe and explore brain activity, since they allow the isolation of neural inputs and systematic altering of the relationships between the neural signals and output. I have used BMIs to explore the process of brain adaptability in a motor-like task. To this end, I trained non-human primates to control a 3D cursor and adapt to two different perturbations: a visuomotor rotation, uniform across the neural ensemble, and a decorrelation task, which non-uniformly altered the relationship between the activity of particular neurons in an ensemble and movement output. I measured individual and population level changes in the neural ensemble as subjects honed their skills over the span of several days. I found some similarities in the adaptation process elicited by these two tasks. On one hand, individual neurons displayed tuning changes across the entire ensemble after task adaptation: most neurons displayed transient changes in their preferred directions, and most neuron pairs showed changes in their cross-correlations during the learning process. On the other hand, I also measured population level adaptation in the neural ensemble: the underlying neural manifolds that control these neural signals also had dynamic changes during adaptation. I have found that the neural circuits seem to apply an exploratory strategy when adapting to new tasks. Our results suggest that information and trajectories in the neural space increase after initially introducing the perturbations, and before the subject settles into workable solutions. These results provide new insights into both the underlying population level processes in motor

learning, and the changes in neural coding which are necessary for subjects to learn to control neuroprosthetics. Understanding of these mechanisms can help us create better control algorithms, and design training paradigms that will take advantage of these processes.

To my parents, Miguel and Martha, and my sister Ingrid

ACKNOWLEDGEMENTS

First and foremost I want to thank my adviser, Steve Helms Tillery, who first accepted me as a summer intern during my senior year of undergrad even before we had personally met, later inspired me to pursue a research career, and further accepted me as a member of his lab upon my returning to ASU for grad school. My dissertation committee, Dr. Jennie Si, Dr. Marco Santello, Dr. Christopher Buneo and Dr. Jeffrey Kleim, for guiding me and providing me with interesting and encouraging feedback of my research through the past couple of years. The members of the SMoRG lab, current and past, who have shared and exchanged with me research ideas, discussed the many intricate aspects of my research, helped me with animal training, and aided me with my experimental design. Special thanks to Flavio daSilva, who had initially started this project, and was patient enough to introduce me to all the different aspects of it so I could start my own experiments. Also to David Dunning, an undergrad FURI fellow in our lab who helped me with the initial phases of the experiments. Rachele McAndrew, a key member of our lab who keeps our monkeys happy, has been a valuable friend, and has provided me with amazing training for animal behavior and handling.

I would also like to acknowledge those friends inside and outside the lab setting who have made this journey more fun and far more enjoyable. Liliana Rincon-Gonzalez and Veronica Clavijo Jordan, you were always a great support, source of fun adventures, and inspiration of how to thrive in life and academia; Mezly Rodriguez Jimenez, who has supported and encouraged me from miles away; David Eberle and Andres Moreno, who helped keep me grounded and swim through all the grad school hurdles, and Utku Ilkturk, with whom I have shared great experiences, and has become an immense support through the past couple of years.

Finally, I want to thank my parents, Miguel and Martha, who have given me their love and encouragement through all my academic, professional and personal endeavors, and have always been my greatest role models; and my sister Ingrid, who has always given me her love and support, and has been an excellent role model of what an outstanding person should be.

TABLE OF CONTENTS

CHAPTER Page

CHAPTER Page

LIST OF TABLES

LIST OF FIGURES

Figure Page

Chapter 1

BACKGROUND

1.1 Motor learning, adaptation and plasticity

Motor learning is a term usually related to the acquisition and retention of behaviors and skills, which were obtained through repeated practice. This term has been generally used when studying any type of adaptation that requires modifications in movements and behaviors, and when measuring specific variables to quantify their improvements (e.g. movement time, velocity, accuracy, etc.). The study of motor learning is not only relevant to understanding how we are able to master such a variety of skills, even as we grow older, but also to help us understand general behavioral and neural mechanisms that might also take place in other types of learning (e.g. during cognitive tasks).

Motor learning can be divided according to the types of compensation or adaptation required, behaviors elicited, whether or not is supervised, etc. Here, I will introduce three possible categories, according to the behavioral and the possible neural changes they might elicit, as discussed by Shmuelof and Krakauer (2011). First, motor adaptation, which can be defined as the changes in motor behaviors after a perturbation is introduced in a task, these changes are concerned with bringing performance and the movements themselves back to baseline levels. Second, skill learning, which involves the acquisition of new behaviors and motor commands (e.g. riding a bike, learning how to swim, playing guitar, etc.), with usually slower improvements than those measured during motor adaptation. Last, a more general third category referred to as action selection. This type of learning includes, but is not limited to,

tasks where subjects perform specific sequence of movements, or learn to relate certain actions to task success (e.g. push a button, press a lever, etc.) (Shmuelof and Krakauer, 2011). It has been suggested that these types of motor learning are not only discerned by the behaviors that accompany them, but also might differ in the neural signals that drive them. I am particularly interested in the common neural processes that might drive these different types of learning.

Much effort has been made to try to understand and dissect motor learning from a neurophysiological perspective. For example, changes in the firing properties of single neural units in motor cortex have been found to be related to training towards specific directions (Paz *et al.*, 2003; Paz and Vaadia, 2004), and activity of single units can correlate to one another according to the epochs and events of the trained task (Vaadia *et al.*, 1995; Salinas and Sejnowski, 2001). Similarly, activity from regions such as cerebellum, basal ganglia (BG), and motor cortex have been linked to different types of learning. For example, error prediction and forward models during motor adaptation have been associated with cerebellar projections and changes in cerebellar activity (Doya, 2000; Shadmehr *et al.*, 2010; Donchin *et al.*, 2012). Skill learning and reinforcement-based learning have been associated with activity in BG, and the projections they have to motor cortices (Jueptner *et al.*, 1997; Doya, 2000; Koralek *et al.*, 2010). On the other hand, re-organization in motor cortex has been related to motor learning and task adaptation (Kleim *et al.*, 1998; Nudo *et al.*, 1996; Kleim *et al.*, 2004). Moreover, damage to projections between motor cortex and deep structures (e.g. BG) has been recently reported to significantly deter the ability to skillfully perform novel tasks (Koralek *et al.*, 2012).

An additional learning classification has also been associated with changes in motor cortex. It has been referred to as unsupervised learning (Doya, 1999, 2000), and includes models that contain both input and output information, and the Hebbian

adaptation that might take place given these inputs. In other words, it is concerned with the representation of an internal model, as well as a model of the external environment.

Furthermore, plastic changes in primary motor cortex (M1) have been previously associated with skill learning and adaptation (Pascual-Leone *et al.*, 1994; Nudo *et al.*, 1996; Kleim *et al.*, 1998; Plautz *et al.*, 2000; Kleim *et al.*, 2004; Shmuelof and Krakauer, 2011). These studies have shown that different behaviors and regimens can actually facilitate adaptations in motor cortex (e.g. movement repetition, timing and synchronization of movements, task relevance, etc.). These regimens have repeatedly been used in a wide range of activities that involve both motor and cognitive learning, and represent main variables when trying to test and measure different aspects of learning (Nudo *et al.*, 1996; Kleim *et al.*, 1998, 2004).

Our understanding of the mechanisms associated with motor learning is an important element in understanding how our brain works, the limitations it may have. These advances are likely to improve our understanding of many pathologies, and may even make suggestions for rehabilitation. Advancements in neuroscience methods and neural interfaces technology have opened new ways to explore and to probe motor cortex plasticity and skill learning. However, these new methods have their own limitations, and bring forth a new set of challenges and considerations that need to be addressed if we want to use them as means to probe motor learning.

In the next section, I will discuss the use of these technologies to explore motor learning, show evidence of plasticity in the use of these neural interfaces, and discuss possible novel applications of these technologies to challenge the motor circuitry.

1.2 Motor learning in brain-machine interfaces

1.2.1 State of the art in brain-machine interfaces

Technology and control algorithms used in brain-machine interfaces (BMIs) have moved a long way since the first demonstrations where non-human primates (NHPs) were able to use a finite number of brain signals to control the movement of a computer cursor (Chapin *et al.*, 1999; Wessberg *et al.*, 2000; Serruya *et al.*, 2002; Taylor *et al.*, 2002; Carmena *et al.*, 2003). These first experiments were successful demonstrations of online multichannel recording and movement decoding. Later work focused on localizing which brain areas might be better suited to extract movement related information (Shenoy *et al.*, 2003; Hatsopoulos *et al.*, 2004, 2005; Wu and Hatsopoulos, 2007). For example, it has been shown that it is possible to control a prosthetic device using movement planning activity from posterior parietal cortex (Shenoy *et al.*, 2003). Similarly, there have been successful attempts to decode movement information from both M1 and pre-motor cortices, using signals prior to and during movement (Hatsopoulos *et al.*, 2004). At the same time, much effort has been made in developing algorithms that allow to process and to use this information to control an increasing number of variables, such as speed and force, and eventually hand configuration information (yaw, pitch, grip aperture, etc.) (Moran and Schwartz, 1999; Shenoy *et al.*, 2003; Carmena *et al.*, 2003; Brockwell *et al.*, 2004; Brown *et al.*, 2004; Ryu *et al.*, 2004; Srinivasan and Brown, 2007; Koyama *et al.*, 2010; Collinger *et al.*, 2013). These experiments have been key instruments to demonstrate the feasibility of BMIs to record, decode and use movement information, while later research has opened the door to explore the variety of devices subjects could interact with by using BMIs technology (Hochberg *et al.*, 2012; Collinger *et al.*, 2013).

More recently, it has been shown that human subjects are able to exclusively use brain signals to control the movement of computer cursors (Donoghue *et al.*, 2004; Friehs *et al.*, 2004; Hochberg *et al.*, 2006) and artificial limbs (Hochberg *et al.*, 2012; Collinger *et al.*, 2013). However, little has been reported about the changes observed in brain activity that allowed subjects to achieve this control. This represents an important gap in knowledge, since understanding of these neural circuits could translate to a better use of this type of technology. For example, a more uniform distribution of preferred directions, which are the estimated directional tuning preferences of individual neural signals, in the workspace might be desired (Koyama *et al.*, 2010), but it will be very unlikely that the small group of signals recorded will be evenly distributed in the workspace (Naselaris *et al.*, 2006). Consequently, questions might arise of whether or not it would be possible to impose some directional preferences to the available neural signals, in order to improve the uniformity of the population. On the other hand, it might be desirable to force neural signals, initially not tuned to the assigned task, to contribute and tune their activity to a specific behavior. Answering some of these questions could help focus research efforts towards solutions that will take advantage of these neural characteristics, whether it involves improvement of calibration methods, development of novel training paradigms or refinement of decoding schemes.

Furthermore, it is expected that as hardware technology progresses, a quadriplegic or locked-in patient, target population of these technologies, would want to interact with more than one device. For example, the subject might like to control the movement of his or her wheelchair, while also controlling the movement of a computer cursor, and typing an email. This rises a new set of questions regarding the possibility of using the same set of brain signals to control more that one external device, or to seamlessly switch the control between these devices. Although some work has

shown that NHPs were able to switch between two different control decoders using the same set of neural signals (Ganguly and Carmena, 2009), subjects were not asked to switch back and forth between different tasks. We consider that understanding the dynamics of the neural population would allow us to make more informed decisions about the decoding and system requirements that would make it possible for a given neural population, to not only learn more than one decoding map, but also that each map will control different output variables.

1.2.2 Evidence of brain plasticity in BMIs

The first single-unit invasive recordings used for online control more than four decades ago, showed that NHPs were able to modulate the activity of a single unit using operant conditioning (Fetz, 1969; Fetz and Finocchio, 1971; Schmidt *et al.*, 1977). Even though these demonstrations were done with technology and methods that have been since greatly improved, they still provided valuable evidence that subjects could drive individual neural activity according to the task at hand.

Several decades after these studies with operant techniques, different groups reported variations in the parameters of the recorded neural populations in NHPs after behavioral training had taken place. It was reported that neuronal mapping changed significantly when subjects switched between manual and brain control (Taylor *et al.*, 2002; Carmena *et al.*, 2003). It has also been reported that neural tuning in M1 occurs even if the subjects are only observing the task and have no active control (Wahnoun *et al.*, 2006; Tkach *et al.*, 2007; Collinger *et al.*, 2014). These studies represent key examples of the brain's ability to adapt its activity to the specifics of the task, and to include information of the actuators involved in such task, that is, whether it was their own limb or the computer cursor performing the movement.

It was recently suggested that BMI technology still constitutes an important tool to study and understand some of the mysteries of the brain, specially when referring to plasticity (Sakurai, 2014). Some groups have started taking advantage of the new opportunities BMIs bring to study brain's adaptability.

Studies with BMI related plasticity have provided understanding of the local effects of global perturbations in a neural ensemble. For example, it is possible to measure the consequences of visuomotor rotation (VMR) on a single neuron's *preferred direction* (PD). Paz *et al.* (2003) performed VMR in specific targets of a two-dimensional center-out task . They measured the changes in the firing activity of motor neurons, and found that cells that had a PD closer to the trained target had significantly increased their firing activity when performing the task. Moreover, when looking at the mutual information (MuI) of these neurons, they found that the information of the neural ensemble did not significantly change between the pre- and post-learning epochs. However, when measuring changes in individual cells they reported that a significant amount had significantly increased their MuI, and these cells were the ones whose PDs aligned with the learned direction. Finally, when they decoded movement using the signals from two different epochs (pre- and post-learning), they observed that prediction of movement was improved when the post-learning activity was used. This improvement was consistent even when using two different types of decoders (population vector algorithm and maximum a posteriori estimator). It is important to note that for this experiment the monkeys always performed overt movements, so the adaptation could be linked to any compensations in kinematics the monkeys executed in order to counteract the introduced perturbations.

Jarosiewicz *et al.* (2008) performed a different type of rotation where, instead of altering the visual feedback of the movement (i.e. VMR), they rotated the PDs of a random subset of neurons, and then computed the output variable (cursor movement).

They rotated the selected subset of neurons towards the same direction and the same magnitude (z-axis as reference, 90°). They showed that the directional preferences of the neural population changed in order to compensate for the error in behavior these rotations introduced. Although the majority of the neural population experienced a shift in their PDs, they reported that the rotated neurons exhibited a more significant shift in their PDs than the non-rotated ones, and this shift followed the direction of the global perturbation. Even though the perturbation was done in the neural space, it could still be compared to a global movement rotation, that is a rotation in the task space. In fact, this was shown when Chase *et al.* (2010) performed further analysis to these data, and reported that the subjects were using re-aiming approaches similar to those observed in other VMR tasks. Furthermore, from this method they were able to estimate the amount of compensation attributed to this re-aiming strategy, and reported as a result that the great majority of the adaptation was due to a global target re-aiming (Chase *et al.*, 2012). It is possible that the brain may have not selectively modulated the activity of the subset of neurons, but rather had a global response to a perturbation that could be translated as a global rotation.

More recently, Sadtler *et al.* (2014) tested the limits of brain adaptation via BMIs. They developed a paradigm where individual brain signals were not directly related to cursor movements or states. Instead, they used dimensionality reduction algorithms (Dempster *et al.*, 1977; Yu *et al.*, 2009) to create a lower dimensional neural space, which could be related to both the task states and the firing activity of the neurons. They refer to this lower dimensional space as the intrinsic manifold. After subjects learned the core task, they introduced two different types of perturbations: a within manifold (WM) where they shifted relationships between the task space (cursor states) and the manifold dimensions, and an outside manifold (OM) where they changed the contribution that each neuron had in the manifold dimensions. The

authors hypothesized that the WM perturbations would be easier to learn, while OM perturbations would have shallower learning rates. They found that subjects adapted to WM perturbations over the course of a single session (1000+ trials), while they were not able to adapt to OM perturbations. It is important to note that in this experiment, is that they did not maintain the mapping between neurons, manifolds, and task dimensions constant across several sessions, so each day the subjects had to re-learn a basic mapping, and then the perturbation (WM or OM) map, not allowing any learning to carry across days. In one additional change from more typical single unit BMI studies, the individual brain signals were only sorted using threshold crossing, which means the signals contributing to the manifold dimensions are already superimposed or summed neural signals. This sorting can affect the weights assigned to each of the manifolds dimensions, and could damp the real contribution each neuron has in the lower dimensional space. Overall, these results suggest that although the brain might be able to adapt to a variety of task credit assignments (Paz and Vaadia, 2004; Jarosiewicz *et al.*, 2008; Sadtler *et al.*, 2014), initial properties of the underlying circuitry might impose constrains in the adaptation of brain signals to more complicated tasks.

1.2.3 Population level measurements during learning

The methods described by Sadtler *et al.* (2014) use different tools than usually applied for single-unit level analysis in other studies (Taylor *et al.*, 2002; Paz and Vaadia, 2004; Paz *et al.*, 2005; Wahnoun *et al.*, 2006; Jarosiewicz *et al.*, 2008). Although methods of dimensionality reduction have been used in different fields for decades (Rubin and Thayer, 1982), they have recently been applied to neuroscience and neural engineering (Mosier *et al.*, 2005; Yu *et al.*, 2009; Churchland *et al.*, 2012; Kaufman *et al.*, 2014; Ranganathan *et al.*, 2014). Given the accelerated development

of better recording hardware in neural interfaces, it is now possible to reliably record from hundreds of neurons; this provides challenges not only at storage level, but also during interpretation and analysis. Comparing single units becomes harder, and data matrices are likely to be ill-ranked, due to much of the information being repeated across different neural units. Moreover, there is evidence that population level analysis could provide a better insight into the underlying structure that governs motor learning and adaptation, and can allow to measure underlying structures and strategies that subjects use when controlling BMIs systems (Braun *et al.*, 2009b; Golub *et al.*, 2013; Sadtler *et al.*, 2014; Addou *et al.*, 2014).

These results suggest that study of neural circuitry might be moving towards population level methods, and use of techniques which allow to simplify the neural data without losing task relevant information. Current literature provides enough evidence that such population level approaches can provide enough information to describe BMIs systems, generate input signals to control these systems, and give key insights of correlations and co-variations in the data that would otherwise be difficult to discern (Braun *et al.*, 2009b; Yu *et al.*, 2009; Ranganathan *et al.*, 2014; Kaufman *et al.*, 2014; Sadtler *et al.*, 2014). However, it is important to recognize that these reduced dimensions may not be directly explained as analogous to anatomical structures or connections in the brain, although they might be considered as representations of functional connections between the measured neural signals.

1.3 Specific aims

Given this evidence, I am interested in dissecting the solutions the brain engages with different learning challenges, and measure the changes both at individual and population levels. For example, how quickly does the brain adapt to a uniform perturbation to the neural system, and how does this adaptation compare to a non-uniform

perturbation in the neural space. Also, if the brain is truly able to selectively alter the tuning of a subset of cells, would this behavior prevail when the perturbations cannot be translated to a global rotation? I hypothesize that compensations and changes across the motor neural circuitry will be similar during different learning processes. Hence, I am interested in measuring changes in these neural signals during task adaptation. Furthermore, if we challenge subjects to the same perturbations across different days, could the suggested neural constrains for learning be overcome? In order to answer some of these questions I propose the following aims:

Specific Aim 1. Determine changes in performance and neural activity when applying a uniform perturbation to the system. This perturbation will be applied to the entire neuronal ensemble, through a VMR, where the intended movement decoded from the brain signals will be rotated around a common axis. For *Specific Aim 1a*, I propose generating learning curves for this perturbation, show the subjects are able to adapt and bring performance back to a baseline, and measure the learning rate for this adaptation. I hypothesize the behavior will be similar to those observed in other VMR tasks, where subjects quickly compensate for the rotation. In *Specific Aim 1b*, I will measure changes in the directional preferences of the neural population during learning and after adaptation, where I expect the neurons used for brain control will on average follow the direction and magnitude of the applied rotation.

Specific Aim 2. Determine changes in performance and neural activity when perturbing internal dynamics of a neural ensemble. Specifically we will apply a focal and non-uniform perturbation to the ensemble. I will try to decouple the activity of a small subset of cells, using rotations in the PDs to alter their contributions to the movement decoding. I will select cell pairs that have correlated firing activity during unperturbed (baseline) brain control, and rotate the PD of one of those cells to an orthogonal plane. In *Specific Aim 2a*, I will generate learning curves that reflect the

changes in behavioral performance, and measure learning rates for this task. I expect the subjects to be able to adapt to the new paradigm but anticipate the curve to be different from those observed in more uniform perturbations (VMR). I expect that the learning rate will be slower than that observed in a uniform perturbation, and the movement might not follow a specific directional shift as in the global perturbation case. In *Specific Aim 2b*, I will measure changes in directional preferences in both individual cells and the neural population during and after task adaptation. I expect that the PDs of the majority of the cells will shift from those observed during normal brain control, and we do not expect to see any significant difference in the amount of change between the rotated and the non-rotated cells.

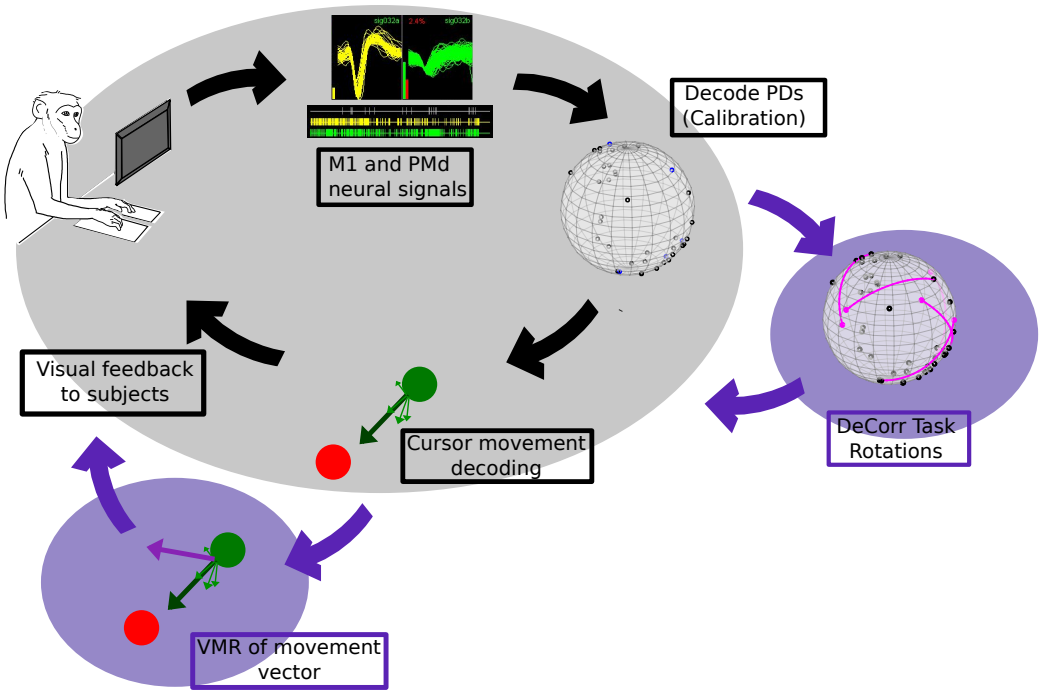

Figure 1.1: Behavioral Paradigm Diagram. Illustration shows proposed system with NHP recordings, PDs estimation, and movement calculation (shaded gray area), and perturbation to the task (purple areas): VMR applied to population vector, before visual feedback, and DeCorr task applied to individual neural signals, before decoding movement.

Figure 1.1 displays a diagram of the behavioral paradigm that was designed to achieve these specific aims. The figure illustrates the flow of the algorithms to estimate PDs from observation, and to control the movement of the cursor (loop over shaded gray area), and it provides a general overview of how each perturbation will be introduced to the system (loops over the purple areas).

In chapter 2, I will outline the methods to probe learning: I will introduce the basic experimental design, and the two task perturbations corresponding to the Specific Aims. In here, I will also introduce the first measurements of individual and population level adaptations. Chapters 3 and 4 will expand the population level analysis: I will use dimensionality reduction algorithms to dissect the neural dynamics during the different tasks, and the different learning stages. In chapter 5, I will summarize the findings and elaborate on possible future work regarding population level techniques to understand neural adaptation, and control BMIs systems.

Chapter 2

UNIFORM AND NON-UNIFORM PERTURBATIONS IN BRAIN-MACHINE INTERFACE CONTROLLED TASK INDUCE SIMILAR ADAPTATION STRATEGIES

This chapter has been submitted as **Armenta Salas, M., Helms Tillery, S.I.**. *Uniform and non-uniform perturbations in brain-machine interface task elicit similar neural strategies*. Initial results of this work have been presented in Armenta Salas and Helms Tillery (2014). The data from the experiments described in this chapter will be used in chapters 3 and 4.

2.1 Introduction

Motor and skill learning are closely related terms often used to describe the acquisition and retention of behaviors through repeated practice (Shmuelof and Krakauer, 2011). Brain-machine interfaces (BMIs) have proven to be a unique environment in which to study the neural correlates of this motor learning. Early reports of BMIs focused heavily on changes in neural coding as subjects adapted to these peculiar output systems and learned to control the movement of an effector that they had never experience before (Wessberg *et al.*, 2000; Taylor *et al.*, 2002; Serruya *et al.*, 2002; Carmena *et al.*, 2003): clearly these systems would require learning and adaptation to even operate. This challenge to neuroprosthetics has become an opportunity in which BMIs provide a novel environment to directly probe and measure the brain's plasticity. BMIs have been used to test the ability of subjects to learn new tasks (Shadmehr and Mussa-Ivaldi, 1994; Taylor *et al.*, 2002; Carmena *et al.*, 2003; Hochberg *et al.*, 2006; Velliste *et al.*, 2008; Orsborn *et al.*, 2014) or to adapt to new environments

(Krakauer *et al.*, 2000; Tong and Flanagan, 2003; Tanaka *et al.*, 2009). It has been possible, using BMIs, to identify the presence of variations in the properties of individual neurons after learning a task (Taylor *et al.*, 2002; Carmena *et al.*, 2003; Ganguly and Carmena, 2009; Ganguly *et al.*, 2011; Chase *et al.*, 2012), as well as the existence of constraints within the neural circuitry which can hamper skill learning (Paz and Vaadia, 2004; Jarosiewicz *et al.*, 2008; Ranganathan *et al.*, 2014; Sadtler *et al.*, 2014). All of these results feed back into neural technologies, and have led to the use of different strategies to challenge neural systems (Ganguly and Carmena, 2009; Ranganathan *et al.*, 2014; Sadtler *et al.*, 2014), and may even lead to potential applications in motor rehabilitation (Hochberg *et al.*, 2012; Collinger *et al.*, 2013, 2014).

Given the present evidence of plasticity in BMI systems, it seems clear that a given neural ensemble is able to adapt to different decoders, suggesting these systems are able to generate strategies that solve a number of diverse challenges. These decoders need not follow exact representations of muscle activation or movement (Ganguly and Carmena, 2009), although the speed of adaptation seems to relate to how closely the decoder follows this relationship (Ganguly and Carmena, 2009; Ganguly *et al.*, 2011; Sadtler *et al.*, 2014). These different adaptations have system-wide impact, changes in neural properties are measured throughout the entire neural ensemble (Hikosaka *et al.*, 1999; Ganguly and Carmena, 2009; Jarosiewicz *et al.*, 2008; Ganguly *et al.*, 2011; Chase *et al.*, 2012; Wander *et al.*, 2013; Addou *et al.*, 2014; Okun *et al.*, 2015). However, not all neurons change in the same manner: the amount of adaptation may correlate with the properties required by the new controller (Paz and Vaadia, 2004; Jarosiewicz *et al.*, 2008; Chase *et al.*, 2012). For example, in tasks with visuomotor rotations or force-field perturbations, the system appears to solve the problem, and respond to the perturbations mostly in a uniform manner across the neural population

(Krakauer *et al.*, 2000; Tong and Flanagan, 2003; Rokni *et al.*, 2007; Tanaka *et al.*, 2009).

Although it has been shown that the neural circuitry can adapt to simple tasks that call for uniform changes across the system (Krakauer *et al.*, 2000), neural systems can also adjust their activity to find a workable solution for tasks that non-uniformly perturb the neural ensemble (Paz and Vaadia, 2004; Ganguly and Carmena, 2009). It remains unclear whether the differences in the measured adaptations are due to differences in the nature of the challenges (e.g. visual rotations, force fields, shuffled decoders, etc.), or due to the overall difficulty of the task. For example, it is not clear at this point how the system would respond to a perturbation that only impacted a focal set of cells. How does the learning process compare across these different tasks: does the neural system try to apply the same adaptation strategies, or does it engage different adaptation processes? Do these strategies change the properties of the signals or can they also alter the underlying dynamics of the area of cortex undergoing adaptation? Lastly, while there is evidence that a neural ensemble can alternate BMI control between a normal and a shuffled decoder (Ganguly and Carmena, 2009), it has not been shown that a given set of neurons can process two very different kinds of perturbations to the decoder, which could have great influence in understanding the limitations of motor adaptation, and might impact the design of motor rehabilitation paradigms.

It was hypothesized that to solve distinct motor learning tasks, the neural population may actually respond as a whole, varying the behavior of the entire neuronal ensemble, even when the perturbation is only across a limited subset of that ensemble. I propose that motor neural circuitry will exhibit changes across the entire neuronal ensemble when challenged with different uniform and non-uniform perturbations, but

both tasks will elicit similar adaptation strategies throughout the learning process, even when the final neural solutions are not similar between the tasks.

In this chapter, I will report the response of the motor cortical system to two different control perturbations: one global and uniform, and a second that is focal and non-uniform. I recorded and characterized the neural behavior during and after learning. I anticipated that any changes to the directional preferences of the neural ensemble, will be achieved with similar exploratory strategies for both uniform and non-uniform perturbations. Furthermore, tuning changes induced by these tasks will be measured in the final adaptations displayed by the entire neuronal ensemble.

For the global uniform perturbation, I used a visuomotor rotation in a BMI controlled 3D center-out task. This rotation was uniformly applied to all movements and all target directions, so I was able to measure corresponding directional tuning changes across the entire neuronal population. Second, to perturb the interactions between motor signals, I decoupled the correlated activity of a small number of neuron pairs. I expected that this would result in non-uniform changes in the directional preferences of the neuronal ensemble, and in their corresponding contribution to the task.

2.2 Methods

2.2.1 Experimental set-up and recordings

All experimental protocols were in accordance with the Guide for the Care and Use of Laboratory Animals, and approved by the Arizona State University Institutional Animal Care and Use Committee (see Appendix A). We implanted two non-human primates (*Macaca mulatta*) with six bilateral (monkey O) and four unilateral (monkey M) 16-channel micro-wire arrays (Tucker Davis Technologies, Inc.), in the hand and

arm regions of the motor and dorsal pre-motor cortices. The coordinates of the cortical regions of interest were acquired with previously described methods (McAndrew *et al.*, 2012), and verified by visual inspection of the implantation sites during surgery. A 96-channel recording system (Plexon, Inc., Dallas TX) was used to capture, filter, and sort single and multi-unit activity. Units were sorted using voltage threshold and waveform shape detection. Action potentials that met both the threshold and waveform criteria were registered as spikes, and sorted as a neural unit. Data from all channels were captured at 40 kHz and saved for post-hoc analysis.

The monkeys were trained to sit on a primate chair and to observe three dimensional center-out movements of a computer cursor in a 3D monitor (SeeReal Technologies), while keeping their hands on pads located on the desk immediately in front of the primate chair (Fig. 2.1A). The task required continuous contact with both left and right hold-pads in order to operate. At least once weekly, and more frequently when recording conditions were changing, the monkeys performed calibration trial blocks. In these calibration blocks, the animals observed the cursor moving automatically to each of the eight targets at a constant speed. In each trial, the cursor took approximately 9.5 seconds to move through a straight path to the target. Neural activity during these epochs exhibited adequate directional tuning to initialize a population vector. From this point, the motion of the cursor was controlled by neural activity using the population vector algorithm (PVA) from Georgopoulos *et al.* (1986). Changes in recording conditions were noted if a neuron's waveform was no longer recorded in a channel, or if the sorted neurons no longer met the previously established sorting criteria. Subjects learned a total of eleven (monkey O) and five (monkey M) different calibration maps during the experiments described here.

The tasks were organized by blocks of 32 trials. During those blocks, the control code remained fixed: cursor and target diameters, successful/failed trials criteria and

cues, and inter-trial times. The cursor and targets were differently colored spheres: the cursor was green for all conditions, and the target was red during calibration blocks and yellow during all brain control blocks. Different background lighting in the virtual-reality (VR) display was also used during the task: white for calibration, and yellow for baseline and perturbations (Fig. 2.1A). Two cases were considered a failed trial: if the subjects did not reach the target in a set time (13-22 seconds), or if the cursor went out of bounds. These bounds were experimenter selected, and they were the virtual limits where the cursor would no longer be visible in the task display. Between trials, the cursor and target were blanked for 0.8-2.4 second inter-trial interval.

Figure 2.1B displays the two possible timelines in a session. The upper timeline illustrates the event sequence with a calibration session; while the bottom timeline represents the days when the monkeys started directly with active brain control. In both cases, the first five minutes of recording were captured without any task display: the monkeys sat quietly on the primate chair with the monitor off. These data were used in a separate study comparing background activity with task-based activity (see chapter 3). Each session consisted of three baseline blocks, 32 trials each, followed by blocks of perturbations (average perturbed blocks = 4.7, s.d. = 1.1). Once the perturbation was introduced, it was kept constant throughout the remainder of the session. If the monkey removed either hand from the copper plates, the task would pause until both plates were pressed, and the task would resume with the cursor back at the center position.

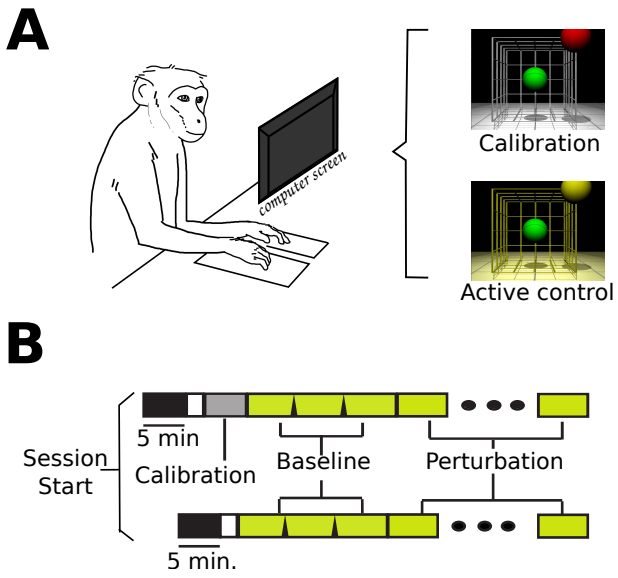

Figure 2.1: Task Set-up, Perturbations and Time Line. **A:** NHP in primate chair set-up, and VR screen with display lighting during calibration and active brain control. **B:** Task time-lines (with and w/o calibration block): task-off, calibration, baseline, and perturbation.

2.2.2 Neural decoding for brain control

I adapted the PVA to decode the movement of the cursor from neural activity. The choice of the population vector was largely on the ease with which changes in neural tuning can be quantified. There are many other possible algorithms, and smoother and better control has been reported with other linear and non-linear decoders such as Kalman filter, particle filters or Bayesian approaches (Carmena *et al.*, 2003; Wu *et al.*, 2003; Hochberg *et al.*, 2006; Velliste *et al.*, 2008; Hochberg *et al.*, 2012; Orsborn *et al.*, 2014); however any parametric changes in neural tuning using these other decoders are more difficult to decipher. Furthermore, in a direct comparison of several of these decoders, most subjects can compensate online for poor preferred directions distributions while using PVA, and have similar performance across different decoders (Koyama *et al.*, 2010).

To begin, I assumed the neurons had cosine tuning profiles as stated in (2.1).

$$f_i = b_0 + m_i cos\theta, \tag{2.1}$$

where f_i refers to the ith neuron's firing rate, b_0 to the tonic activity of the ith neuron, m_i is the depth of modulation for the ith neuron, and θ is the angle between the *preferred direction* (PD) of the cell and the intended movement direction. Since these neurons also display a preferential tuning when observing movement in a VR environment (Wahnoun *et al.*, 2006), I calculated the preferred directions from recordings during the calibration trials. I estimated each neuron's *calibration preferred direction* (cPD) using a multivariate linear regression, which related the neuron's change in firing rate from their baseline to the target direction at any given moment during the task. The firing rate was calculated online from the spiking activity of non-overlapping 50 milliseconds bins and a running mean for each neuron using a rectangular kernel (Nawrot *et al.*, 1999). The estimated directions were converted to unitary vectors and used to control the movement of the cursor, unless the 90% confidence interval for all three coefficients spanned zero. These cPDs were used to compute the population vector shown in (2.2).

$$\overrightarrow{PV} = \sum_{i=1}^{N} \left(f_i - \bar{f}_i\right) \overrightarrow{cPD_i}, \tag{2.2}$$

where $\overrightarrow{cPD_i}$ is the ith neuron's preferred direction, f_i is the instantaneous firing rate, $\bar{f}_i$ is the baseline firing rate, computed as a running mean for each cell across the entire block, N is the total number of neurons used for active brain control, and $\overrightarrow{PV_t}$ is the final population vector for that time step. The population vector was calculated every 50 ms, and the position of the cursor was updated using this vector. The population vector was smoothed using a two time-step window moving average filter.

Equations (2.3) and (2.4) display the formulas used to update the cursor position for monkeys O and M, respectively.

$$\overrightarrow{C_t} = \overrightarrow{C_{t-1}} + \left[\overrightarrow{PV_t} \cdot g \cdot (1-h) + \overrightarrow{Tar_{t-1}} \cdot h\right] s \cdot L; \tag{2.3}$$

$$\overrightarrow{C_t} = \overrightarrow{C_{t-1}} + \left[\overrightarrow{PV_t} \cdot g(1-h) + \overrightarrow{Tar_{t-1}} \cdot h\right] s, \tag{2.4}$$

where vectors $\overrightarrow{C_t}$ and $\overrightarrow{C_{t-1}}$ refer to the current and previous cursor position, respectively. The vector $\overrightarrow{PV_t}$ represents the current smoothed population vector, and the scalar g is the population vector gain factor ($\mu_O = 34.94$, s.d. 18.6; $\mu_M = 412.58$, s.d. 4.36). Additional parameters include active assistance factor ($h_O = 8\%$ and $h_M = 0.8\%$), speed gain (s : experimenter selected), and length of the population vector (L). The vector $\overrightarrow{Tar_{t-1}}$ is the direction to target from the previous cursor position, normalized to be a unitary vector.

2.2.3 Learning challenges in BMI-controlled task

I introduced two types of perturbation to the task: 1) a visuomotor rotation (VMR), around the axis into the monitor, of 30° in CCW and CW directions; and 2) a decorrelation perturbation (DeCorr), in which we chose a subset of the pairs of neurons with highest peak cross-correlation values, and constrained their contribution to the population vector to be uncorrelated by assigning them orthogonal preferred directions.

In the VMR task, I selected the antero-posterior axis as our reference vector, with positive directions into the VR display. I then rotated the computed PV using a rotation matrix derived from the Rodrigues' rotation formula (2.5).

$$R = \begin{bmatrix} cos\theta & 0 & sin\theta \\ 0 & 1 & 0 \\ -sin\theta & 0 & cos\theta \end{bmatrix}, \tag{2.5}$$

where θ is the angle of rotation around the selected axis. The rotation was applied to the PV before updating the cursor position. A positive theta yielded a CCW rotation, and a negative theta a CW rotation. Figure 2.2A displays the rotation of an arbitrary movement vector in CCW direction, where the blue vector is the initial intended movement, and the magenta vector is the outputted movement after the rotation. The y-axis was selected as reference for the rotation, which places the rotation in the plane of the display screen.

For the DeCorr perturbation, we used the cross-correlation function between the firing rates of neurons to identify functional connections between the cells (Vaadia *et al.*, 1995; Salinas and Sejnowski, 2001). I calculated the cross-correlations between all neuron pairs from activity recorded in the baseline intervals, and then selected the pairs which displayed the highest maximum cross-correlations. One neuron was randomly selected from each pair, and the cPD of the selected neuron was rotated to a new direction orthogonal to the starting cPD. To select the specific direction within that orthogonal plane, I projected the cPDs of the entire ensemble to that same plane, and identified the region of the plane with the fewest projected cPDs. The new cPD for the selected cell was chosen to fill the most substantial gap in that orthogonal plane. This process was repeated four to six times, with no single cell involved in more than a single rotation. Figure 2.3A shows the distribution of angles between all the cPDs for a given decoding map of monkey O and monkey M before (black) and after (purple) the perturbation. Figure 2.3B displays the distribution of angle differences between the rotated pairs before (black) and after (purple) the

DeCorr perturbation of the same ensemble cPDs for both monkeys. The sum of the individual rotations did not result in substantial rotation to the output (two-sample test, circular data, $p > 0.05$, Zar, 1996).

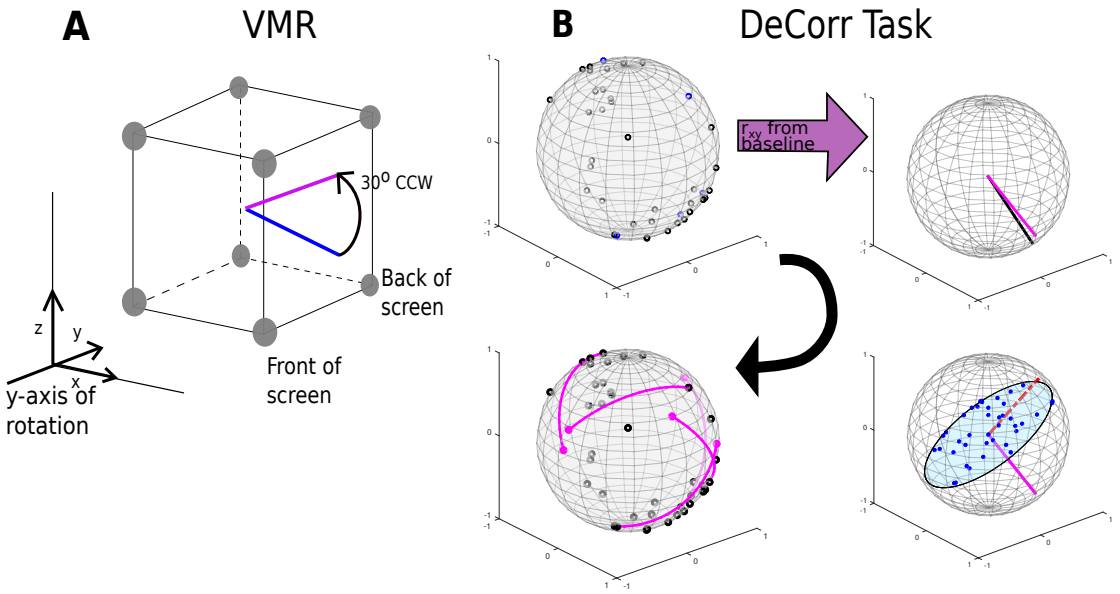

Figure 2.2: VMR and DeCorr. **A**: Diagram displays the VMR applied to the original population vector (blue) and the resulting rotated vector (magenta), which was used to update the cursor movement. **B:** DeCorr procedure (read clockwise from top left corner): from a given cPD distribution, the cross-correlation coefficients were computed (r_{xy}), and top correlated pairs were then selected. A neuron was randomly selected from the pair (magenta vector), and the rest of the cPDs were projected into an orthogonal plane. The cPD for the selected neuron was rotated towards the region of the plane with fewer neurons (red dashed vector). This process was repeated for a small number (4-6) of neuron pairs.

2.2.4 Control for chance performance

In order to test whether the subjects were able to rely on active assistance to perform the tasks, I simulated the task offline using the stored firing activity during baseline, VMR and DeCorr trials, but manipulated the relationships between firing and device motion in two ways. First, I employed the same cPDs used during active

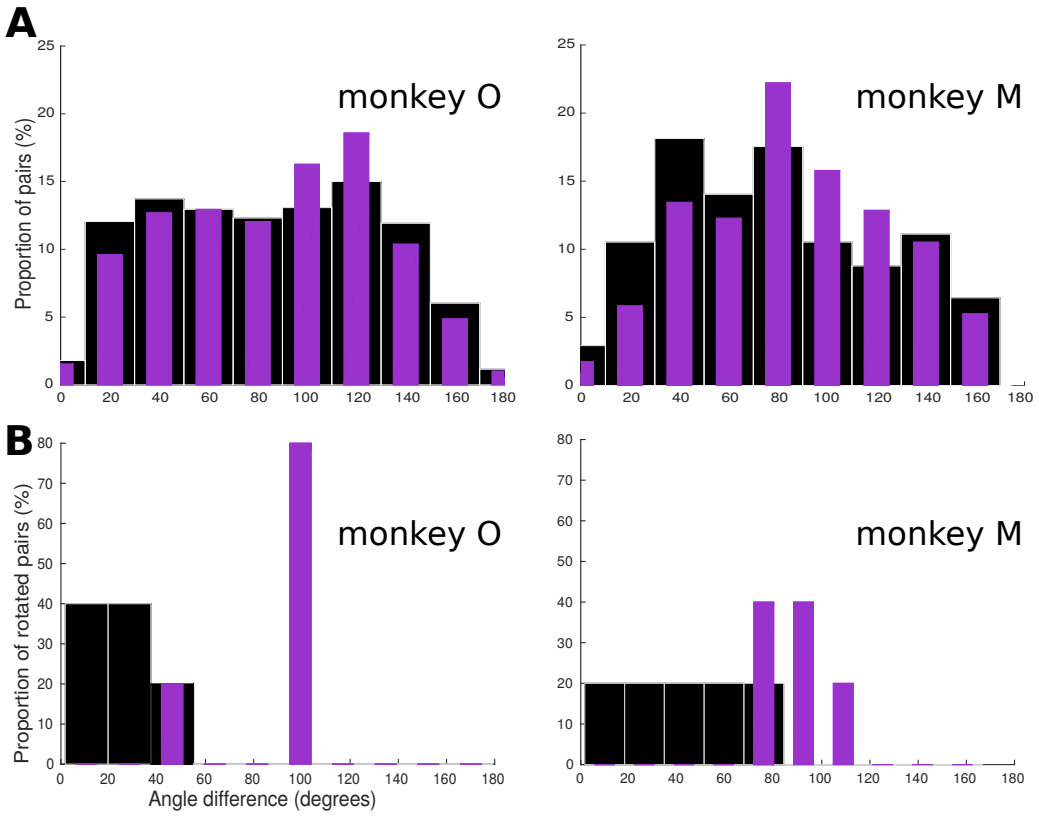

Figure 2.3: Changes in Preferred Directions Distributions in DeCorr Perturbation. **A:** Distribution of angle differences between neurons used for active brain control for a single baseline session. Histograms display the percentage of cell pairs vs. angle in degrees. **B:** Distribution of angle differences between cell pairs before (black) and after (purple) the DeCorr perturbation.

brain control but shuffled the relationship between the neurons' cPDs and their firing activity. The goal was to keep the same directional distribution and neuron firing rates, but to alter the relationship between neurons and their preferred directions. Second, I estimated the population vector and cursor motion as if the firing activity had not varied from its mean value. In both cases, the population vector was recalculated using (2.2), and updated the cursor position using (2.3) and (2.4). All task parameters were kept the same as those used during active brain control. From these simulations, I computed the estimated target hits and angular errors between population vector and target direction. These controls provided a measure of the

extent to which the cursor motion was due to active assistance, and how much was due to subjects modulating their activity. In cases using modulated firing rates, I would observe only 2 or 3 target hits in 96 trials. If only the help was included (no firing rate modulation), there were no target hits (see Fig. 2.4 for details).

Figure 2.4 shows examples of the effects of active assistance in the task for both subjects, where the purple trace shows the average distance to target across the simulated trials (shaded area represents standard error). A minimum distance of seven centimeters was considered a target hit. The effects of the active assistance were larger for monkey O (left panel) than for monkey M (right panel); however, they were not significant enough to explain the success rate of the monkey. Bottom right insets display the cumulative distribution functions of angles between the target and cursor, for the simulated (red) and the actual (purple) population vectors ($p < 0.001$, one-sided two-sample K-S test).

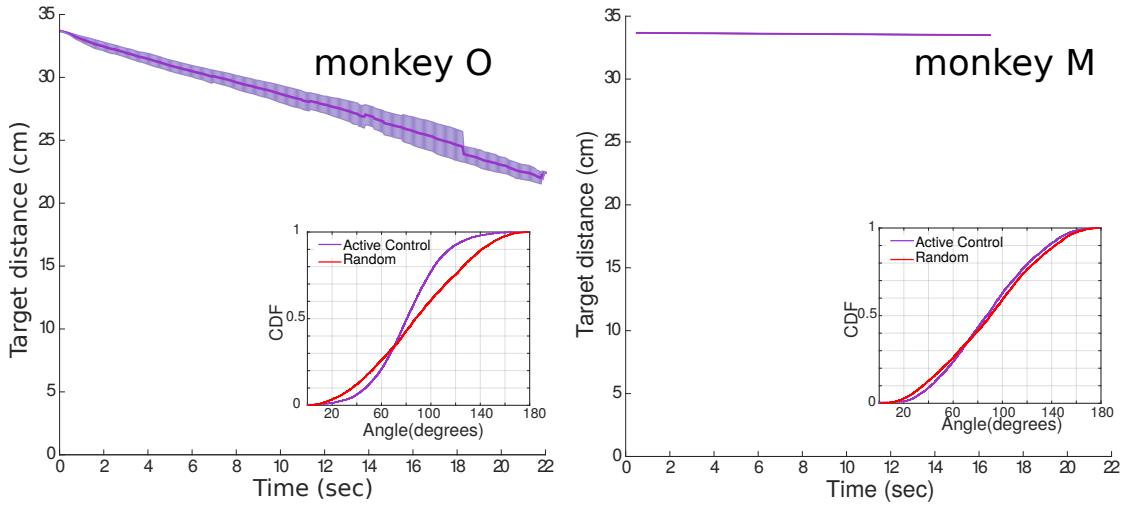

Figure 2.4: Control for Chance Performance. Simulated movements from shuffled cPDs from monkey O (left panel) and monkey M (data). Average distance to target if maximum trial time was allowed. Shaded areas represent mean +/- one standard deviation. Bottom right inset in each panel displays the CDF of angles between PV and target from the active brain control (purple trace), and the simulated movements (red trace).

2.2.5 *Changes in tuning properties and neural ensemble dynamics*

Tuning was expected to change between tasks, and specifically, I expected preferred direction to change (Taylor *et al.*, 2002; Jarosiewicz *et al.*, 2008; Chase *et al.*, 2010). Therefore, a key measure of changes in the neural system was observed by calculating the preferred directions associated with action in the virtual task (*action PDs* or aPDs), using the same tuning equation shown in (2.1). Many of the main results reflect differences in the aPDs between conditions. As a primary measure of changes in cell properties, I calculated the angle between the aPDs of baseline and perturbed trials for both successful and failed trials. I measured angle changes in the aPDs between the baseline trials and the perturbations.

To measure any possible changes in neuronal ensemble dynamics, I calculated the cross-correlation function during both the baseline trials and the perturbations using one millisecond bins and a Gaussian kernel of 200 milliseconds (Nawrot *et al.*, 1999). I then compared the peak cross-correlation coefficients for each trial across the different paradigms. I also compared the peak cross-correlation coefficients during the first phases of task learning to those from when the animals were fully adapted.

The tasks are three-dimensional, and so the control of the tasks is over-specified by the neural ensemble. Because of this, it is possible that each of the tasks is eventually controlled in separate neural spaces. To capture this, I used dimensionality reduction techniques to identify control manifolds specific to each task, and to explore whether the neural activity could be expressed in terms of latent dimensions (Rubin and Thayer, 1982; Sadtler *et al.*, 2014). This method allowed us to estimate a subspace or manifold that related the activity of each of the recorded neurons to the solution space for a given phase of the task. This space may indicate latent variables driving the activity of the recorded neurons (Santhanam *et al.*, 2008; Yu *et al.*, 2009). These

analyses can express neural activity as a function of unobservable variables (latent dimensions) that reflect an intrinsic manifold (Sadtler *et al.*, 2014). We used existing algorithms and MATLAB scripts (Yu *et al.*, 2009; Cowley *et al.*, 2013) to estimate these intrinsic manifolds and latent variables from the raw neural data. I estimated these manifolds using a fixed number of latent dimensions ($n = 12$) across the different trials.

Finally, we computed the principal angles (PAs) between these estimated manifolds for baseline and perturbation trials. These PAs capture the intersections between subspaces. For dimensions that two subspaces share, the PAs are near zero. For dimensions that the two manifolds do not share, the PAs are closer to 90°, indicating that the subspaces are distinct. I used an algorithm and MATLAB function which allows for precise estimation of small angles between subspaces (Knyazev and Argentati, 2002). I then measured the changes in the distribution of the PAs as subjects improved performance in both perturbations.

2.3 Results

Both subjects were trained on both perturbations. For monkey O, I was able to observe full adaptation back to initial levels of performance in both tasks. Monkey M was only able to complete adaptation in the VMR task: after three days in the DeCorr task, the recording implants failed. After the subjects had been trained with both types of perturbation, we measured the variations in behavior and performance across days where perturbations were constant. For all the performance measurements of VMR sessions, the rotation directions (CCW and CW) were merged, as I did not find significant differences in performance or movement errors among them (one-way ANOVA, $p > 0.8$). Pertinent corrections for rotation direction were made when

measuring the angle shift in aPDs, and movement errors. For examples of movement shifts please refer to Appendix B.

Figure 2.5 summarizes task success of the perturbations for both monkeys across several sessions. Figure 2.5A displays the percentage success for VMR sessions for monkey O (solid purple lines) and M (dashed black lines). Illustrated trials belong to sessions where the cPD distributions and the perturbation were kept constant. Percentage success was normalized according to the maximum success rate during the baseline trials. The red trace represents model fitting of a modified Wright's (1936) learning curve ($y = 100 - ax^b$), the coefficient b represents how quickly or slowly the subjects improved in the task. Values close to zero mean the learning was slow, while values close to negative one mean the subjects adapted quicker as they performed more trials. I observed similar learning rates for both subjects in VMR trials, as shown in Fig. 2.5A. Subject M had a slightly faster adaptation with an estimated coefficient b = -0.10, while subject O had an estimated b = -0.08. Similarly, Fig. 2.5B displays the increase in performance in the DeCorr trials for both subjects. Subjects O and M had estimated coefficients of b = -0.19 and b = -0.03, respectively.

As we can observe in Fig. 2.5B, monkey M performed fewer trials of the DeCorr task, although he showed improvement in the task, he did not reach accuracy similar to the baseline trials and displayed slower learning than monkey O. However the improvements were similar along the initial learning phases, and we will compare the initial phases of learning between subjects. For example, during the first couple of sessions ($\sim$500 trials) both had an increase of approximately 20% of initial performance (Fig. 2.5B), and there was not a significant difference between the normalized performance of these trials (one-way ANOVA, F = 0.7, p > 0.4).

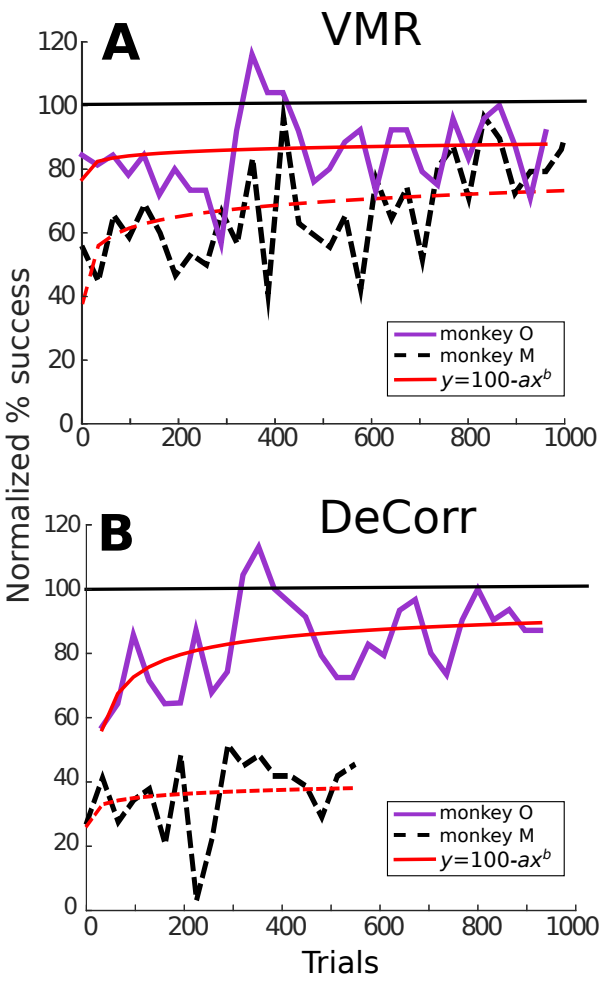

Figure 2.5: Task Performance. **A:** VMR performance for monkey O and monkey M in solid purple and dashed black lines, respectively. Trials span across different days. Percentage success was normalized with maximum performance in baseline trials. Red trace shows fit for Wright's learning curve ($y = 100 - ax^b$), with coefficients a_O = 22.11, b_O = -0.08 and a_M = 58.1, b_M = -0.10. **B:** DeCorr performance for monkey O and monkey M in solid purple and dashed black lines, respectively. Trials span across different days with the same perturbed cPDs. Coefficients a_O = 47.43, b_O = -0.19 and a_M = 74.91, b_M = -0.03. Format is the same as top panels. (*: monkey M had less data, trials span for approx. 500 trials)

2.3.1 Tuning property variations with learning

As a first measurement of responses in the neural signals, I compared the firing rates across days where we used the same decoding cPD distributions for cursor con-

trol, and I did not find significant differences between baseline and the perturbations (see Appendix B). I also looked for specific differences between the firing activity of the rotated and non-rotated neurons in the DeCorr task, and I also found no significant variations between these groups.

In order to quantify tuning changes in individual signals while the subjects adapted to the task, I calculated the angles between aPDs of baseline and perturbed trials. I calculated these aPDs during learning and after subjects had reached good performance in the perturbed tasks. To measure changes during learning, I used data sets of 16 trials to calculate the aPDs after introducing the perturbations, measuring the angle shift between subsequent trial sets until subjects had reached between 90 and 100% accuracy within those trials. This way, I tracked the behavior and tuning changes in individual neurons while subjects learned the tasks. Figure 2.6 shows the average arc lengths between aPDs for VMR and DeCorr trials for monkey O (purple) and M (black). I fitted simple linear first order models to the average arc lengths, shown in the red traces. I observed a decreasing trend for both task types, but did not observe any significant differences in the aPD variations of rotated and non-rotated neurons during the initial stages of learning (performance $< 65\%$) for either subject. For monkey M, the DeCorr trials did not have a strong fit to any model but did display a slight decreasing trend (see Fig. 2.6B).

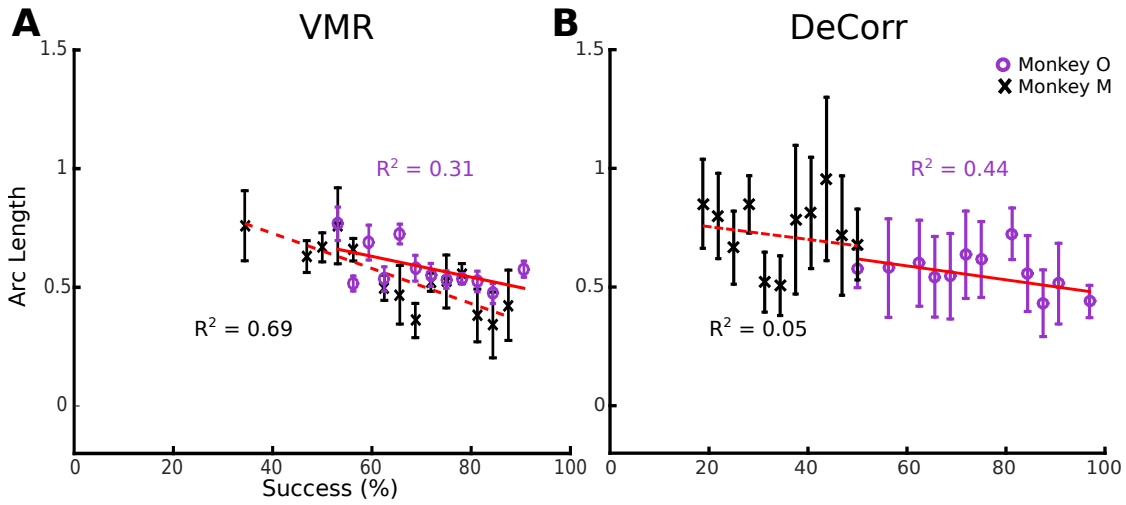

Figure 2.6: Preferred Directions Variations During Learning. **A:** Average arc length vs. percentage success in VMR task for monkey O (purple circles) and monkey M (black cross), error bars display standard error. Red traces display fit for linear model ($y = ax + b$), with coefficients a_O = -0.004, b_O = 0.894, a_M = -0.007, b_M = 1.023. **B:** Average length vs. percentage success in DeCorr task for both subjects, error bars display standard error. Red traces display fit for linear model, with coefficients a_O = -0.003, b_O = 0.765, a_M = -0.003, b_M = 0.808.

I also estimated the final aPDs once the monkeys had learned the perturbations. Figure 2.7 displays the final shifts of aPDs between baseline and perturbed trials, using only successful trials across several days (200+ trials) with movement still decoded with the same cPDs. Figure 2.7A displays examples of aPD shifts during VMR trials for monkey O in CW direction, where the black end of each trajectory represents the baseline aPD, and the red end shows the aPD during perturbation. Similarly, Fig. 2.7B shows the change in aPDs in the DeCorr trials, the magenta trajectories highlight the rotated neurons during the perturbation. Figure 2.7C displays changes in VMR aPDs across all days for monkey O. In the majority of the sessions, the aPDs displayed an average angle shift of 30° in the direction of the induced rotation ($p < 0.05$, one-sample test for mean angle; Zar, 1996). On the other hand, Fig. 2.7D shows the distribution of aPD shifts for the rotated (magenta) and non-rotated (blue) cells for the same subject in the DeCorr task. I observed a significant difference between

these sub-populations ($p < 0.05$, two-sample test for mean angle; Zar), with a larger shift in the rotated neurons. I observed similar behaviors in monkey M's aPDs during the VMR and DeCorr tasks (see Fig. 2.8). In this monkey there was also an overall 30° rotation in the VMR task, and significant difference between the rotated and non-rotated sub-populations in the DeCorr task.

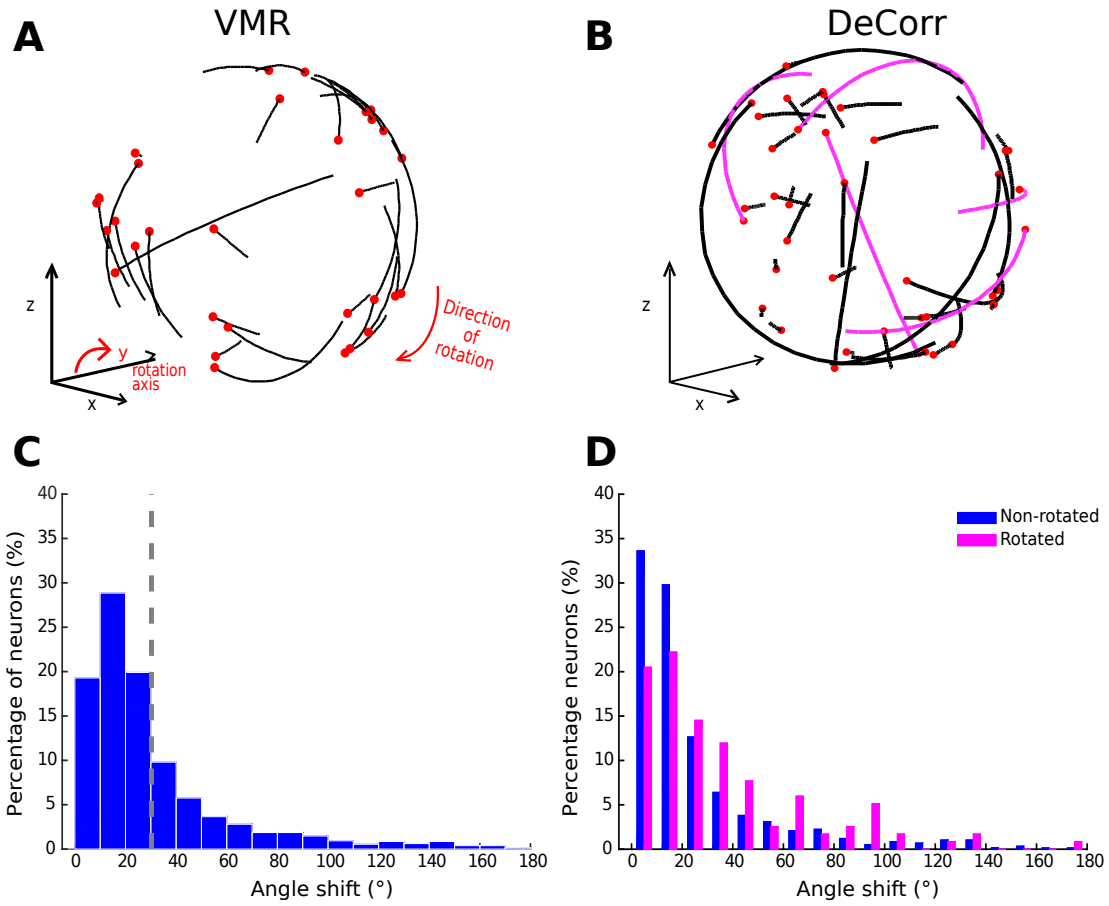

Figure 2.7: Preferred Directions Changes in VMR and DeCorr Task for Monkey O. **A:** aPDs changes during VMR task (CW direction): aPDs during baseline (black end) and after perturbation (red dot) are displayed for each neuron used for brain control. **B:** aPDs changes during DeCorr task (5 rotated pairs): aPDs during baseline (black end) and after perturbation (red dot) are displayed for each neuron used in brain control, magenta trajectories highlight the rotated neurons. **C:** Shift in neurons aPDs, pooled data are displayed for all VMR sessions for monkey O. Dashed gray line illustrates ideal 30° shift. **D:** Shift in neurons aPDs, pooled data for all DeCorr trials for monkey O. Blue bars show data for non-rotated neurons, and magenta bars display data for rotated neurons.

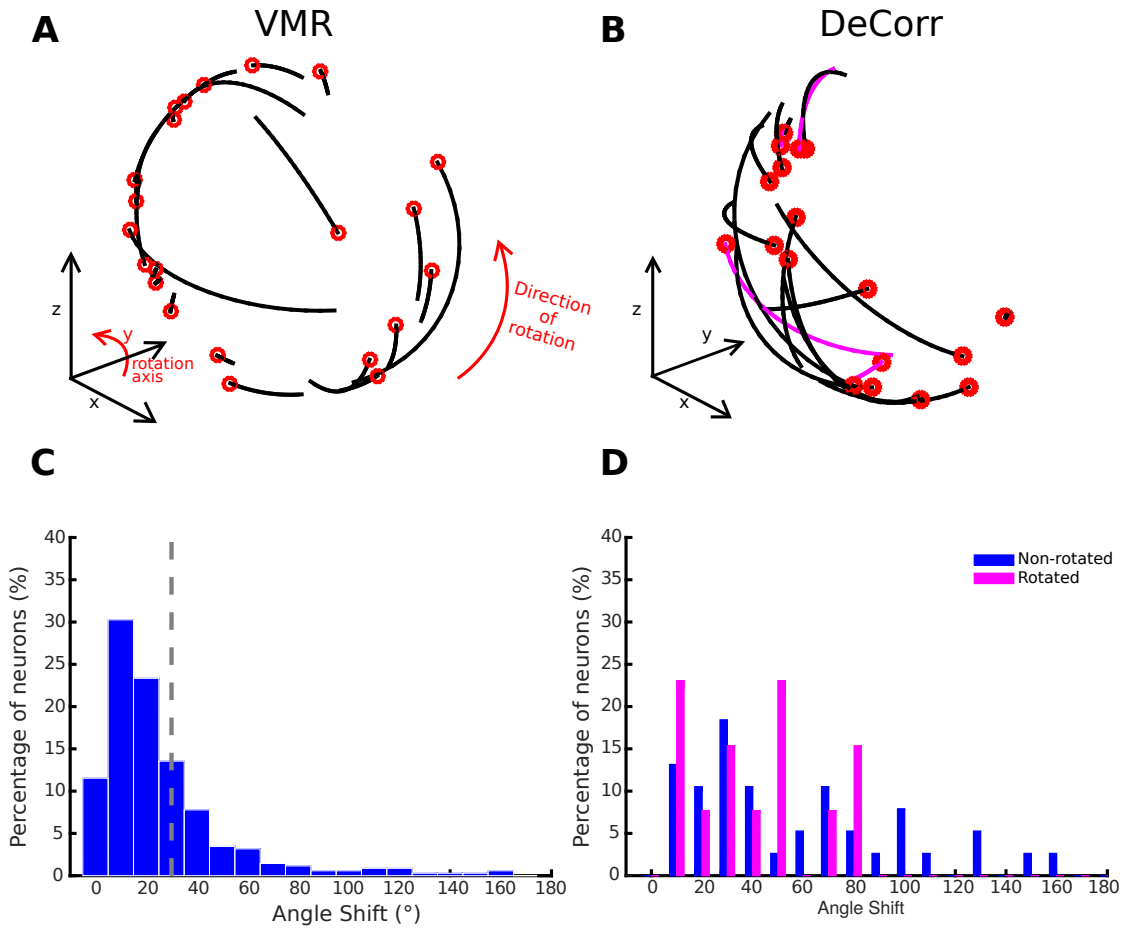

Figure 2.8: Preferred Directions Changes in VMR and DeCorr Task for Monkey M. **A:** aPDs changes during VMR task (CCW direction): aPDs during baseline (black end) and after perturbation (red dot) are displayed for each neuron used for brain control. **B:** aPDs changes during DeCorr task (4 rotated pairs): aPDs during baseline (black end) and after perturbation (red dot) are displayed for each neuron used in brain control, magenta trajectories highlight the rotated neurons. **C:** Shift in neurons aPDs, pooled data are displayed for all VMR sessions for monkey M. Dashed gray line illustrates ideal 30° shift. **D:** Shift in neurons aPDs, pooled data for all DeCorr trials for monkey M. Blue bars show data for non-rotated neurons, and magenta bars display data for rotated neurons.

2.3.2 Changes in population dynamics during learning

A key goal in this experiment was to measure whether the tasks, and specially the DeCorr task, resulted in changes in the internal dynamics of the ensemble. The first measure of changes was to determine whether the overall profile of the cross-

correlations between neurons of interest changed with the task. Thus, I compared changes in the peak cross-correlations from the neurons used to control the movement of the cursor after the tasks had been learned. Here I found no significant changes in the peak coefficients during baseline and DeCorr trials. I also examined correlation coefficient along sets of trials while subjects learned the tasks. For half of the DeCorr sessions, there was a significant drop in cross-correlation coefficients after the perturbation was introduced for both subjects (13/24, one-way ANOVA, $p < 0.01$). During these sessions, I also observed an increase in the coefficients of all cell pairs as subjects improved performance; however this trend was not present across all days (see Fig. 2.9). I also compared changes in correlation between the rotated and non-rotated neurons, and did not find any significant differences between them during most sessions for both subjects (16/24 sessions, $p \geq 0.1$).

These results suggest that the network dynamics are changed during learning, but that once learning is completed, the ensemble properties appear to revert to their baseline state.

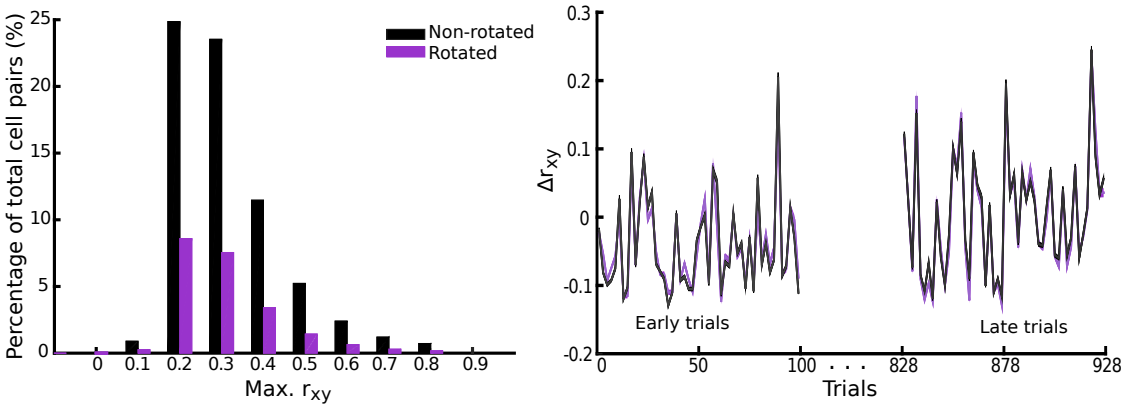

Figure 2.9: Changes in Peak Cross-Correlations. Left panel displays cumulative percentage from total rotated (purple bars) and non-rotated (black bars) pairs during DeCorr trials. Right panel shows the average change from baseline trials in peak cross-correlations with standard deviations (shaded area), for rotated (purple) and non- rotated (black) pairs. Data illustrate the first and last 100 trials of data set of approx. 1000 trials with DeCorr perturbation for one subject.

The state of the ensemble was also measured by examining the spaces in which the ensemble encoded movement. To this end I applied factor analysis methods to discern key dimensions of the neural control (Yu *et al.*, 2009; Sadtler *et al.*, 2014). I estimated manifolds which captured the observed firing patterns among the neural ensembles with a smaller set of latent dimensions. I found that with at most 12 dimensions we could capture the key elements of neural activity that were associated with control of the cursor. When I examined the manifolds corresponding to baseline performance and those associated with the perturbations, I found that there was a great degree of overlap between the manifolds, reflected in small PAs between axes of the manifolds (solid bars in Fig. 2.10) (Knyazev and Argentati, 2002). There were generally only 1 or 2 dimensions which were distinct between manifolds in the perturbed cases and those from the baseline cases. In Fig. 2.10, I arbitrarily split the principal angles into "small" angles (0°-30°) indicating dimensions of overlap between manifolds, and "large" angles (60°-90°), indicating dimensions that were separate between the manifolds. In both the VMR (panel A) and DeCorr (panel B) tasks, the bulk of PAs were small angles (solid colors). I further broke that analysis down into the cases where the animal was performing well ($\geq 70\%$ performance) and where the animal was performing poorly ($\leq 50\%$ performance). The asterisked bars indicate cases that were found to be statistically different by ANOVA ($p < 0.01$). Only the DeCorr trials for one subject displayed significant variations. I also measured the absolute value of the largest and smallest angles in each perturbation. I observed a decreasing trend in the largest angles of the VMR trials, and mixed responses for the DeCorr trials of both subjects. Consistent with our finding that the correlations between neurons changed only transiently, and only during the DeCorr task, the dimensional coding for the movement of the cursor was clearly impacted by learning in the case of the DeCorr task.

Finally, I found a general decreasing trend in the average PAs as subjects improved performance. As shown in Fig. 2.11A, a decreasing linear model explained most of the variability in the DeCorr trials ($R^2 \geq 0.5$) for one subject, and this was also observed across the VMR trials for both subjects even if they did not have a good fit. Figure 2.11 shows data from both subjects during VMR and DeCorr trials, with the red trace representing the linear fit for each data set. To test whether the perturbation type or the improvement in performance had effects in the average PAs, between the manifolds of baseline and each perturbation, I used one-way and two-way ANOVA for circular data. I tested the levels of task type (VMR and DeCorr), and the performance in each set of trials. We assigned levels of performance of low ($\leq$ 30%), medium (30-60%), and high ($>$ 60%) accuracy. While I found that for one subject performance had a significant effect in the average PAs (p = 0.003, $F_{(2,31)} = 10.01$), the perturbation type did not have a significant effect for either of the subjects (p = 0.091, $F_{(1,31)} = 3.04$), and I found significant interactions between task type and performance level (p = 0.037, $F_{(1,31)} = 4.74$).

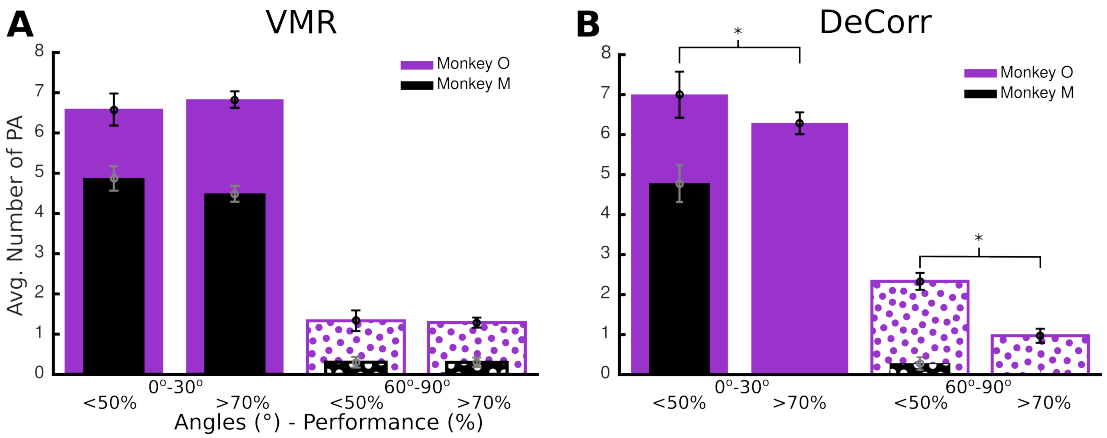

Figure 2.10: Principal Angles between baseline and perturbations. **A:** Histogram count of PA for VMR trials, for monkey O and M in purple and black color, respectively. Data shows average number of angles between 0°-30°(solid bars) and 60°-90°(dotted bars), during low performance ($< 50\%$) and high performance ($\geq 70\%$). Error bars show standard error for each data set. **B:** Histogram count of PA for DeCorr trials, monkey O and M in purple and black color, respectively. Format is the same as in panel B. (* = significant change between low and high performance, one-way ANOVA, $p < 0.01$)

2.4 Discussion

It is clear that motor learning and adaptation are captured in changes in cortical mapping of movement (Taylor *et al.*, 2002; Paz and Vaadia, 2004; Wahnoun *et al.*, 2006; Jarosiewicz *et al.*, 2008; Ganguly and Carmena, 2009; Ganguly *et al.*, 2011). Neurons can change basic tuning properties like preferred directions (Paz and Vaadia, 2004; Jarosiewicz *et al.*, 2008), and can even adapt to entirely arbitrary mappings between neural activity and motor output (Ganguly and Carmena, 2009). Here I describe findings which show that although mapping outcomes can be extremely different, part of the neural mechanism for achieving those outcomes is similar. A learning challenge acts as a perturbation to the system (He and Weber, 2002; Cai *et al.*, 2004), and that perturbation induces an increase of the overall system entropy (Cordier *et al.*, 1994), which enables the system to search a larger space for solutions

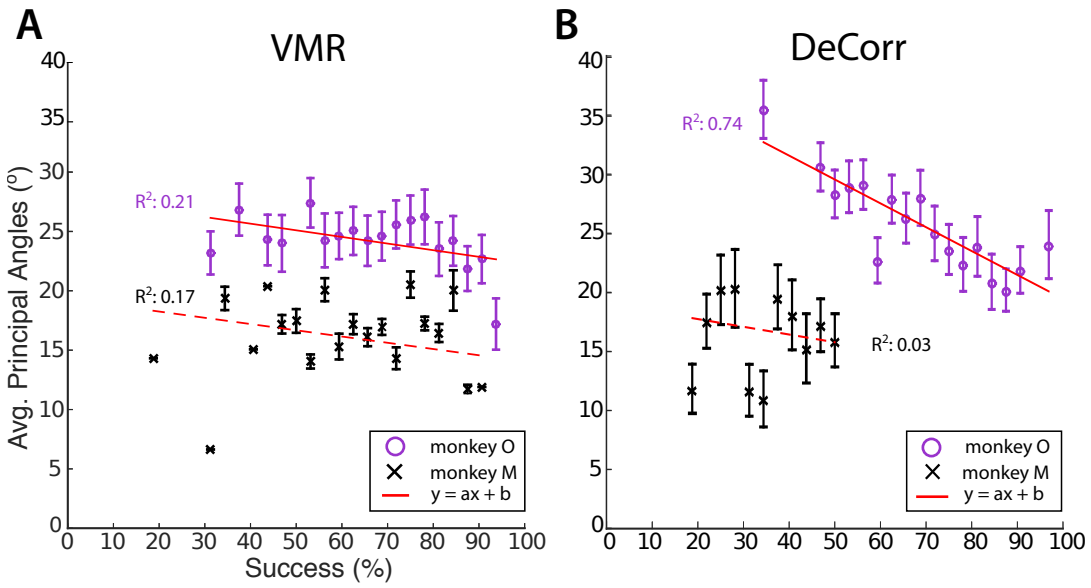

Figure 2.11: Principal angles of reduced neural manifolds in VMR and DeCorr tasks. **A:** Average principal angles between baseline and VMR trials versus percentage success, for monkey O (purple circles) and monkey M (dark cross). Error bars represent one standard deviation. Red line shows linear fit ($y = ax + b$) for each subject, with coefficients a_O = -0.056, b_O = 27.90, a_M = -0.052, b_M = 19.29. **B:** Average principal angles between baseline and DeCorr trials versus percentage success, for monkey O (purple circles) and monkey M (dark cross). Error bars show one standard deviation. Red line shows linear fits with coefficients a_O = -0.202, b_O 39.64, a_M = -0.065, b_M = 19.08.

which are almost certain to be local (Goffe *et al.*, 1994; Schollhorn *et al.*, 2009). If the perturbation has a relatively simple solution, as does the VMR task, the system may be able to identify a global solution, such as altering preferred directions by a fixed amount (see Figs. 2.7A and 2.8A). On the other hand, if the problem is more complex (e.g. non-uniform DeCorr task), the system is able to identify local solutions which may have some correlation with the ideal solution (see Fig. 2.7B and 2.8B), and thus enables the system to achieve its goals, which in this case was to place the cursor into each of eight targets.

Neural adaptations and correlates are described here during two very distinct motor learning paradigms: a uniform VMR perturbation, which induced expected errors

in movement and behavior (Krakauer *et al.*, 2000; Paz and Vaadia, 2004; Jarosiewicz *et al.*, 2008), and a non-uniform DeCorr task, which generated bigger and more random errors in the behavior (Sadtler *et al.*, 2014) (see Fig. 2.5). This chapter's major findings indicate important similarities in the mechanisms that allow subjects to reach the solutions for each task. The neural signals display a population wide adaptation to both tasks (Figs. 2.6, 2.7, 2.8 and 2.9), which implies there is a global response to both perturbations, and eventual global or local solutions are found for the tasks (Figs. 2.7 and 2.8). I also measured transient changes in the tuning properties of the neural signals, and found that success rate had a more significant effect in these dynamic changes than the type of perturbation (Figs. 2.6 and 2.10). This suggests that learning might be encoded in these transient variations in individual tuning, and agrees with recent findings that motor cortical activity modulates with both movement direction and previous trial success or failure (Yuan *et al.*, 2014).

2.4.1 Directional tuning changes during learning

I found significant correlations between task performance and changes in the aPDs of both tasks (Fig. 2.6). When subjects learn a task, or try to solve a novel problem, there is often an increase in global entropy in systems, and an eventual reduction in this uncertainty as learning progresses (Cordier *et al.*, 1994; Schollhorn *et al.*, 2009; Suminski *et al.*, 2010). The transient changes in aPDs that we observed appears to mirror those changes in entropy, which suggests an exploratory strategy that the brain engages in when trying to solve challenges posed by a novel task.

Each of the tasks could be solved in principle if the subjects were able to solve the credit assignment problems offered by the two perturbations. In order to verify whether the subjects were able to solve the credit assignment problems, we measured the final changes in aPDs from baseline, as shown in Figs. 2.7 and 2.8. In the

VMR task, the preferred directions yielded expected shifts across the entire neuronal ensemble (Figs. 2.7A, 2.8A, 2.7C, 2.8C), which would correspond to solving the credit assignment problem. However, this was a global perturbation, and the solution could be obtained with a simple global solution, which is simply for the structures which drive motor cortex to change their control of the output, thus providing an accurate solution to the rotation. To verify this, I also measured possible re-aiming strategies using the latent target calculation developed by Chase *et al.* (2010), which can estimate new target directions that better explain the firing rate changes in the recorded neurons. Using this algorithm, I found that changes in firing properties during VMR trials were indeed explained by re-aiming strategies, where the new targets were on average shifted 30° in the opposite direction of the VMR (mean test for circular data, $p < 0.05$; Zar, 1996).

In the DeCorr task, on the other hand, such a simple global solution was not possible. The only "correct" solution would be to identify those few neurons for which I had altered the cPDs, and change the system to use those neurons with their new assigned preferred directions. Instead, the entire population had aPD shifts during the DeCorr task, without the uniformity we observed in the VMR case (Figs. 2.7B and 2.8B). This non-uniformity was expected, since the task itself was designed to disrupt the neuronal dynamics in a non-uniform manner. However, I did not observed adaptation only on specific subsets of neurons, but rather compensations distributed across the entire neuronal ensemble. I observed a larger shift in the aPDs of the rotated neurons during the DeCorr task ($\mu = 56.72°$), when compared to the non-rotated sub-population ($\mu = 29.69°$), as shown in Figs. 2.7D and 2.8D. However if I measured the shift in the rotated neurons only in direction of the perturbed cPDs, we observed a smaller and non-significant shift ($\mu = 33.6°$) in the aPDs. In other words, while the perturbed cells did have larger aPD shifts, those shifts were not

uniformly in the directions required to compensate for the DeCorr perturbation as would be expected if the brain was solving the credit assignment problem (Paz and Vaadia, 2004; Jarosiewicz *et al.*, 2008). This points to a distributed and non-uniform ensemble adaptation rather than a selective one. Finally, although the DeCorr perturbation improved the uniformity of the cPD distribution, this did not translate to an immediate improvement in performance.

2.4.2 Changes in population dynamics correlate to task improvement

As shown in Fig. 2.9, I found that cross-correlation coefficients did vary between baseline and each task, but these changes were not consistent across the different sessions and subjects, and I did not measure any significant differences between the rotated and non-rotated pairs in the behavior of their cross correlations. These results suggest that the changes in neural dynamics were more dependent on the stage of the learning process than on the type of task the neural system was trying to solve.

In addition to changes in preferred directions or cross correlations, it is possible that wider changes could be observed in the underlying space of the neural representations of the tasks. It is conceivable that a change in the neural space would not be directly reflected in changes in aPDs, and so I estimated reduced neural spaces for the tasks and tasks states. In order to further characterize changes in neural dynamics during learning of both tasks, I measured the principal angles between these subspaces during baseline and each perturbation. In Figure 2.10 I showed that during VMR trials, there were few significant differences in either intersecting axes (small PAs), or axes indicating independent spatial dimensions (large PAs). On the other hand, in the DeCorr perturbation, I found a shift from small to large PAs, indicating that the system was operating in a separate neural subspace. Thus, the DeCorr task required larger changes in the intrinsic manifold of the neural signals. If more neuron

pairs were rotated, it might be possible to measure larger changes in the manifolds of baseline and perturbed tasks, although the subjects would need more time to bring performance back to baseline.

On the other hand, I found that task improvement had a stronger effect in the average PAs between these subspaces (see Fig. 2.11). While I expected to find very distinct ranges in the PAs of the two tasks, it was surprising to see that as performance in the perturbation tasks improved the average PAs of both tasks steadily decreased, and eventually fell in the same range. Once subjects adapted the neural system returned to a manifold that was similar to that in the baseline condition.

As Sadtler *et al.* and Ranganathan *et al.* have already shown, there might be some internal constraints in the neuronal ensemble that make it more or less likely for a subject to become proficient at a task. This chapter's results suggest that indeed there are certain limitations as to how much can we ask the neuronal population to change its internal mapping or dynamics. Keeping a stable map across several days allows subjects to adapt and learn new and complicated mappings between neuronal activity and desired output. However, this certainly does not seem to be enough to alter underlying functional relationships across different neural units, at least not for the long term as is shown in our results (Figs. 2.6 and 2.10).

The similarities between the two tasks and the analogous neural changes during learning give evidence that the neural circuitry engaged similar strategies when adapting to each task, even though the "correct" solution is quite different between the tasks. The results also suggest that underlying functional connections between neural units are not easily decoupled, so it is understandable that a task that requires this from the system will take longer to learn.

Overall, the results show that the brain uses similar strategies to solve strikingly different tasks. It remains unclear whether these similarities in the adaptation process

might interfere with learning, or if subjects will still be able to perform the tasks when alternating between perturbations within a single session, as suggested by Ganguly and Carmena (2009). Similarly, these results indicate that system wide changes are responsible for task adaptation, so these processes should be measured in tasks that allow the exploration of neural ensembles as a modular system. Experiments like the ones described in here can provide better information about dynamic adaptations in neural systems and reveal limitations to the challenges the brain can solve.

Chapter 3

NEURAL TRAJECTORIES IN REDUCED NEURAL SPACES CORRELATE TO DIFFERENT TASK STATES

Initial results and figures of this work have been presented in Armenta Salas and Helms Tillery (2015). The following chapter will use the neural data from the experiments described in chapter 2.

3.1 Introduction

Motor adaptation and skill learning bring forth challenges of planing, execution and evaluation. All these stages require the brain to orchestrate the activity of multiple cortical areas, muscles and feedback sensory signals (Wolpert *et al.*, 1995; Scott, 2004; Koralek *et al.*, 2013; Wolpert *et al.*, 2011). Motor adaptation further requires these neural systems to overcome challenges of redundancy, synchronization and optimization (Wolpert *et al.*, 2011; So *et al.*, 2012a; Koralek *et al.*, 2013). I am interested in how the neural circuitry might use different strategies to overcome these challenges, and evaluate whether these strategies can be measured through novel techniques that simplify analysis of the measured neural signals.

Motor skill learning has been related to growth and reorganization of synapses in motor cortex (Nudo *et al.*, 1996; Kleim *et al.*, 1998, 2004), changes in activity of cortical areas, which correlates to both movements, to error correction and rewards (Jueptner *et al.*, 1997; Doya, 1999, 2000; Koralek *et al.*, 2010, 2012), and properties of the underlying circuitry that might control these signals (Braun *et al.*, 2009b; Ranganathan *et al.*, 2014; Sadtler *et al.*, 2014). These last studies have taken advantage

of algorithms that reduce the number of variables in the neural space, in order to simplify the study and the understanding of neural and behavioral data, and have found strong correlations between the new low dimensional space and task parameters. For example, non-human primates (NHPs) were able to control the movement of a computer cursor using these latent dimensions instead of directly modulating individual neural activity (Sadtler *et al.*, 2014). Furthermore, it was recently suggested that overlapping and redundancy in these simplified spaces can relate to learning interference and task facilitation (Ranganathan *et al.*, 2014).

Former studies with dimensionality reduction algorithms and population level analysis have helped identify key differences in planning and execution stages of motor tasks. Studies with the uncontrolled manifold (UCM), a motor control hypothesis which identifies important variables for task functionality (Scholz and Schoner, 1999), have suggested that motor systems pay closer attention to joint angles and muscle movements that will have a direct effect on the task, and allows for more variability in those that do not directly affect task performance (Scholz and Schoner, 1999; Domkin *et al.*, 2005). Similarly, null space approaches, that methods which identify the input variable space which does not affect task output, allow the identification of control signals which can facilitate or interfere skill acquisition (Mosier *et al.*, 2005; Ranganathan *et al.*, 2014). Coupled with brain-machine interfaces (BMIs) recordings, these new neural spaces have shown to include information of execution and planning of motor tasks, even though these relationships cannot be clearly measured from the initial raw neural signals (Churchland *et al.*, 2012; Kaufman *et al.*, 2014). Studies in these lower dimension spaces also captures prominent covariability in the data, and identify cross-talk across different recording channels that may cloud any other analysis in the data (Yu *et al.*, 2009).

It has become more clear that system level analysis can provide better insight of how the brain solves different tasks (Braun *et al.*, 2009b; Kaufman *et al.*, 2014; Ranganathan *et al.*, 2014), and the type of changes that happen across several cortical areas during these adaptations (Hikosaka *et al.*, 1999; Addou *et al.*, 2014; Okun *et al.*, 2015). These tools can be used to analyze large data samples, like those that come from the recent advancements in neural recording interfaces, and have even been used as input for decoding algorithms in BMI controlled systems (Sadtler *et al.*, 2014). We can still use these tools to explore the differences in brain states during these BMI controlled tasks, the transition between different tasks, and the adaptation processes that take place across the neural circuitry during motor learning.

Although it has been shown that different stages of a motor task can be differently represented in the trajectories of reduced neural spaces (Kaufman *et al.*, 2014), these states have not been described in the context of a purely brain controlled task, they have mostly been studied with overt movements. It is unclear whether these new neural spaces provide similar representations for these brain controlled tasks, and whether or not the new neural trajectories will provide information about different task types and stages (e.g. calibration, active control, perturbations, etc.). There is also little evidence whether these latent dimensions might help track changes in brain states and parameters during motor learning and adaptation.

In this chapter, I will try to address the first questions, regarding task state representation. I will study the neural signals from the BMI-controlled task discussed in chapter 2, and identify the possible neural states during passive task observation, active brain control, resting activity, and inter-trial periods. Using dimensionality reduction techniques to explore different methods that might help dissect the variability of the neural data, and identify how these different behavioral states are represented in these latent neural dimensions.

I hypothesize that, similar to overt movement cases, the brain will allow for increased variability during states where the output is not as important (e.g. inter-trial period, pre-movement epochs) or when it is exploring for new solutions for a credit assignment problem (e.g. motor learning), but will be constrained during states were precise output is required (i.e. during skillful active brain control). Also, I expect that the brain trajectories will not be as smooth as those seen during tasks with overt movements, however they will still have relevant information about the task at hand.

3.2 Methods

3.2.1 Behavioral task and neural data

The neural data collected from the experiment described in chapter 2 was used in the following analysis. The behavioral experiment is a BMI controlled task, where two NHPs performed 3D center out movements in a virtual reality (VR) monitor. The subjects were naive to the task and were only trained with a brain controlled paradigm, and did not have any prior training in task related manual 3D movements. I used the population vector algorithm (PVA) from Georgopoulos *et al.* (1986) to control the movement of the cursor in the VR monitor, using (2.1), (2.2), and (2.3).

In this Chapter, I will use the neural data from the beginning of each session (*task-off*, see Fig. 2.1), the baseline brain control task (non-perturbed trials), and the inter-trial period (see Chapter 2.2.2). The neural data correspond to days when subjects (monkey O and monkey M) were mostly adapted to the baseline task (performance $> 50\%$). Neural recordings were captured from microwire arrays (Tucker Davis Technologies Inc.) implanted over primary motor cortex and dorsal pre-motor cortex. I used a 96-channel recording system (Plexon Inc., Dallas TX) to filter, sort and record single-unit and multi-unit neural signals (see Chapter 2.2.1).

For the *task-off* data, the neural signals were parsed in segments of ten seconds, and were considered as separate trials, as this was the average duration of the calibration and the active baseline control trials. Data from baseline and calibration were grouped per target. I used the raw spike count data stored at each different stage, and used the methods described below to calculate the firing rate and latent dimensions of the neurons used during active brain control.

3.2.2 Dimensionality reduction algorithms in neural data

I used two different algorithms to reduce the high-dimensional neural space (n > 25) to a low dimensional space (n < 10). I will compare the different characteristics that each dimensionality reduction method is able to capture from the neural data given four different task stages: task-off, active baseline brain control, inter-trial intervals (ITI), and calibration.

Factor Analysis

The expectation-maximization algorithm (EM) was first developed by Dempster *et al.* (1977), as a tool to deal with incomplete data sets or estimate unobservable variables from observable measurements. His work was further expanded by Rubin and Thayer (1982), who applied this maximum likelihood algorithm to Factor Analysis (FA), which is a statistical tool used to explain the variability of data with new unobservable factors. It assumes that the covariance relationship of a data set with p variables can be explained, almost completely, by q unobservable *factors*, given that $q < p$. The EM algorithm provides an estimate of the unobservable or latent variables and, more specifically, of how each observable variable relates to the latent factors.

The methods developed by Rubin and Thayer were more recently modified and applied to neural systems by Yu *et al.* (2009). They considered a system where

neurons are recorded, $y \in \mathbb{R}^{p\times 1}$, and assumed that the activity of these neurons are influenced by unobservable factors $z \in \mathbb{R}^{q\times 1}$, where $q < p$. The activity of the recorded neurons has the conditional probability distribution given by (3.1).

$$y \mid z \sim \mathcal{N}(\mu + \Lambda z, \Psi), \tag{3.1}$$

where y represents the standardized firing activity of the recorded neurons, and z the unobservable latent factors. The firing of the neurons is conditional of the activity of the latent factors following a normal distribution, with mean $\mu + \Lambda z$, and a covariance Ψ. Only the diagonal of the matrix Ψ is considered, which has the variance of each neuron's firing rate. The matrix $\Lambda \in \mathbb{R}^{p\times q}$ has the coefficients or loadings which relate the recorded neurons with the latent factors, these loadings are referred as the intrinsic manifold, represented in the column space of Λ. The latent factors z were taken to follow (3.2):

$$z \sim N(0, I), \tag{3.2}$$

which states that the unobservable factors z will also follow a Normal distribution with zero mean, and identity covariance matrix.

Yu *et al.* and Rubin and Thayer standardized the firing activity of the neurons, so that the μ term would equal zero, and the the Λ and Ψ could be estimated using the EM algorithm (see Chapter 3.2.2).

Expectation-Maximization Algorithm

The EM algorithm is a tool used to calculate the maximum likelihood of data sets that are incomplete or when the desired variables can not be directly measured (i.e. they are unobservable). The problem arises when trying to solve the maximum likelihood

of these variables, we find that it is necessary to have the complete data set likelihood function, which involves the known variables $\mathcal{Y}$, the unknown parameters Θ, and the unobservable variables $\mathcal{Z}$. The EM algorithm bypasses this problem by iteratively solving the following two steps:

1. **Expectation step (E-step):** generates a function $Q(\Theta|\Theta^{t-1})$ for the expected value of the log-likelihood function at the current time step, evaluated with the most current estimate of the parameters Θ^{t-1}, as shown in (3.3):

$$Q\left(\Theta|\Theta^{t-1}\right) = E_{\mathcal{Z}|\mathcal{Y},\Theta^{t-1}}\left[\log L\left(\Theta;\mathcal{Y},\mathcal{Z}\right)\right]. \tag{3.3}$$

2. **Maximization step (M-step):** computes parameters Θ that maximize the expected log-likelihood function $Q(\Theta|\Theta^{t-1})$ found in the E-step. That is, it finds (3.4):

$$\Theta^t = \arg\max_{\Theta} Q\left(\Theta|\Theta^{t-1}\right) \tag{3.4}$$

The algorithm repeats the E- and M-steps until the parameter values converge (e.g. error $\leq 1^{-8}$). For a more detailed description of the EM algorithm and its application to solve FA problems, refer to the Appendix C.

Principal Component Analysis: Basis Changes

Another commonly used method to analyze neural data is principal component analysis or PCA, which is a dimensionality reduction multivariate regression tool that captures the variance in data with large set of variables p with a lower number of q principal components. These components provide a new basis for the data, and represent the dimensions of maximum variability. They follow the direction of the eigenvectors of the covariance matrix of the measurements, these eigenvectors are normalized and orthogonalized, and the variability due to a specific component will be proportional to its corresponding eigenvalue.

PCA assumes that the new basis will have a linear relationship with the measurement basis, so the principal component can be defined as a linear combination of them. It also considers that data points with low variability are essentially noise. If there are any non-linearities in the relationships of our measurement basis, then PCA will inadequately express the data with the reduced dimensions. Since PCA generates linearly uncorrelated variables that will represent the new principal components.

PCA will provide relevant results if we consider that only a few neural signals will have task relevant information, and it will generate components that maximize the variance of the neural data. FA, on the other hand, will provide information about underlying latent factors that maximize the covariance among the observable signals. FA can also assume observation noise, whereas PCA does not, these assumptions can better explain neural firing activity variability (Cowley *et al.*, 2013).

DataHigh Toolbox

Cowley *et al.* (2013) consolidated different dimensionality reduction algorithms (e.g. FA, PCA, Gaussian-process FA, etc.) to generate a MATLAB (The Mathworks Inc.) toolbox which allows researches to use these dimensionality reduction techniques on neural data, and to visualize these high-dimensional data in a more helpful way. I used functions from this toolbox, and those provided by (Yu, 2013) to perform cross-validation of data sets, and reduce the dimensions of our neural data ($n = 8$), following the format indicated by Cowley *et al.*, and performed PCA and FA reduction using the adapted code from Ghahramani (1996).

Figure 3.1 shows the expected relationships between the neural signals and a latent manifold, for the case of FA, and displays how these algorithms can simplify the study of the neural signals. Each data set in the experiment will have a high dimension ($n > 25$) neural space that will change across time, and across the different trials (left

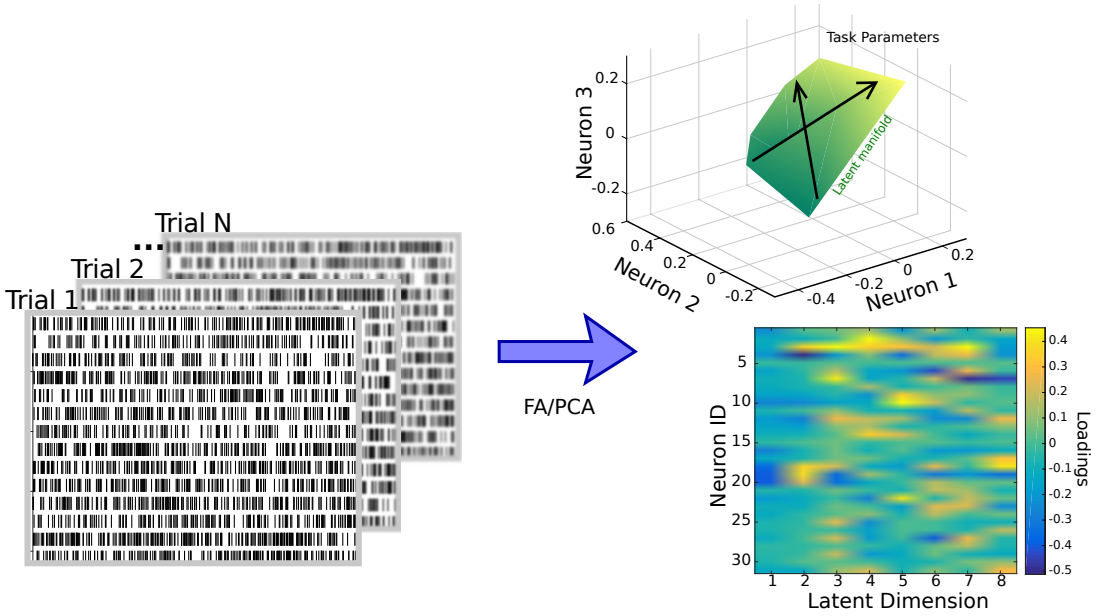

Figure 3.1: Diagram of Dimension Reduction Procedure in Neural Data: from a given data set of n neurons, and N trials of different time lengths, a latent manifold can be estimated (right 3D plot, green surface), which relates to the firing activity of the neurons (heatmap loading matrix), and traces task related information (black arrows).

side spike rasters). A latent manifold can be estimated, where each neuron linearly relates with the manifold (bottom right heatmap), and the different task parameters and conditions can still be projected and traced in this new reduced dimensions space (top right plot). The loadings matrix can also help identify cross-talk between recording channels, for example when one or two channels are the only contributors of a latent dimension (e.g. the first and second dimensions on the map).

3.2.3 Comparison of neural trajectories and firing rates

After estimating the latent factors during each task state, and the corresponding average neural trajectories in these new reduced dimensions, I measured how much each trajectory spread in the neural space. In order to do this, I measured the convex hull of the trajectories in the first three principal components or latent factors, which

explained 65% or more of the data variability (or covariability). I compared the volume of each convex hull in each state across several days, and performed analysis of variance to check if any of the task states had any significant effect in the trajectories volume.

As a next measure to compare the changes of the trajectories in the reduced space, I estimated the information in these paths in the first three dimensions. I considered the neural trajectories as three dimensional curves, and computed the entropy of these curves using (3.5)(Balestrino *et al.*, 2008).

$$H\left(\Gamma\right) = \log_2\left(\frac{2L}{d}\right), \tag{3.5}$$

where the entropy H of the plane curve Γ is described as the logarithm of the length of the plane curve (L), and the diameter (d) of the smallest hypersphere that covers the curve Γ. This diameter can be found by determining the minimum covering sphere of the convex hull polygon, I used Semechko (2014) MATLAB function from the MinBoundSuite to estimate the sphere radius. Figure 3.2 illustrates the procedure to determine the convex polygon, its volume, and the minimum diameter of the sphere that encloses the curve. The entropy measurement can be further normalized by (3.6), where N is the number of segments in the plane curve Γ (Balestrino *et al.*, 2008):

$$H = \frac{\log\left(Ld\right)}{\log\left(N-1\right)}. \tag{3.6}$$

Firing Rate and Population Vector Estimation

From the average activity of each target and condition, I estimated a single manifold for each session of the experiment, and then used the first three factors (or principal components) of the model (loading matrix Λ) to estimate the average neuron firing

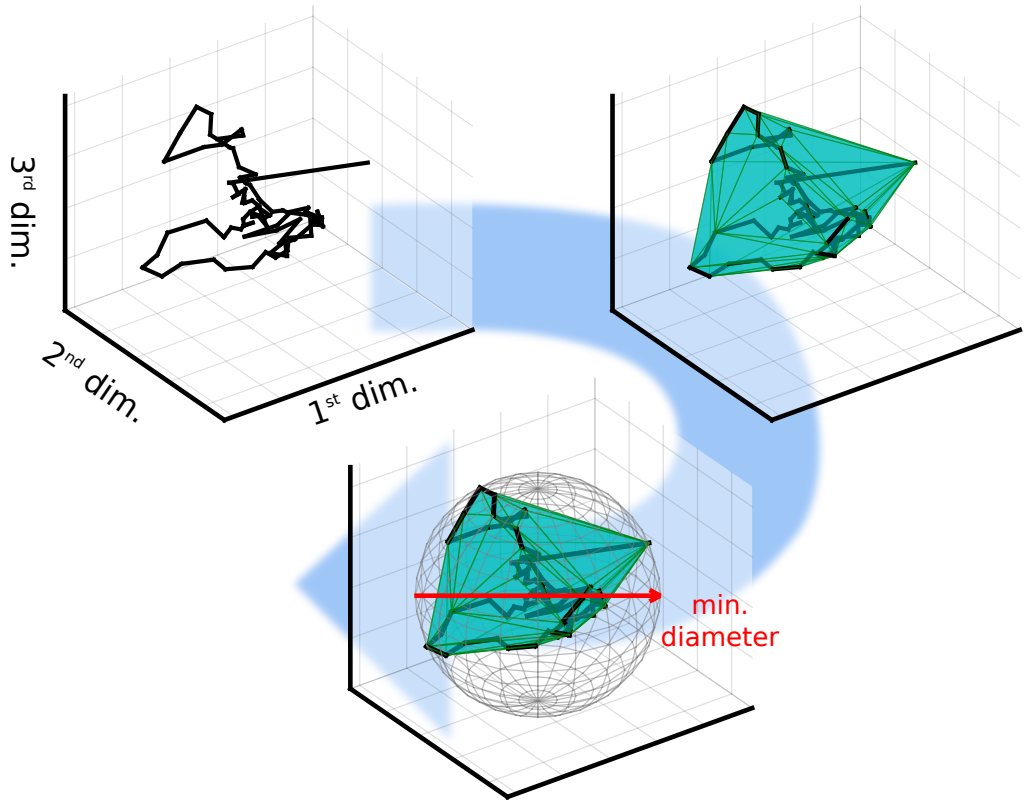

Figure 3.2: Convex Hull and Hypersphere Diameter. From an initial plane curve (neural trajectory in black), you estimate the minimum convex polygon that encloses this curve (top right plot), from this polygon we determine the minimum diameter that generates a sphere which encloses the polygon and plane curve (bottom plot).

rate from the neural trajectories. Using the same task parameters and preferred directions, I re-estimated the population vector using the modified PVA equation shown in (2.2), and estimated the average target direction during each trial.

For calibration and baseline data, I also measured the angle between the estimated vectors and the actual target direction, and calculated a 95% confidence interval cone to determine if the estimated PV pointed in the direction of the target.

3.3 Results

Using data across the different states for each day (calibration, task-off, baseline and ITI), I estimated the underlying manifold from the neural activity of the neurons used to control the movement of the cursor. For the purpose of this chapter, I will focus on data from successful trials. In chapter 4 I will discuss the variations as subjects learned the tasks described in chapter 2.

I used the FA (Ghahramani, 1996) and the PCA (The Mathworks, Inc.) algorithms to estimate underlying factors and principal components, with distinct conditions for each target location during baseline control and calibration, and for the pooled ITI and the task-off data. This allowed me to calculate a single manifold common across all the conditions. Neurons that did not have an average firing rate of at least 1 Hz were removed from the data set, as well as those channels that displayed cross-talk (i.e. when two or three recording channels were the sole contributors of a latent dimension or principal component). In order to estimate average trajectories across the different conditions, I averaged the firing activity of all the trials for each condition. The following results will show the data of these averaged trajectories.

3.3.1 Neural trajectories vary during brain control states

Figure 3.3 illustrates exemplar neural trajectories for a single subject in the top three latent dimensions estimated with FA, which explain 97.3% of the average data covariability across all conditions. The left side plots show the trajectories for the ITI (dark gray), the task-off (light gray), the baseline (top left, colored traces), and the calibration (bottom left, colored traces) trials. The right side plots show a more detailed view of the traces during baseline (top) and calibration (bottom) for four targets, each different color represents a different target location in the task space.

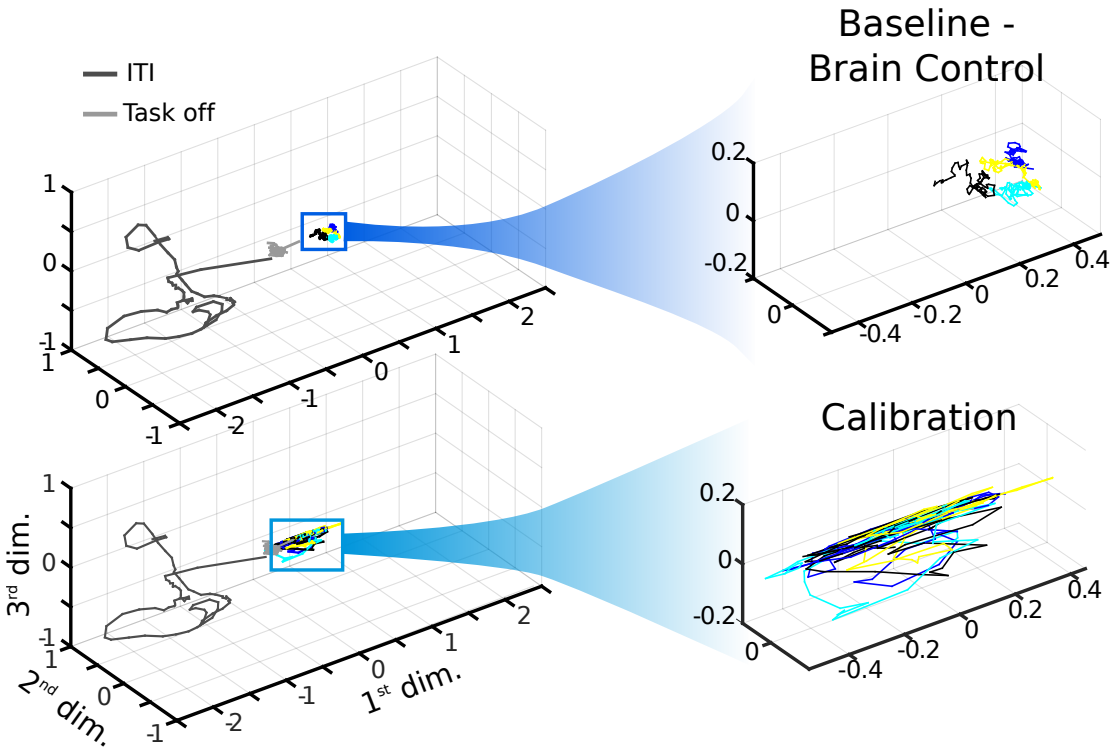

Figure 3.3: Neural Trajectories in FA Reduced Space. Left side plots display trajectories for ITI (dark gray), task-off (light gray), baseline (top panel, colored traces), and calibration (bottom panel, colored traces). Right side plots show zoomed view of baseline (top panel) and calibration (bottom panel) for four target locations.

Only four target locations are shown for ease of view. Similar trajectories and clusters were observed for the second subject (data not shown).

Figure 3.4 displays examples of neural trajectories estimated with PCA for the same session and subject. The first three components of the data explain 96.6% of the variability across all conditions. The figure follows the same format as Fig. 3.3, and the target locations displayed for baseline (top plots) and calibration (bottom plots) are also the same. We can observe there is less separation in the individual clusters of each target, but overall the trajectories show a similar trend between the FA and PCA reduced spaces: larger trajectories during ITI, small and centered trajectories during task-off, spread and overlapping trajectories for calibration, and

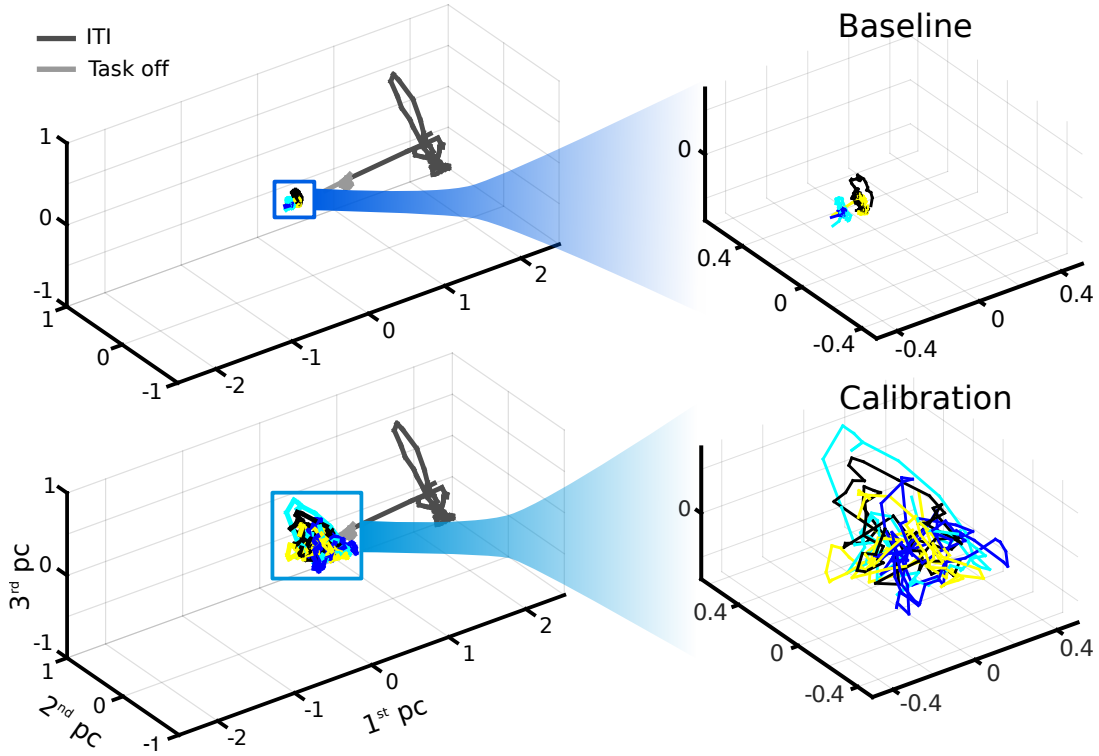

Figure 3.4: Neural Trajectories in PCA Reduced Space. Left side plots display trajectories for ITI (dark gray), task-off (light gray), baseline (top panel, colored traces), and calibration (bottom panel, colored traces). Right side plots show zoomed view of baseline (top panel) and calibration (bottom panel) for four target locations

small and separate clusters during the baseline task. The PCA trajectories did not yield individual clusters for each target location, but rather clusters of left-right or top-bottom targets.

In order to measure the variations in the reduced spaces trajectories, I estimated the convex hull polygon that enveloped the average path for each condition, I then computed the normalized entropy from these average trajectories. Figure 3.5 displays a summary of the changes in these volumes for both subjects across the different conditions. Figure 3.5A displays the average volumes and standard errors for subject O (purple) and subject M (black), of the trajectories estimated with FA. I found that the calibration and the ITI trials had the largest volumes, and the conditions

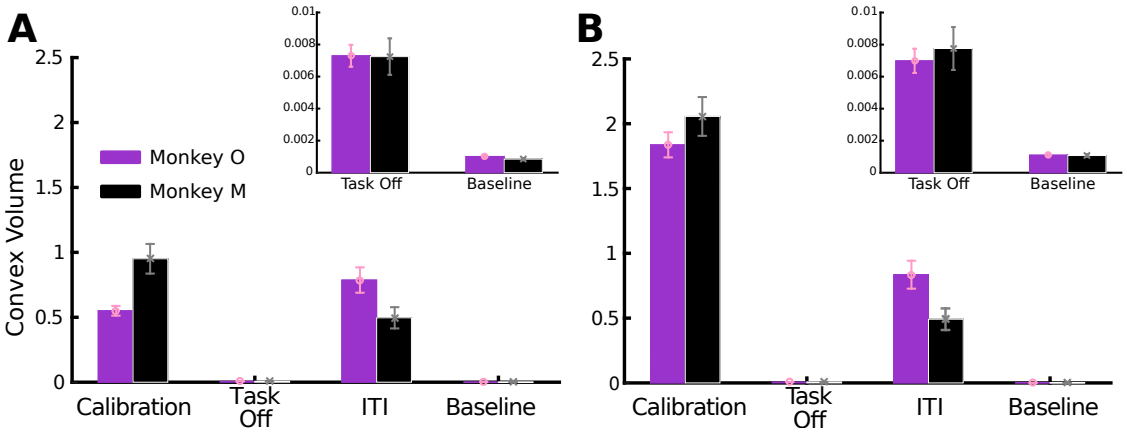

Figure 3.5: Histogram Count of Trajectories Volumes. **A:** Average trajectories volume across all task states estimated with FA algorithm for monkey O (purple) and M (black). Error bars display standard error. **B:** Average volume across all task states computed with PCA trajectories for both subjects. (* All tasks had significant difference between each other)

were significantly different between each other. The upper diagonal of Tables 3.1 and 3.2 show the results for the ANOVA test and the post-hoc multicomparison analysis with adjusted degrees of freedom using the Games-Howell test for subjects O and M, respectively. The analysis indicated that the mean volumes of calibration and ITI were indeed the largest across all the conditions, and all the conditions means were significantly different from each other. Similarly, the trajectories obtained through PCA analysis displayed larger volumes for calibration and ITI trials (see Fig. 3.5B and upper diagonal of Tables 3.1 and 3.2).

3.3.2 Information encoded in reduced neural trajectories

Using the estimated average trajectories, I computed the entropy and normalized entropy at each different task state, with both algorithms. Figure 3.6 displays a summary of the normalized entropy for monkey O (purple bars) and monkey M (black bars). Left panel A illustrates the entropy from FA, and the right panel B from PCA reduction. We found similar trends between the algorithms, where the

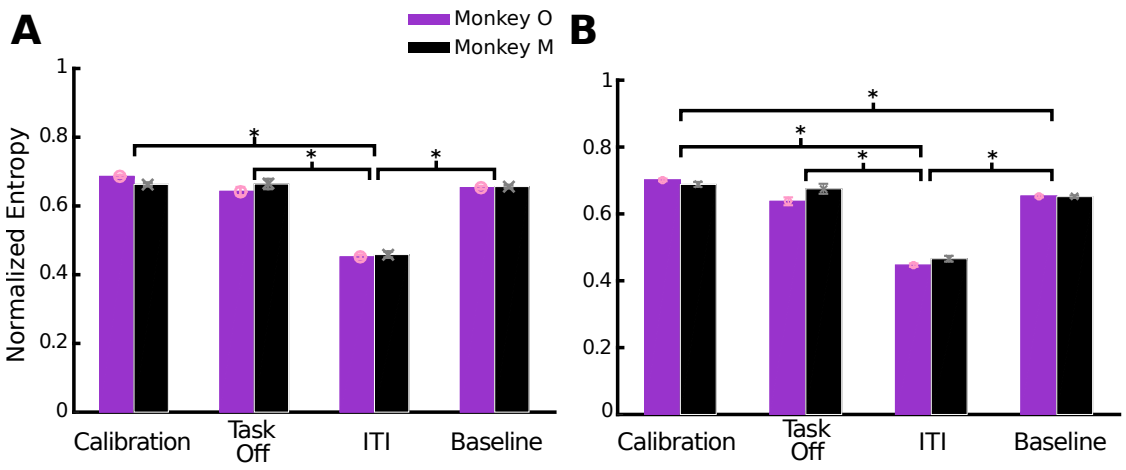

Figure 3.6: Histogram Count of Normalized Entropy. **A:** Normalized entropy across all task states of FA trajectories for monkey O (purple) and M (black). Error bars display standard error. **B:** Normalized entropy across all task states of PCA trajectories for both subjects. Asterisks indicate significant difference between means of the entropies ($p < 0.01$).

calibration trials and the task-off had the higher values for normalized entropy, and the ITI trials had the lowest amount of information. Tables 3.1 and 3.2 show, in their lower diagonal, the analysis of variance, and post-hoc p-values of the multicomparison test between the treatments. For both subjects baseline and task-off did not have any significant difference between their means, although the measurements in the task-off had slightly higher variance.

3.3.3 Population vector reconstruction

Using the same modified PVA equation 2.2, I re-estimated the population vectors and movement from the first three latent factors and principal components, using the average neural trajectories across the calibration, baseline and ITI states. The movement reconstruction did not follow the original movements during baseline and calibration trials; however, the PVs followed closely the target location.

Task states	ITI	Task-off	Baseline	Calibration
ITI	–	**FA:** $F_{(3,34)}= 11.30$, $p = 0.001$. **PCA:** $F_{(3,34)}= 10.86$, $p = 0.001$.	**FA:** $F_{(3,34)}= 11.39$, $p = 0.001$. **PCA:** $F_{(3,34)}= 10.94$, $p = 0.001$.	**FA:** $F_{(3,44)}= 3.20$, $p = 0.122$. **PCA:** $F_{(3,82)}= 9.78$, $p < 0.001$.
Task-off	**FA:** $F_{(3,50)}= 20.26$, $p = 0.001$. **PCA:** $F_{(3,46)}= 20.93$, $p = 0.001$.	–	**FA:** $F_{(3,35)}= 11.97$, $p = 0.006$. **PCA:** $F_{(3,35)}= 10.98$, $p = 0.001$.	**FA:** $F_{(3,63)}= 20.53$, $p < 0.001$. **PCA:** $F_{(3,27)}= 63.0$, $p < 0.001$.
Baseline	**FA:** $F_{(3,83)}= 38.00$, $p < 0.001$ **PCA:** $F_{(3,88)}= 45.09$, $p < 0.001$.	**FA:** $F_{(3,45)}= 1.17$, $p = 0.838$. **PCA:** $F_{(3,44)}= 1.78$, $p = 0.595$.	–	**FA:** $F_{(3,63)}= 20.78$, $p < 0.001$. **PCA:** $F_{(3,27)}= 63.0$, $p < 0.001$.
Calibration	**FA:** $F_{(3,66)}= 46.00$, $p < 0.001$. **PCA:** $F_{(3,74)}= 56.30$, $p < 0.001$.	**FA:** $F_{(3,42)}= 4.88$, $p = 0.008$. **PCA:** $F_{(3,42)}= 7.22$, $p = 0.001$.	**FA:** $F_{(3,234)}= 7.57$, $p < 0.001$. **PCA:** $F_{(3,212)}= 11.98$, $p < 0.001$.	–

Table 3.1: Statistics of Volume and Entropy Measurements for Monkey O. Upper diagonal of table display one-way ANOVA statistics with adjusted degrees of freedom with Games-Howell post-hoc test, and its corresponding p-value for the volume data of the trajectories for ITI, task-off, baseline and calibration. Lower diagonal shows the results for the same test, on data from the normalized entropy of the same task states trajectories.

Task states	ITI	Task-off	Baseline	Calibration
ITI	–	**FA:** $F_{(3,19)}$= 8.45, p = 0.002. **PCA:** $F_{(3,19)}$= 8.22, p = 0.002.	**FA:** $F_{(3,19)}$= 8.56, p = 0.002. **PCA:** $F_{(3,19)}$= 8.33, p = 0.002.	**FA:** $F_{(3,58)}$= 4.58, p = 0.011. **PCA:** $F_{(3,56)}$= 12.93, p < 0.001.
Task-off	**FA:** $F_{(3,32)}$= 17.24, p = 0.001. **PCA:** $F_{(3,30)}$= 17.09, p = 0.001.	–	**FA:** $F_{(3,19)}$ = 7.94, p = 0.002. **PCA:** $F_{(3,19)}$= 7.05, p = 0.002.	**FA:** $F_{(3,39)}$= 11.68, p = 0.001. **PCA:** $F_{(3,39)}$= 19.37, p = 0.001.
Baseline	**FA:** $F_{(3,28)}$= 28.62, p = 0.001 **PCA:** $F_{(3,27)}$= 27.78, p = 0.001.	**FA:** $F_{(3,22)}$= 0.70, p = 0.960. **PCA:** $F_{(3,22)}$= 2.14, p = 0.447.	–	**FA:** $F_{(3,39)}$= 11.76, p = 0.001. **PCA:** $F_{(3,39)}$= 19.43, p = 0.001.
Calibration	**FA:** $F_{(3,37)}$ = 26.93, p = 0.001. **PCA:** $F_{(3,46)}$= 27.29, p = 0.001.	**FA:** $F_{(3,26)}$= 0.10, p = 0.999. **PCA:** $F_{(3,29)}$= 1.10, p = 0.866.	**FA:** $F_{(3,234)}$= 7.57, p < 0.001. **PCA:** $F_{(3,60)}$= 6.06, p = 0.001.	–

Table 3.2: Statistics of Volume and Entropy Measurements for Monkey M. Upper diagonal of table display one-way ANOVA statistics with adjusted degrees of freedom with Games-Howell post-hoc test, and its corresponding p-value for the volume data of the trajectories for ITI, task-off, baseline and calibration. Lower diagonal shows the results for the same test, on data from the normalized entropy of the same task states trajectories.

Figure 3.7 shows example reconstruction of PVs for baseline (left panel), calibration (middle panel) and ITI (right panel) average trajectories. Each actual target location is represented by the different colored circles (red, blue, black and green). The surfaces represent the 95% cone of confidence, estimated with each computed PV for each different target per session, the colored traces illustrate the average PV from these estimations. The average PVs and the actual target locations were converted to unitary vector for ease of view. We can observe that the baseline trajectories had an overall accurate reconstruction of the target directions, while the calibration trials only had information about top-bottom target locations.

Figure 3.8 shows the summary of correct target estimations for calibration, ITI and baseline trials for monkey O (purple bars) and monkey M (black bars). Figure 3.8A shows the average correct target locations estimated from the average trajectories from the FA. Similarly, Fig. 3.8B displays the average of the correctly estimated target locations from PCA trajectories. There was a statistically significant difference between the correct estimated target locations from FA and PCA trajectories for the ITI and the baseline trials (two-sample t-test, $p< 0.01$) for one of our subjects. While the second subject had significantly higher target location estimation with the calibration trials.

3.4 Discussion

It has been shown that as task requirements vary dynamically through an experimental session, the neural circuitry will need to encode different information during these different task epochs, whether it is planning for the next movement (Paz *et al.*, 2003; Kaufman *et al.*, 2014) or saving learning from previous perturbations (Paz *et al.*, 2003; Paz and Vaadia, 2004; Jarosiewicz *et al.*, 2008). Modulation in the neural activity can reflect these changes, and recordings from cortical areas are usually

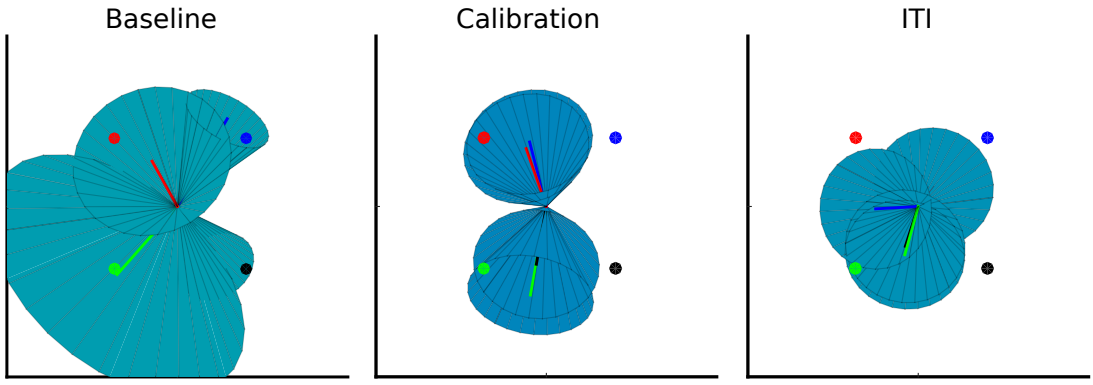

Figure 3.7: Population Vector Estimation from Reduced Dimensions. From left to right: estimations of four target locations for calibration, ITI and baseline trials. Each colored vector shows the average trajectory for each target, with their corresponding 95% cone of confidence. Same target locations are shown across all task states.

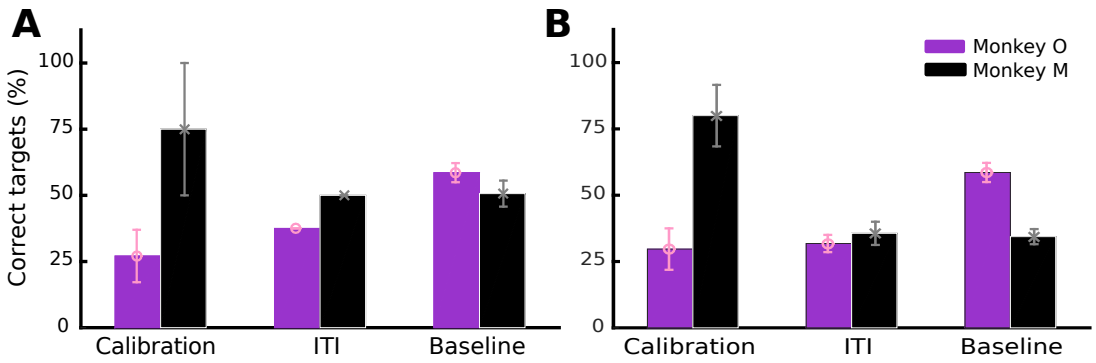

Figure 3.8: Correct Target Estimation across Task States. Average of correct target directions estimation from the population vector reconstructed with the reduced neural trajectories. Error bars show standard error. Data shown for subject O (purple bars), and subject M (black bars). **A-B:** Population vector and target location estimation from FA and PCA average trajectories, respectively.

considered to track these variations. However, some changes are not easily traceable through these direct recordings, and it might be necessary to analyze the variability and covariability of neural signals' firing activity, and the underlying connections between these signals, in order to extract valuable task related information (Churchland *et al.*, 2012). In this chapter, I have described findings which show that neural circuitry variability and covariabilty capture different states of a motor tasks, and represent them differently in the neural space.

3.4.1 Task states are represented in different regions of the reduced neural spaces

Figures 3.3 and 3.4 provide evidence that neural systems highly control signal outputs which are relevant to the task at hand, and these signals have all the necessary information to complete the task. Across the different sessions for both subjects we observed either small clusters of trajectories for each target during baseline or clusters of general target distribution (left/right or top/bottom), overlapping and larger trajectories during calibration trials, small and centered clusters for the task-off, and larger trajectories during ITIs. I found that these neural trajectories had similar representations whether they were estimated through FA or PCA; however there were significant differences in the length and volume of the trajectories during the calibration trials. Although it has been considered that FA can more closely represent neural activity, and the underlying inputs these signals receive (Yu *et al.*, 2009; Cowley *et al.*, 2013), it seems that both algorithms are able to track task epoch variations during a BMI controlled paradigm, and find similar relationships between the neural activity and the task parameters (see Figs. 3.1 and 3.2).

In addition, the volumes covered by these trajectories (both FA and PCA), and consequently the information and uncertainty in them, further indicated to significant differences across the task states (see Tables 3.1 and 3.2), which agree with the initial

assumption that task irrelevant periods or learning periods will have significantly different representations in these reduced spaces.

Scholz and Schoner (1999) and Domkin *et al.* (2005) have previously suggested, using the UCM, that motor variables which do not impact directly motor tasks have higher variability than those which directly impact task performance. In this chapter, we measured larger trajectories in the reduced spaces during states that did not have an immediate impact on task outcome (ITI state), however this did not mean that these signals had higher task related information (Fig. 3.6). Following these assumptions, we would expect to find smaller trajectories for the calibration trials, similar to what we observed during baseline trials; however, it appears that as subjects try to learn the task, the information and exploration in the neural space is actually increased (see. Figs. 3.5 and 3.6). This initial increase might correlate to the adaptation strategies the neural system uses in order to find the correct solution path for the credit assignment problem (Cordier *et al.*, 1994; Schollhorn *et al.*, 2009)

3.4.2 Neural trajectories convey final goals

In addition to describing the neural system behavior during different task epochs, I also assumed that distinct task parameters (e.g. movement direction, speed) could be tracked in the new reduced neural space. To this end, I re-estimated firing activity, population vectors and movements from the average neural trajectories with both algorithms. I found that the information in these reduced spaces allows an estimate of the intention of the subjects during the different states (see Figs. 3.7 and 3.8). The reduced spaces were better at tracking the end-goal of each trial, and did not have exact representation of point-to-point movements. These results agree with studies where subjects using signals with lower neural resolution (e.g. EEG, LFPs, ECoG) were able to better control prosthetic devices using goal-selection algorithms, rather

than process control ones (Royer and He, 2009). Furthermore, from these estimated PVs, it seems likely that subjects were still practicing the task during the ITIs (see Fig. 3.8), even though the patterns of neural activity significantly differ from baseline and calibration trials (see Figs. 3.1 and 3.2). There were no significant differences in target location reconstruction between FA and PCA trajectories, except for the calibration trials, where reconstruction was higher for the PCA trajectories (unpaired t-test, $p < 0.05$).

The results discussed in this chapter indicate that task epochs have distinct representations in the neural space, and it might be possible for subjects to switch between different neural states within a single task (Kaufman *et al.*, 2014). Although the information and uncertainty varies across these states, task parameters are still encoded in these neural trajectories, and they could be used for external device control instead of individual neural units (Sadtler *et al.*, 2014). However these type of discrete states cannot explain the overlap in neural trajectories during the calibration trials, and how they still encode target location information. Neither is it clear how subjects can eventually have individual clusters for different target locations. The next step will be to study the adaptation process in these reduced neural spaces, and measure the dynamic changes that take place across the entire neuronal population. Analysis in these reduced spaces can provide insight about the ongoing changes in the signals that control or relate to the recorded neural units.

Chapter 4

DYNAMICAL CHANGES IN REDUCED DIMENSION SPACES DURING LEARNING

Initial results and figures from this chapter have been presented in Armenta Salas and Helms Tillery (2015).

4.1 Introduction

Motor learning and, in general, problem solving requires the synchronized activity of different cortical areas, the activation of these different regions according to the learning elicited by the tasks, and the stage of the adaptation process itself (Doya, 2000; Koralek *et al.*, 2010; Addou *et al.*, 2014). It is this adaptation process that could help identify key similarities and differences between the different types of motor learning (Shmuelof and Krakauer, 2011). Some of these similarities have been recently hypothesized as part of a structural learning, which suggests that an underlying learning structure can be generated across different tasks, which will allow for faster adaptation when exposed to new but similar tasks (Braun *et al.*, 2009b; Wolpert *et al.*, 2011). For example, if you are familiar with riding a road bicycle, riding a mountain bike will not be that difficult, and the learning process will most likely be faster, and you can possibly adapt to more than one bicycle type with the same ease (Braun *et al.*, 2009b). However, the process of how the neural systems can generate such structure is still not very well defined, neither are the task characteristics which can help create this structure.

These motor learning processes can also be related to changes in overall system information and uncertainty, which appear to be a key and necessary component of this process, regardless of the learning type. For example, in some artificial systems, noise increase and task space exploration is necessary to reach the global solution, or optimize the system behavior (Rutenbar, 1989; Ingber, 1993; Chen and Aihara, 1995). Evidence of these strategies in neural systems agrees that uncertainty and noise increase in motor tasks are key components of problem solving (Cordier *et al.*, 1994; Braun *et al.*, 2009b,a; Schollhorn *et al.*, 2009), and noise augmentation might have clinical benefits which improve sensory and motor information (Rokni *et al.*, 2007; McDonnell and Ward, 2011; Medina *et al.*, 2012).

It is clear that previous experience and characteristics of the neural system can indeed facilitate or constrain the amount of adaptation and the type of skills a subject is able to learn (Cordier *et al.*, 1994; Ranganathan *et al.*, 2014; Sadtler *et al.*, 2014). The learning from these experiences can carry across several days, and might be key to overcoming some of the limitations in the neural system's first encounter (Ganguly and Carmena, 2009). However, it is not clear how much of these initial constrains can be overcome by increasing the noise and exploration in the system, similar to the simulated annealing algorithm (Rutenbar, 1989; Ingber, 1993), or whether we could facilitate learning if we artificially introduce this noise (Manjarrez *et al.*, 2007).

In this chapter, I will follow the population level analysis described in chapter 3, and address these questions, regarding the variations in system information and uncertainty as subjects adapt to new tasks, and the possible necessary changes in these neural systems for motor adaptation. I will measure the changes in the underlying structure of the neural system when it is challenged with two distinct tasks, a uniform and a non-uniform perturbation. I expect the neural system to increase task and neural space exploration when initially adapting to the tasks, with changes similar to

those observed in individual directional preferences (see Fig. 2.6 in chapter 2), and hypothesize that a similar learning process will be observed for both tasks. However, the adaptation rates at which the neural system will perform this exploration might vary according to the task structure, and the eventual task solution the subjects reach.

4.2 Methods

4.2.1 Behavioral tasks and neural data

The data used for this chapter were the same data collected in the experiments described in chapter 2. The behavioral experiment is a BMI controlled task, using recordings from primary motor and pre-motor cortex. The baseline task was a 3D center-out task, where subjects had to move a computer cursor from the center of a cube to each of the corners (see Fig 2.1). I trained two subjects (monkey O and M), and recorded neural activity using microwire arrays implanted over motor areas (M1 and PMd). I used the Plexon recording system (Plexon Inc., Dallas, TX) to filter, sort and record single and multiunit activity from these signals (for details see Chapter 2.2.2).

Two different learning challenges were introduced to the task, a uniform and a non-uniform perturbation. These perturbations intended to disrupt the system in two ways: 1) by evenly altering the relationship between the subject's movement intention and the actual movement displayed on the virtual reality screen, which was done through a visuomotor-rotation (VMR); and 2) by decoupling the activity of the neural signals when performing the task, which was done through rotations of individual neurons preferred directions (PDs). For a more detailed description of these experiments, please refer to Chapter 2.2.3.

4.2.2 Factor analysis and PCA

As described in chapter 3, I used Factor Analysis (FA) (Ghahramani, 1996; Yu *et al.*, 2009; Cowley *et al.*, 2013) and principal component analysis (PCA) algorithms to estimate underlying variables (factors) and principal components that helped described the neural data covariability and variability. These factors help decrease the number of dimension of the data set, and estimate possible control signals from the recorded neurons (Sadtler *et al.*, 2014). These same algorithms were used with neural data from the learning challenges previously described in chapter 2. Refer to chapters 3.2.2 and 3.2.2 to find more details of each algorithm. In general, FA estimates underlying variables which condition the firing rate of the measured neurons, and such factors can be found by analyzing the covariability of the recorded signals (neural units). PCA, on the other hand, will find the linear combinations of neural signals that explain the most variability in the data, creating a new basis for our system (i.e. the principal components).

I compared the similarities in the trajectories as subjects adapted to each task, and once they had adapted to them, in order to determine if the task solution was similarly represented in the reduced dimension neural space.

Similarly, I calculated the convex hull volume and entropy information of the neural trajectories in the reduced spaces using (3.5) and (3.6). These metrics were used to measure any differences in the task strategies, and changes in uncertainty of the neural trajectories. I fitted a power learning model (Wright, 1936) and double exponential learning models (Krakauer *et al.*, 1999) to estimate the learning rates of the entropy in the trajectories. I also used one-way and two-way analysis of variance to test if task type or learning state (task performance) had a significant effect in the entropy of the reduced trajectories.

4.2.3 Estimation of population vector

I re-estimated the population vector (PV) from the average trajectories for each perturbation, keeping the same preferred directions and task parameters that subjects had during active brain control, and also using the action preferred directions estimated from online control (see 2.2.5). I used the first three factors or principal components to estimate the firing rates, and reconstruct the PVs and cursor movements. Similar to chapter 3, I computed the 95% cone of confidence to determine if the estimated PVs pointed in the direction of the assigned target with the estimated manifolds from each algorithm (FA and PCA).

I also generated shuffled maps of the latent manifold, to decorrelate the contribution each neuron had in each latent dimension or principal component, and its correspondence with the preferred directions to estimate the population vector. I used these shuffled maps to estimate PVs and target locations with the same average trajectories, across the different tasks. These allowed me to generate chance levels margins of target the estimation.

4.3 Results

Using the data from unperturbed baseline, VMR and DeCorr trials for each day, I estimated the underlying manifold or principal components from the neural activity of the neurons used to control the movement of the cursor. I used data from all the trials, successful and failed, in order to measure the effect that task improvement (i.e. learning) had in these reduced neural trajectories.

I used FA (Ghahramani, 1996) and PCA (The Mathworks, Inc.) algorithms to estimate the reduced neural spaces and trajectories across the different trials. I also discarded neural units that had firing rates lower than 1 Hz, and channels that had

cross-talk between them (i.e. latent dimensions or principal components represented by 2-3 units). I estimated both the average trajectories and single trial trajectories during each condition.

Figure 4.1 shows an example of single trial and average trajectories during the VMR task for a single subject using FA reduction. The top left plot shows the baseline (black trace) and rotated (red trace) trajectories for the first trial of the first session after the VMR was introduced, the trial was a target hit. The top right panel shows the average trajectories, for the same target and the same session, of baseline trials and rotated trials. Accuracy for that target was only 25%, the majority of these failed trials (7/16) were timed out, and were on average in the direction of the target. The bottom panel shows the average trajectories for baseline (black) and rotation (red) for later sessions, for the same target, once the subject had reached 100% accuracy.

Figure 4.2 illustrates the variations in the average trajectories of baseline (black traces) and DeCorr (red traces) data for the same subject, using FA reduction. The top left panel shows single trajectories for baseline and perturbed trials, the DeCorr trial was from the first session where we introduced the DeCorr perturbation, and was a target hit. The top right plot illustrates the average trajectory during baseline and perturbation for the same target, during the first session in which the subject had reached 60% accuracy. The bottom panel shows the average trajectories for a later session for the same target, once the subject had reached 100% accuracy.

Similarly, Fig. 4.3 displays average baseline, initial and final rotated (red) trajectories for VMR and DeCorr trials using PCA, for a single subject. The sessions and targets are the same as those shown for FA (Figs. 4.1 and 4.2). The top panels show the first trial, the average trajectory after the first session (25% success), and the average trajectories of the 13th session (100% success) for the VMR task.

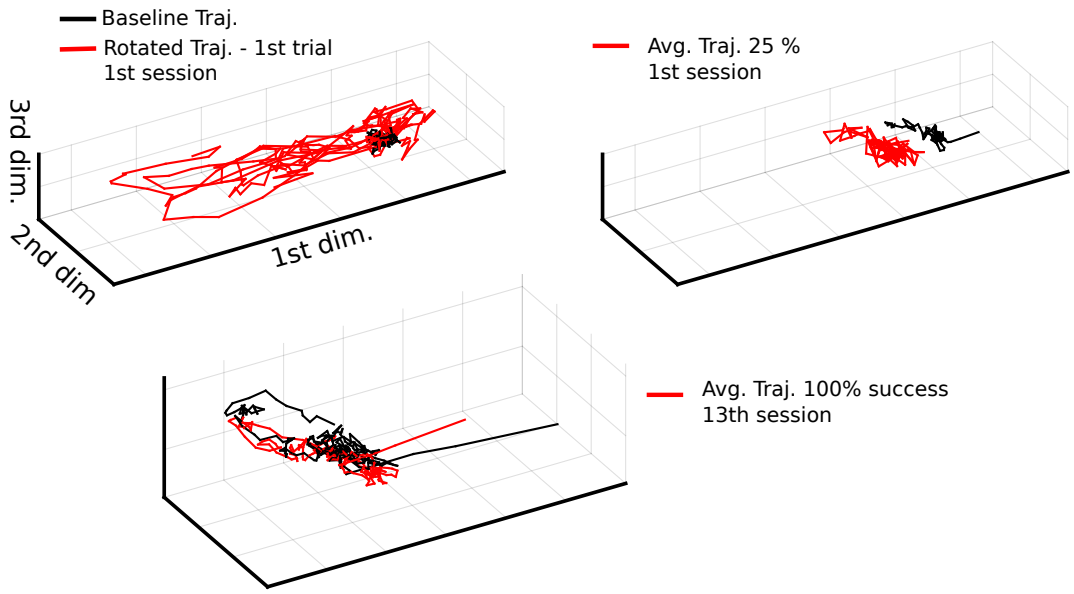

Figure 4.1: Neural Trajectories for VMR Task with FA. Top left panel shows baseline trajectory (black) and first rotated trajectory (red) for the VMR task. Top right panel displays the average baseline (black) and rotated (red) trajectories for the same target and the same session. Bottom panel shows the trajectories for the same target, and the same rotation direction, for a session where accuracy reached 100%.

The bottom panels display the first trial, the average trajectory after the first session (60% success), and the average trajectory after the 16th session (100% success) for the DeCorr task.

4.3.1 Neural trajectories volume and information during learning

In order to quantify the observed differences in the neural trajectories during task adaptation, I estimated the convex hull polygon that enveloped these trajectories, and the information encoded in them (see chapter 3.2.3).

Figure 4.4 shows the variations in the normalized entropy of the average trajectories for subject O (purple) and subject M (black), for the VMR (Fig. 4.4A) and DeCorr (Fig. 4.4B) tasks. I fitted power learning curves ($y = ax^b$, Wright

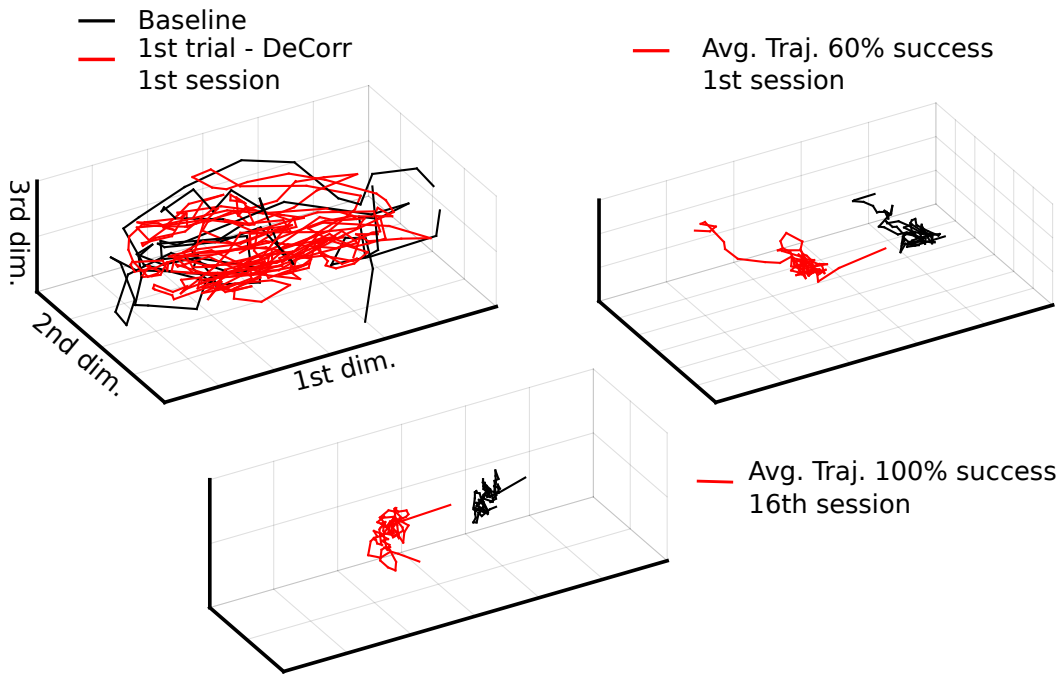

Figure 4.2: Neural Trajectories for DeCorr Task with FA. Top left panel shows baseline trajectory (black) and first rotated trajectory (red) for the DeCorr task. Top right panel displays the average baseline (black) and rotated (red) trajectories for the same target and the same session. Bottom panel shows the trajectories for the same target, and the same rotation direction, for a session where accuracy reached 100%.

(1936)) shown as the red traces in Fig. 4.4, and a double exponential learning curve ($y = ae^{bx} + ce^{dx}$, Krakauer *et al.* (1999)) for each subject. The coefficients estimated for the power curves were b_{VMR_O} = -0.25, b_{VMR_M} = -0.13, b_{DeCorr_O} = -0.09, and b_{DeCorr_M} = -0.02, which indicate a faster rate of adaptation for the VMR task (coefficient closer to negative one describes faster learning rate). The double exponential model had a better fit with most of the data, except for the DeCorr task in subject M, who did not have enough data to fit the model. The estimated coefficients for the exponential curves are reported in Table 4.1 for both FA and PCA trajectories.

Figure 4.5 displays the variations in normalized entropy of the average PCA trajectories for monkey O (purple) and M (black) for the VMR (Fig. 4.5A) and DeCorr (Fig. 4.5B) tasks. The entropies display similar behaviors as those measured in the

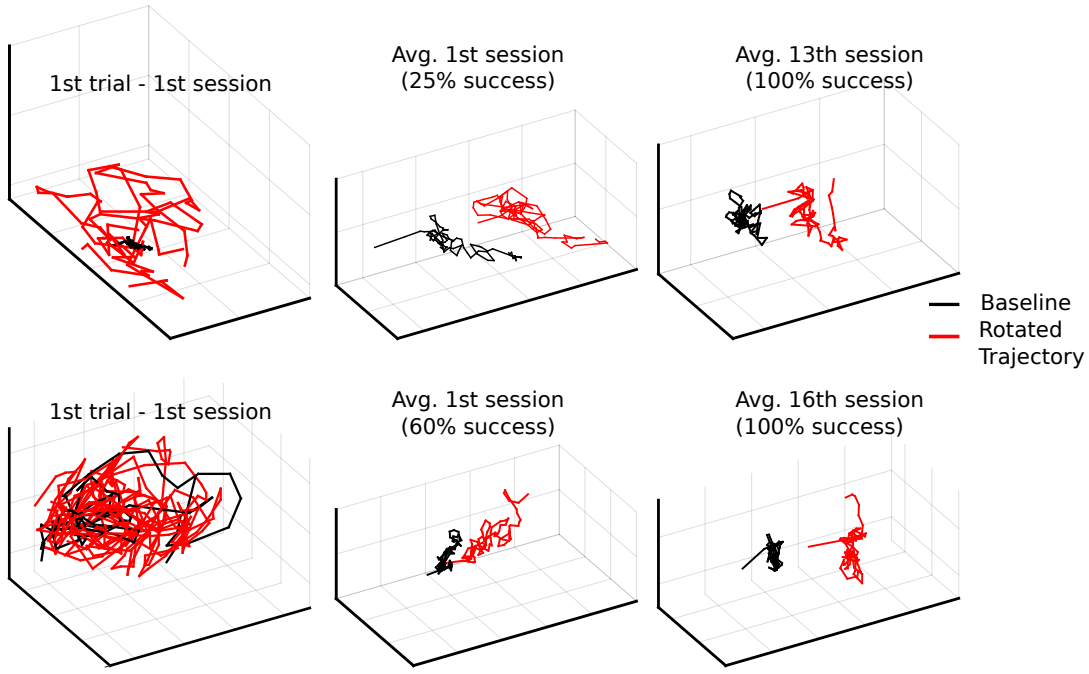

Figure 4.3: PCA Neural Trajectories of Learning Challenges. Top row displays the trajectories during the VMR task for a single target location. From left to right: first rotated trial trajectory (red) and baseline trial (black) for a single target, averages at the end of first session (25% success for that target, and averages at the end of the 13th session (100% success for that target). Bottom row displays the trajectories during DeCorr task for a single target location. Format is the same as top row: first trials for DeCorr perturbation and baseline, averages at the end of first session (60% success for that target), and averages at the end 16th session (100% success).

FA trajectories. I observed and measured similar inversely proportional relationship between the normalized entropy and task success, highlighted by the power learning curve in the plots (red traces). The coefficients estimated for the power curves were b_{VMR_O} = -0.26, b_{VMR_M} = -0.14, b_{DeCorr_O} = -0.13, and b_{DeCorr_M} = 0.05, which again suggest faster adaptation in the VMR task for both subjects. The estimated coefficients for the double exponential model are shown in Table 4.1.

Table 4.2 shows the statistical test results which compare the differences of the volume and entropy means for both subjects in the FA trajectories. We measured significant differences in the entropies of one subject, and had similar ranges for the

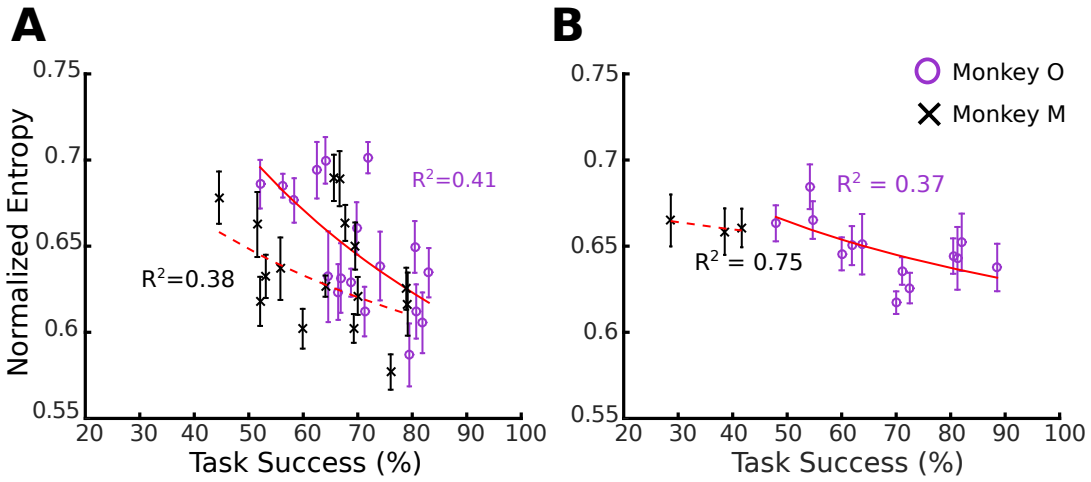

Figure 4.4: Normalized Entropy of Neural Trajectories from FA. **A:** VMR task estimations of average normalized entropy changes vs task performance for subject O (purple) and M (black). Error bars display standard error, and red traces show power function fit ($y = ax^b$). Coefficients were a_O = 1.923, b_O = -0.257, a_M = 1.082, b_M = -0.131. **B:** DeCorr task estimations of average normalized entropy for both subjects. Same format as panel A. Coefficients were a_O = 0.939, b_O = -0.088, a_M = 0.715, b_M = -0.022.

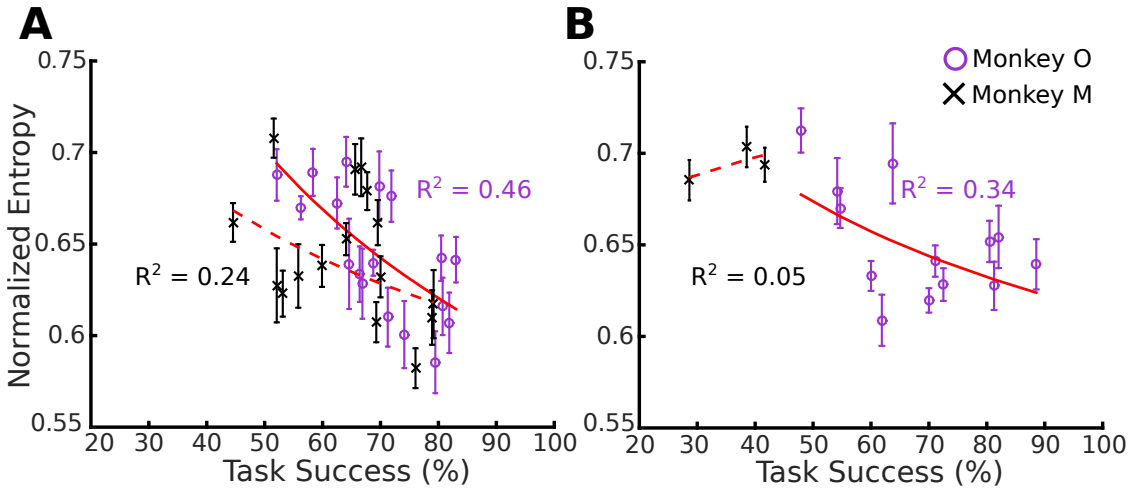

Figure 4.5: Normalized Entropy of Neural Trajectories from PCA. **A:** VMR task estimation for average normalized entropy vs task performance for subject O (purple) and M (black). Error bars display standard error, and red traces show power function fit ($y = ax^b$). Coefficients were a_O = 1.947, b_O = -0.261, a_M = 1.120, b_M = -0.136. **B:** DeCorr task estimations of average normalized entropy for both subjects, with power function fit (red trace). Coefficients were a_O = 1.138, b_O = -0.134, a_M = 0.586, b_M = 0.048.

	Subject O	Subject M
FA	a_{VMR}:1.923, b_{VMR}: -0.257 c_{VMR}: 0.272, d_{VMR}: -0.015. a_{DeCorr}: 0.007, b_{DeCorr}: 0.034 c_{DeCorr}: 0.854, d_{DeCorr}: -0.005.	a_{VMR}:0.004, b_{VMR}: -0.314 c_{VMR}: 0.676, d_{VMR}: -0.001.
PCA	a_{VMR}: 0.893, b_{VMR}: -0.004 c_{VMR}: -1.15e^5, d_{VMR}: -0.308. a_{DeCorr}: 10.04, b_{DeCorr}: -0.086 c_{DeCorr}: 0.463, d_{DeCorr}: 0.004.	a_{VMR}: 57.47, b_{VMR}: -0.014 c_{VMR}: -57.06, d_{VMR}: -0.014.

Table 4.1: Learning Curve Coefficient Estimates of PCA and FA Entropy. Coefficients for both tasks and both subjects estimated from double exponential curve ($y = ae^{bx} + ce^{dx}$).

VMR and DeCorr tasks across subjects ($\mu_{VMR_O} = 0.647$, s.d. $= 0.006$; $\mu_{DeCorr_O} = 0.647$, s.d. $= 0.006$; $\mu_{VMR_M} = 0.636$, s.d. $= 0.010$; $\mu_{DeCorr_M} = 0.661$, s.d. $= 0.010$). I measured significant differences in the normalized entropy of VMR trajectories as performance increased in both subjects, and there was an inversely proportional relationship between them (see Figs. 4.4 and 4.5). The highest mean entropy was when performance ranged between 40% and 50% in both tasks ($\mu_O = 0.685$, s.d. $= 0.027$; $\mu_M = 0.678$, s.d. $= 0.034$), and the lowest when performance was between 75% and 78% in both tasks ($\mu_O = 0.586$, s.d. $= 0.039$; $\mu_M = 0.577$, s.d. $= 0.034$). Table 4.2 displays the results of the one- and two-way ANOVA, with corrected degrees of freedom with Games-Howell post-hoc test for the trajectories calculated with FA.

Similar behaviors were measured in the volumes of the trajectories of both tasks. There was not a significant difference between the average volumes of the VMR and the DeCorr trajectories, although the latter ones had larger volumes, as calculated with Tukey's multicomparison test ($\mu_{VMR_O} = 0.254$, s.d. 0.021; $\mu_{DeCorr_O} = 0.283$, s.d. $= 0.021$; $\mu_{VMR_M} = 0.227$, s.d. $= 0.020$; $\mu_{DeCorr_M} = 0.038$, s.d. $= 0.028$). Task

	Task type (one-way ANOVA)	Task success (one-way ANOVA)	Task type and success (two-way ANOVA)
Subject O - Volume	$F_{(1,278)}$= 1.88, p = 0.17.	$F_{(12,267)}$= 3.13, p < 0.001.	**Task*Succ.:** $F_{(6,260)}$= 9.37, p < 0.001.*
Subject M - Volume	$F_{(1,158)}$= 20.85, p = 0.003.	$F_{(10,149)}$= 15.92, p < 0.001.	**
Subject O - Entropy	$F_{(1,278)}$= 0.03, p = 0.983.	$F_{(12,267)}$= 4.05, p < 0.001.	**Task*Succ.:** $F_{(6,260)}$= 2.28, p = 0.03.*
Subject M - Entropy	$F_{(1,158)}$= 5.98, p < 0.016.	$F_{(10,149)}$= 4.71, p < 0.001.	**

Table 4.2: Test Statistics of Volume and Entropy Changes of FA Trajectories. (*: Interaction effect. **: Not enough trials to test full model)

success had a significant effect in the trajectories' volumes in both tasks for both subjects.

Table 4.3 displays the statistical results for the volume and entropy comparison of the trajectories from the PCA reduction. I observed similar ranges in the entropies of the trajectories between both tasks, where a significant effect was measured for one subject (μ_{VMR_O} = 0.647, s.d. = 0.006; μ_{DeCorr_O} = 0.651, s.d. = 0.006; μ_{VMR_M} = 0.645, s.d. = 0.010; μ_{DeCorr_M} = 0.694, s.d. =0.010). Task success also had a significant effect in the PCA estimated trajectories. The highest entropy was measured when performance was between 45% and 52% in both tasks (μ_O = 0.712, s.d. = 0.039; μ_M = 0.705, s.d. = 0.033), and lowest when task success was between 75% and 78% (μ_O = 0.585, s.d. = 0.039; μ_M = 0.582, s.d. = 0.033). Again, it appears

	Task type (one-way ANOVA)	Task success (one-way ANOVA)	Task type and success (two-way ANOVA)
Subject O - Volume	$F_{(1,260)}$= 1.02, p = 0.469.	$F_{(12,267)}$= 3.21, p < 0.001.	$F_{(6,260)}$= 2.9, p < 0.001.*
Subject M - Volume	$F_{(1,108)}$= 13.66, p = 0.007.	$F_{(10,149)}$= 12.76, p < 0.001.	**
Subject O - Entropy	$F_{(1,278)}$= 0.49, p = 0.479.	$F_{(12,267)}$= 5.39, p < 0.001.	**Task*Succ.:** $F_{(6,260)}$= 2.62, p = 0.017.*
Subject M - Entropy	$F_{(1,51)}$= 9.41, p = 0.010.	$F_{(10,149)}$= 6.66, p < 0.001.	**

Table 4.3: Test Statistics of Volume and Entropy Changes of PCA Trajectories. (*: Interaction effect. **: Not enough trials to test full model)

that both dimensionality reduction algorithms are able to capture similar variations and transitions in the neural trajectories as subjects adapted to each task.

Similar to what was observed with FA trajectories, task type had a significant effect in the trajectories volume for only one subject, as shown by one-way ANOVA with corrected degrees of freedom and p-values with Games-Howell test (see Table 4.3). Task success, on the other hand, had significant effects across both subjects and both tasks, similar to what was measured in the FA trajectories.

4.3.2 Population vector and target location estimation

As a next measure of possible dynamical changes across the different tasks, I re-estimated the population vector (PV) and cursor movements with the same parameters used during online control, using (2.2), (2.3), and (2.4), and the average

trajectories in the reduced spaces calculated from FA and PCA. I used the first three dimensions of these reduced neural trajectories.

Similar to the estimated PVs and movements calculated in chapter 3, I found that the information in the average trajectories described well the final target location, but did not estimate correctly the actual movement trajectories. Figures 4.6 and 4.7 display the summary of these correctly estimated target locations from FA and PCA trajectories, for both subjects and both tasks (VMR and DeCorr). Figure 4.6 shows the correct target locations versus the task success, across all the sessions of VMR (Fig. 4.6A) and DeCorr (Fig. 4.6B), for monkey O (purple bars) and monkey M (black bars) using the FA trajectories. Error bars display standard errors, and the light gray squares show the chance level estimations calculated from the shuffled manifolds. I did not observe any trend in the average of the correctly estimated targets as subjects improved in the tasks. There was a slight increase for one subject in the DeCorr task, but could not be compared to the second subject.

Figure 4.7 displays the correct target locations versus task success for the PCA trajectories, for monkey O (purple bars) and monkey M (black bars). Figure 4.7A shows the percent correct targets for the VMR task, and Fig. 4.7B for the DeCorr task. Light gray squares show the chance level estimation with the shuffled manifolds. The estimations had a slight positive slope, directly proportional to task improvement, although it was only significant for one subject in the DeCorr task.

4.4 Discussion

Motor neural signals can vary their individual properties (Gandolfo *et al.*, 2000; Paz and Vaadia, 2004; Jarosiewicz *et al.*, 2008; Ganguly *et al.*, 2011), and even modify the relationships between them in order to adapt to new tasks (Vaadia *et al.*, 1995; Paz and Vaadia, 2004; So *et al.*, 2012b). However, these changes are usually measured at

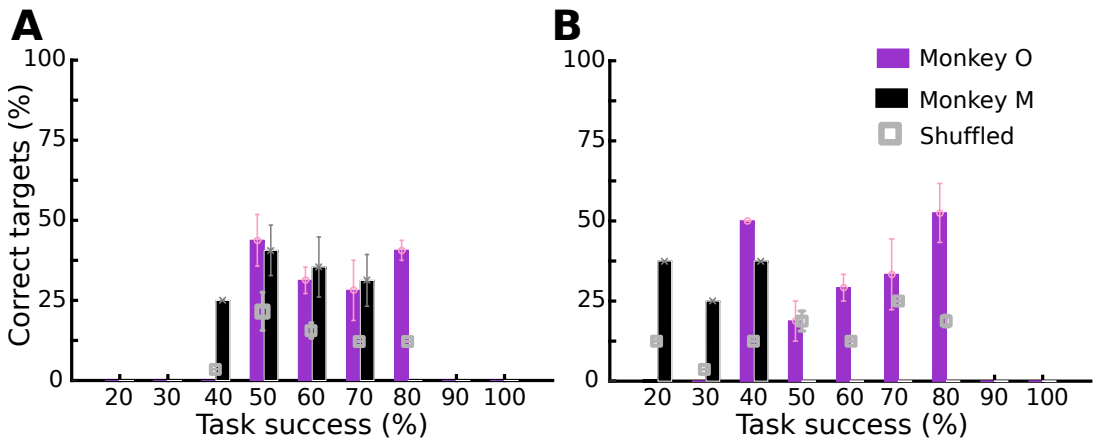

Figure 4.6: Target Location Estimation with FA Trajectories. **A:** Average of percentage correct target estimations versus task success during VMR trials for subject O (purple bars) and subject M (black bars). Pink and dark grey bars show standard error. Light gray squares and error bars show chance levels with shuffled manifolds. **B:** Average correct target estimations versus task success during DeCorr trials for both subjects (purple and black bars). Error bars show standard error, and light gray squares show chance levels with shuffeld manifolds.

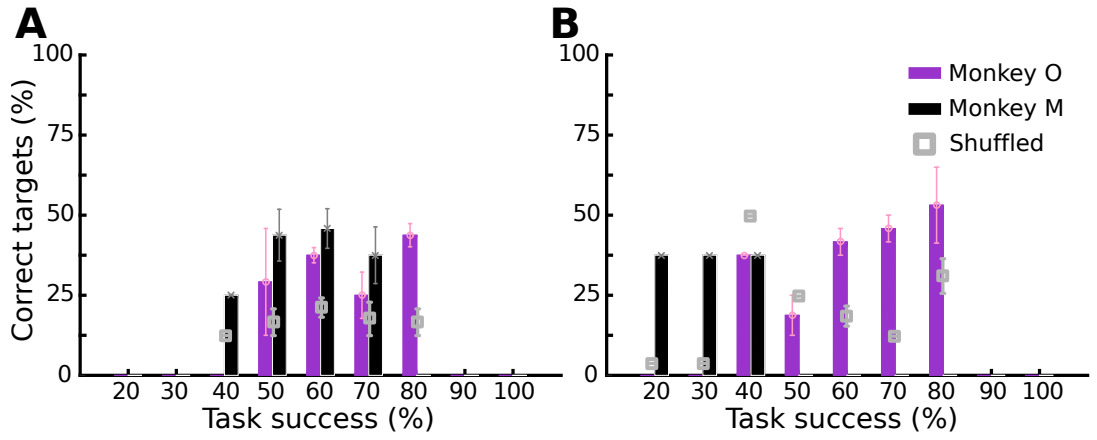

Figure 4.7: Target Location Estimation with PCA Trajectories. **A:** Average percentage correct target estimations versus task success during VMR trials for subject O (purple bars) and subject M (black bars). Same format as in Fig. 4.6. **B:** Average correct target vs. task success for DeCorr trials. Light grey square markers show chance levels with shuffled manifolds.

the end of the adaptation process, and for a single adaptation task. Moreover, it has been previously shown (Churchland *et al.*, 2012) that some properties of the neural signals can be better understood when measuring population wide adaptations, since some learning challenges may require modifications not only in the motor cortex, but also in the signals which control and connect with these neurons (Doya, 2000; Tanaka *et al.*, 2009; Koralek *et al.*, 2012). In this chapter, I report findings which highlight similarities in the dynamical changes across the neural population, and the signals which control them when adapting to two very different tasks.

It was previously shown, in chapter 2, that subjects were able to bring their performance back to baseline in both tasks, with slightly faster adaptation rates during the VMR trials (see Fig. 2.5). Moreover, I measured changes in the tuning preferences of the neural signals after subjects adapted to the tasks, but also measured transient variations in these directional preferences as subjects learned each task (see Fig. 2.6). It seems possible that the adaptation processes are actually similar between the tasks, so it might be likely that the signals controlling these recorded neurons also have similar transient changes during this adaptation process.

4.4.1 Paths and information of reduced neural trajectories during learning

The results reported in here quantify some of the variations in the neural population activity as subjects adapt to the two learning challenges (VMR and DeCorr tasks), and describe two relevant findings concerning population dynamics in motor learning. First, the process of adaptation after a perturbation in a motor-like task is similarly represented in the neural ensemble and its controlling signals, as measured by the estimated latent variables (see Figs. 4.1 and 4.2), and variations in their principal components (see Fig. 4.3). The neural trajectories had similar behaviors regardless of the underlying characteristics of the perturbation (e.g. uniform or

non-uniform). Second, this adaptation can be compared to an exploratory process, where the neural ensemble, and its corresponding control latent variables, increase the volume (or hypervolume) covered in the neural space, and the information they encode (see Figs. 4.4 and 4.5).

The information and uncertainty of these neural trajectories varies dynamically during each learning challenge, and they are more dependent on the stage of adaptation, than on the underlying task parameters (see Figs. 4.5 and 4.6, and Tables 4.2 and 4.3). The increase in the trajectories' uncertainty could be linked to the initial performance errors, although higher values were not consistently measured during the DeCorr task, which had more initial errors than VMR. So it seems likely that an increase in the neural trajectories' uncertainty is part of a general adaptation strategy. This uncertainty augmentation has been previously hypothesized as a strategy in motor systems and learning (Schollhorn *et al.*, 2009), and related to exploration-exploitation strategies identified during reinforcement learning in the basal ganglia (Ishii *et al.*, 2002; Schweighofer and Doya, 2003). Furthermore, the individual changes measured in the preferred directions (see Fig. 2.6) are mirrored by these transient changes in the reduced space neural trajectories, which indicates that these estimated latent factors might indeed account for the dynamical changes in synaptic connections which happen during motor adaptation (Kleim *et al.*, 1998, 2004).

Although the adaptation processes were similar across tasks, the final task solutions were not always similarly represented in the reduced neural spaces (see Figs. 4.1 and 4.2). I measured a bigger overlap between the baseline and VMR trajectories, than between baseline and DeCorr trials. Similar to individual neural unit changes (see chapter 2), the neural solutions differ across the tasks. Sadtler *et al.* (2014) have previously suggested that neural circuitry might have learning constraints which interfere with skill acquisition, and that subjects could not adapt to perturbations that

shifted from the space of the intrinsic manifold of the neural signals. However, our subjects were able to adapt to the DeCorr task, which might require the neural activity to shift outside this intrinsic manifold. By asking the neural system to decouple the activity of specific neural signals, it was essentially required that the signals will move from their internal or intrinsic manifold, and it seems that the subjects found a way to solve this problem. This solution is shown in the shifted representations of target locations in the reduced spaces (see Fig. 4.4). It appears that the subjects were still able to adapt to the DeCorr perturbation, even if this required a shift from the intrinsic manifold, however they had shallower adaptation rates, which were measured in the variations of the individual signals and the whole neural population (see Figs. 2.6, 4.4 and 2.5). Another key element of this adaptation was the use of the same calibration preferred directions distribution, and perturbations across several days, which allowed for learning and savings to transfer across different sessions (Ganguly and Carmena, 2009; Orsborn *et al.*, 2014).

4.4.2 Task related information did not vary with learning

Together with the estimation of the neural trajectories volume and entropy, I measured the task related information contained in them; in other words, information about neural firing activity and the target direction during each trial set. I found that task related information did not vary dynamically as subjects improved in the task (see Figs. 4.6 and 4.7), and this estimation was not improved even when using the preferred directions estimated during active brain control. It seems that even if the neural representation was doing an exploratory process, the end goal information (task location) remained constant throughout this process. These results agree with what was measured during the calibration trials (see Figs. 3.7 and 3.8), where target location was recovered even if the neural trajectories were highly variable and over-

lapped between each target, and could be used as an indication that subjects were engaged in the task, and actively trying to solve them (bring cursor to each target).

Overall, these results highlight further similarities between the adaptation process of the two tasks. There are similar variations not only in the directional preferences of individual neurons, but also in the ensemble activity, and the activity of the signals which control these neurons. These variations indicate that the neural systems might require an increase in the system noise and the neural space exploration during motor learning, in order to find the solution to learning challenges. It was also shown that the rate of this adaptation might eventually depend on task complexity, and how easily the system could arrive to a solution. For example, if the system only needs to uniformly shift directional preferences or aim towards a virtual target, the direction of the global solution could be easily found; however if several signal configurations could help solve the task (neurons re-weighing, target re-aiming, directional re-mapping, etc.), then the system might have several local solutions which are "good enough" to solve the task. Therefore, it remains to be determined if the workable solutions reached by the subjects were really the global solution to the tasks, specifically in the case of the DeCorr task, and if we can aid these neural systems during the exploratory phase. This aid could speed the adaptation rates and help the neural systems to arrive to the global solution for the task (e.g. through feedback stimulation, artificial noise increments in the system, training trials which induce the neural and task space exploration, etc.).

Chapter 5

SUMMARY AND CONCLUSIONS

The work described in this dissertation has focused in the underlying mechanisms that allow motor adaptation, studied directly with brain-machine interfaces (BMIs). In order to achieve this, a BMI controlled task was designed to track changes in neural circuitry as subjects adapted to two different tasks. These tasks introduced uniform and non-uniform perturbations to the neural system, the first through a visuomotor rotation (VMR) of the decoded movements, and the second one through a non-uniform novel decorrelation (DeCorr) task, which aimed to decouple the activity of individual neural signals. The results of these experiments, and their possible contributions to the study of motor learning and adaptation are briefly summarized below.

5.1 Neural adaptation to distinct learning challenges

It has been shown that neural systems can separately adapt to uniform perturbations in the task space (e.g. VMR, force field, movement gains), and non-uniform perturbations (e.g. subset rotation) in the neural space (Krakauer *et al.*, 2000; Paz and Vaadia, 2004; Jarosiewicz *et al.*, 2008; Krakauer, 2009). However, little work has been done to directly compare if subjects can adapt, using the same neural signals, to both of these learning challenges (Ganguly and Carmena, 2009), and compare the similarities and differences of the adaptation to these tasks. As a first step to address this, I designed two distinct learning challenges which introduced uniform and non-uniform perturbations to the neural signals (see chapter 2). In the first task, the relationships between neural signals remained the same, but we altered the re-

lationship of the final output of the population vector decoder (PVA, Georgopoulos *et al.*, 1986) and the visual feedback given to the subjects. In the second task, we altered the relationship between individual neural signals, by selectively decoupling their preferred directions (PDs), but did not alter the decoder output and the visual feedback.

By comparing movement errors and tuning changes, I was able to track whether the neural system was able to solve each task, and also track transient changes for each task as subjects adapted. I found that the adaptation rates differ between the tasks, measuring faster learning rates for VMR than for DeCorr trials in both subjects. Similarly, the movement errors varied between the tasks, showing more uniform shifts during the VMR trials than during the DeCorr trials. In addition, we did not measure significant changes in neuronal firing rates between the tasks, but we did measure significant variations in the final tuning properties of the neurons. The neuronal ensemble had population wide responses to both tasks, however the eventual solution did differ between the them (i.e. the final preferred directions matched the underlying parameters of the task).

5.1.1 Neural exploration necessary for task adaptation

When tracking the dynamical changes in the individual PDs as subjects adapted to each task, I found significant variations that were dependent on task success. In other words, the shifts in neuronal directional tuning converged as subjects became more proficient in the tasks. The rate of this convergence differ between the tasks, but both tasks displayed an inversely proportional relationship between PD's shifts and performance.

These dynamical changes hint to an increase in the neural exploration in order to successfully complete motor adaptation, for example the second subject (monkey M)

was not able to fully adapt to the DeCorr task, and we did not measure a decreasing trend in his PD shifts, and these had higher values than the shifts measured for monkey O, who did achieve higher performance.

Similarly, I found that cross-correlations, which hint to possible functional connections between signals, also had system wide responses during adaptation, and these changes also had transient variations as subjects improved performance in these tasks. However, there was not a significant difference between the responses of the rotated and non-rotated sub-populations, during the DeCorr task. Furthermore, an initial look to the estimated underlying inputs of the neural signals pointed towards significant differences between the tasks, and possible dynamical changes in these signals as well (see chapter 2). Future work will have to focus on studying these underlying connections, and systematically altering and measuring these transient changes in preferred directions correlated to task adaptation.

Regardless of the similar adaptation strategies measured across both subjects, and during both tasks, the second subject (monkey M) had a larger decrease in task performance after the perturbations were introduced, and his learning was slower than for monkey O. A possible reason of these variations would be the difference in location and amount of neural units available for control. Monkey O had bilateral implants over shoulder (96 recording channels), arm and hand representation of motor and pre-motor cortices (see chapter 2), these locations were determined before surgery, and verified with electrical micro-stimulation after implantation. Furthermore, four of the six microwire arrays were located over primary motor cortex, and we measured twitches and movement responses from cortical stimulation. On the other hand, Monkey M only had unilateral implants over the same cortices (64 recording channels), with verified twitch and movement responses over shoulder and arm regions from two of the four arrays. The rate and amount of adaptation subjects can achieve in BMI

systems differs between M1 and PMd signals (Carmena *et al.*, 2003), so the measured adaptation differences can be a result of the type of signals which were driving the movement of the cursor. However, the adaptation processes were still similar between the subjects, and both eventually adapted to the VMR task, and had comparable changes at the beginning of the adaptation for the DeCorr task.

5.2 Neural trajectories in a brain controlled task

As part of the strategies the neural systems engage when solving tasks, it is possible that the measured adaptation during learning is due to changes in the connections that the motor neural signals receive, rather than changes only in the properties of the measured signals. It is then necessary to measure not only the modulation in individual firing rate and tuning properties, but also to quantify changes in these underlying connections and their variations during task adaptation. To this end, I estimated neural trajectories that described this population level adaptation in both tasks (VMR and DeCorr). I used dimensionality reduction algorithms which allowed me to estimate the signals responsible for the covariance (possible shared connections or inputs between the neurons) and the variance (possible independent inputs to neurons) of the measured neural signals. The algorithms used (factor analysis, FA, and principal component analysis, PCA) allowed an estimate of the underlying manifold composed of these controlling inputs (see chapter 3). Using these manifolds as the new neural space, I was able to track neural trajectories for the different learning challenges and unperturbed baseline trials, and also estimate neural trajectories during different task epochs.

5.2.1 Distinct neural trajectories during observation, resting and active brain control

I found that neural trajectories traced over the same manifold space had separate representations of different task stages. Overall, I found that the neural trajectories have more variability and span a bigger region of the manifold hyperspace, when the neural activity does not have a direct impact in the task outcome, but the subjects are still engaged in the task (see chapter 3), as had been suggested by the uncontrolled manifold hypothesis (Scholz and Schoner, 1999; Domkin *et al.*, 2005). Similarly, a larger variability was measured during passive task observation (i.e. calibration trials), which could relate to the subjects trying to figure the task out. On the other hand, neural trajectories that did not diverge from the center (zero coordinates), could usually be related to a resting state, and possibly to low attention. Furthermore, even though active brain control did not exhibit as much variability as the passive observation, it was not zero centered, and I found discrete regions and separate neural trajectories that matched the separate target locations in the task space.

Kaufman *et al.* (2014) showed that it was possible to track neural firing activity in null- and output-potent spaces, which correlated to movement preparation and overt movements, respectively. The results shown in chapter 3 complement these initial studies, by showing that we can obtain different representations of resting states (task off), passive observation (calibration), inter-trial periods, and active brain control, all in a brain controlled only task. Moreover, I was able to extract task related information from these reduced dimension neural trajectories, in other words to re-estimate firing activity and movement intention with less dimensions. I found that the neural trajectories during passive observation still had significant end-goal information, regardless of the increased variability in these neural trajectories. Inter-

trial intervals also had relevant previous-target information, which was not observed during resting periods. These results and intention estimations can shed light about the internal process, and possible rehearsal the subjects engage during the tasks.

5.2.2 Neural space exploration and learning

Similar to the measurements in dynamical changes done with the PDs and the cross-correlation coefficients, I tracked the dynamical variations in the neural trajectories during learning in active brain control trials (baseline, VMR and DeCorr). Some studies have suggested the need to increase movement variability during motor adaptation, and the possibility to increase a system's noise in order to reach the global solution of the tasks (Latash *et al.*, 2002; Schollhorn *et al.*, 2009; Shadmehr *et al.*, 2010). This led to the hypothesis that the neural trajectories at the beginning of learning would be more noisy and have more variability than those measured during later stages of the adaptation process.

I compared the neural trajectories of unperturbed baseline trials, and those during VMR and DeCorr trials (see chapter 4), and estimated the changes in the volume and the entropy (uncertainty) that these neural trajectories had. I found that indeed the neural trajectories had more variability and entropy during early stages of the adaptation process, for both tasks. The uncertainty of the neural trajectories decreased as performance increased, and the rate of this decrease was faster during the VMR trials. Furthermore, I measured a more significant overlap between the final trajectories of VMR and unperturbed trials, than between DeCorr and unperturbed baseline trials. The shift observed in the neural trajectories of the final task adaptation could be the graphical representation of the non-uniform changes in the contribution of the input signals, necessary to adapt to the task. For the VMR task, the input signals

needed only to uniformly change their contributions to the neural signals, and this was reflected in the overlapping final neural trajectories.

Finally, when re-estimating the target direction from the neural trajectories for VMR and DeCorr trials, I found that performance did not have a significant effect in this target estimation. This means that the neural trajectories still had task relevant information, even when performance was low and their variability was high, similar to what was observed during the calibration trials. Future work should focus in further understanding how these variability and noise increase are able to help motor and task adaptation, and look at the possibility to use this noise to enhance and improve motor adaptation.

5.3 Implications for neuroprosthetics

In addition to their individual contributions to learning with BMIs, the results presented and discussed in this dissertation can have significant contributions in the neuroprosthetics field and, more generally, in the field of motor learning and adaptation.

5.3.1 Motor adaptation and learning

We have studied and compared motor adaptation processes across two very different learning challenges in a BMI motor-like paradigm. The results show that the overall general strategy used by the neural circuitry has a lot of similarities between the tasks, but the eventual solutions differ between them. In neuroprosthetics, and BMI tasks, it is common to calibrate the BMI systems every day (Taylor *et al.*, 2002; Jarosiewicz *et al.*, 2008; Sadtler *et al.*, 2014), and train subjects across different tasks (Hochberg *et al.*, 2012; Collinger *et al.*, 2013). However, we have shown that the adaptation process has striking similarities across tasks of different complexity, this

could mean that it is not necessary to have subjects train in complex task in order to exert a better and more complex control over the neuroprosthetics or external devices. It might be possible to get the same overall neural activation with more simple tasks, which can keep the subjects engaged during training, and will still allow them to explore the neural space. However, it remains to be tested whether subjects training in different levels of complexity can eventually adapt with similar rates to a different task. These studies would have to involve two groups which train in distinct paradigms such as VMR and DeCorr, and later measure their ability to use the same neural signals in a separate task, possibly with a more functional goal (e.g. bring food or drink to mouth, grasp physical objects, type e-mail, etc.).

On the other hand, when studying the underlying connections that control the measured neural signals, it was found that these latent variables also have dynamical changes during adaptation. These results hint that the measured adaptation will involve dynamical changes across several cortical and subcortical areas (Hikosaka *et al.*, 2002; Addou *et al.*, 2014), so focusing on isolated cortical regions might only give a limited understanding of the underlying process that happen during motor adaptation. Future work should focus on comparing these variations in the estimated variables and recordings from different cortical and subcortical areas. These studies might not provide a direct relationship or causality of the changes in the underlying variables, but might help us identify important correlations and better understand the mechanisms which allow the motor signals to adapt to a variety of tasks, acquire new skills, and also understand certain learning constraints, and how can we facilitate this learning process.

5.3.2 Brain decoding and applications to brain-machine interfaces

Recent work with invasive recordings have shown that it is possible to directly use reduced dimension neural signals to control external devices (Sadtler *et al.*, 2014), similar strategies have been used with EEG recordings, where the information does not have as good spatial resolution as invasive recordings (Bulea *et al.*, 2013; Kilicarslan *et al.*, 2013). I have shown that it is possible to extract task relevant information of three dimensional movements from a very small number of reduced dimensions (n = 3), even after the signal properties are not calibrated daily. Moreover, these same reduced dimensions can be used to estimate the intention during passive observation, and different task epochs. Use of these latent variables instead of individual neural units could help lengthen the life of invasive implants once the recordings decrease their signal-to-noise ratio, and can also bypass the necessity to calibrate and sort the signals for these systems daily, since they could be more robust to day-to-day variations.

Similarly, it seems that developing algorithms which constraint movement noise and uncertainty is not necessarily the answer to faster adaptation. We have shown, and it has been previously suggested (Braun *et al.*, 2009b; Schollhorn *et al.*, 2009), that neural exploration and tuning properties vary dynamically and increase their variability during the initial stages of learning, and this increase might be indeed a necessary part of the adaptation process. However, more work needs to study this noise increment, and the possibility to use it as a tool to enhance learning (Ranganathan *et al.*, 2014), and maybe aid subjects to improve performance after they have reach a plateau during their training.

5.4 Future directions

The next steps for the experiments described in this dissertation, would be to determine the "optimal noise" levels that allow motor adaptation to occur, through systematic perturbations. Some groups have proposed that there is an inverse "U" shape between the amount of noise and motor learning (Manjarrez *et al.*, 2007; Scholl-horn *et al.*, 2009), but this is yet to be measured experimentally. It has recently been shown that, at a cellular level, it is possible to enhance evoked potentials and increase firing rates when injecting artificial noise to the system (Manjarrez *et al.*, 2015). Other groups have proposed the existence of random background noise in the neural systems, which underlies the neural modulation and tuning we observe during motor adaptation (Rokni *et al.*, 2007). We were able to measure an increase in the neural trajectory's entropy and its eventual decrease during learning of both tasks, which had different adaptation rates. It might be possible to artificially introduce this noise to the system (e.g. through TMS, ICMS) which might not evoke motor responses (twitches, movements, etc.) but which might increase the noise in the motor signals and the neural system, and affect the adaptation rates for both tasks.

Another approach that could be used to increase the noise in the neural system, would be to randomly increase the error in the task (increase angle in VMR or number of rotated pairs in DeCorr) for a short set of trials, in order to increase the noise/uncertainty within the neural system itself. This would be similar to increasing the temperature during simulated annealing (Rutenbar, 1989), and then let the system "solve" the task (VMR or DeCorr) again, this would be analogous to the "cool down" phase of simulated annealing. This noise increase could aid the neural system to eventually solve the credit assignment problem, specially in tasks where the solution space has several local minima (e.g. DeCorr task).

In addition to understanding the process which allows and facilitates motor adaptation, similar BMIs paradigms could be used to determine constraints in this motor adaptation. Some studies have signaled that overlap of underlying manifolds between tasks will interfere with learning (Ranganathan *et al.*, 2014), and tasks which require to move outside this manifold will not be learned (Sadtler *et al.*, 2014). Further experiments with BMIs could compare whether random shuffling of calibration preferred directions would have a similar effect as our DeCorr tasks. It would be interesting to explore whether selecting highly correlated neural units was the driving factor of the slow adaptation process, or whether it was the non-uniformity of the perturbation.

Finally, it would also be interesting to study and measure the adaptation of more structures usually involved in motor learning (e.g. cerebellum, basal ganglia), and compare the dynamical changes in motor and pre-motor cortices, and these deeper structures. Moreover, we could discern whether the dynamical changes in the underlying manifolds relate to variations in activity of these deeper structures that send and receive connections from motor cortical areas. Parallel studies of these structures might bring new challenges regarding hardware and recording technologies, however it might be possible to use less invasive tools (e.g. ECoG, micro-ECoG, fMRI, EEG, etc.) that would still allow to get a general picture of the adaptation processes and the structures engaged.

Addou, T., N. Krouchev and J. Kalaska, "Motor cortex single-neuron and population contributions to compensation for multiple dynamic force fields", Journal of Neurophysiology , 113, 487–508 (2014).

Armenta Salas, M. and S. I. Helms Tillery, "Neural ensemble response to learning challenges in brain-machine interfaces", in "Society for Neuroscience Conference", Poster session (Washington, D.C., 2014).

Armenta Salas, M. and S. I. Helms Tillery, "Neural ensemble dynamics during brain-machine interface controlled motor-like task", in "Society for Neuroscience Conference", Nanosymposium (Chicago, Il., 2015).

Balestrino, A., A. Caiti, E. Crisostomi and G. Grioli, "A generalised entropy of curves: an approach to the analysis of dynamical systems", pp. 1157–1162 (Cancun, Mexico, 2008).

Braun, D. A., A. Aertsen, D. M. Wolpert and C. Mehring, "Learning Optimal Adaptation Strategies in Unpredictable Motor Tasks", J of Neuroscience **29**, 20, 6472–6478 (2009a).

Braun, D. A., A. Aertsen, D. M. Wolpert and C. Mehring, "Motor Task Variation Induces Structural Learning", Current Biology **19**, 4, 352–357, URL `http://www.ncbi.nlm.nih.gov/pmc/articles/PMC2669412/` (2009b).

Brockwell, A. E., A. Rojas and R. Kass, "Recursive Bayesian Decoding of Motor Cortical Signals by Particle Filtering", Journal of Neurophysiology **91**, 4, 1899–1907, URL `http://jn.physiology.org/content/91/4/1899.abstract`, 00191 (2004).

Brown, E. N., R. E. Kass and P. P. Mitra, "Multiple neural spike train data analysis: state-of-the-art and future challenges", Nat Neurosci **7**, 5, 456–461, URL `http://dx.doi.org/10.1038/nn1228`, 00565 (2004).

Bulea, T., S. Prasad, A. Kilicarslan and J. Contreras-Vidal, "Classification of stand-to-sit and sit-to-stand movement from low frequency EEG with locality preserving dimensionality reduction", in "Engineering in Medicine and Biology Society (EMBC), 2013 35th Annual International Conference of the IEEE", pp. 6341–6344 (2013).

Cai, X., Y. Shimansky, D. Weber and H. Jiping, "Disassociation between primary motor cortical activity and movement kinematics during adaptation to reach perturbations", in "Engineering in Medicine and Biology Society", pp. 4665–4668 (San Francisco, CA, 2004).

Carmena, J. M., M. A. Lebedev, R. Crist, J. E. O'Doherty, D. Santucci, D. Dimitrov, P. Patil, C. Henriquez and M. A. L. Nicoleilis, "Learning to Control a Brain-Machine Interface for Reaching and Grasping by Primates", PLoS Biology **1**, 2, e42, 01146 (2003).

Chapin, J. K., K. A. Moxon, R. S. Markowitz and M. A. L. Nicolelis, "Real-time control of a robot arm using simultaneously recorded neurons in the motor cortex", Nat Neuroscience **2**, 7, 664 – 670, URL http://www.neuro-it.net/pdf_dateien/summer_2004/Chapin%201999.pdf, 00821 (1999).

Chase, S. M., R. E. Kass and A. B. Schwartz, "Behavioral and neural correlates of visuomotor adaptation observed through a brain-computer interface in primary motor cortex.", J of Neurophysiology (2012).

Chase, S. M., A. B. Schwartz and R. E. Kass, "Latent Inputs Improve Estimates of Neural Encoding in Motor Cortex", J of Neuroscience **30**, 41, 13873–13882 (2010).

Chen, L. and K. Aihara, "Chaotic simulated annealing by a neural network model with transient chaos", Neural Networks **8**, 6, 915–930, URL http://www.sciencedirect.com/science/article/pii/089360809500033V (1995).

Churchland, M. M., J. P. Cunningham, M. T. Kaufman, J. D. Foster, P. Nuyujukian, S. I. Ryu and K. V. Shenoy, "Neural population dynamics during reaching", Nature **487**, 7405, 51–56, URL http://dx.doi.org/10.1038/nature11129 (2012).

Collinger, J. L., R. Vinjamuri, A. D. Degenhart, D. J. Weber, G. P. Sudre, M. L. Boninger, E. C. Tyler-Kabara and W. Wang, "Motor-related brain activity during action observation: a neural substrate for electrocorticographic brain-computer interfaces after spinal cord injury", Frontiers in integrative neuroscience **8**, 00000 (2014).

Collinger, J. L., B. Wodlinger, J. E. Downey, W. Wang, E. C. Tyler-Kabara, D. J. Weber, A. J. McMorland, M. Velliste, M. L. Boninger and A. B. Schwartz, "High-performance neuroprosthetic control by an individual with tetraplegia", The Lancet **381**, 9866, 557–564, URL http://www.sciencedirect.com/science/article/pii/S0140673612618169, 00152 (2013).

Cordier, P., M. M. France, J. Pailhous and P. Bolon, "Entropy as a global variable of the learning process", Human Movement Science **13**, 6, 745–763, URL http://www.sciencedirect.com/science/article/pii/0167945794900167 (1994).

Cowley, B. R., M. T. Kaufman, Z. S. Butler, M. M. Churchland, S. I. Ryu, K. V. Shenoy and B. M. Yu, "DataHigh: graphical user interface for visualizing and interacting with high-dimensional neural activity", Journal of Neural Engineering **10**, 6, URL http://iopscience.iop.org/1741-2552/10/6/066012/ (2013).

Dempster, A. P., N. M. Laird and D. B. Rubin, "Maximum likelihood from incomplete data via the EM algorithm", Journal of the Royal Statistical Society. Series B (Methodological) pp. 1–38, 39956 (1977).

Domkin, D., J. Laczko, M. Djupsjbacka, S. Jaric and M. Latash, "Joint angle variability in 3d bimanual pointing: uncontrolled manifold analysis", Experimental Brain Research **163**, 1, 44–57, URL http://dx.doi.org/10.1007/s00221-004-2137-1, 00066 (2005).

Donchin, O., K. Rabe, J. Diedrichsen, N. Lally, B. Schoch, E. R. Gizewski and D. Timmann, "Cerebellar regions involved in adaptation to force field and visuomotor perturbation", Journal of neurophysiology **107**, 1, 134–147, 00031 (2012).

Donoghue, J. P., A. Nurmikko, G. Friehs and M. Black, "Chapter 63: Development of neuromotor prostheses for humans", in "Supplements to Clinical Neurophysiology", vol. Volume 57, pp. 592–606 (Elsevier, 2004), URL `http://www.sciencedirect.com/science/article/pii/S1567424X0970399X`, 00000.

Doya, K., "What are the computations of the cerebelum, the basal ganglia and the cerebral cortex?", Neural Networks **12**, 7-8, 961–974 (1999).

Doya, K., "Complementary roles of basal ganglia and cerebellum in learning and motor control", Current opinion in neurobiology **10**, 6, 732–739, 00370 (2000).

Fetz, E. E., "Operant Conditioning of Cortical Unit Activity", Science **163**, 3870, 955 – 958, 00281 (1969).

Fetz, E. E. and D. V. Finocchio, "Operant Conditioning of Specific Patterns of Neural and Muscular Activity", Science **174**, 4007, 431–435, URL `http://www.sciencemag.org/content/174/4007/431.abstract`, 00157 (1971).

Friehs, G. M., V. A. Zerris, C. L. Ojakangas, M. R. Fellows and J. P. Donoghue, "Brain-machine and brain-computer interfaces", Stroke **35**, 11 suppl 1, 2702–2705, URL `http://stroke.ahajournals.org/content/35/11_suppl_1/2702.abstract`, 00094 (2004).

Gandolfo, F., C.-S. R. Li, B. J. Benda, C. P. Schioppa and E. Bizzi, "Cortical correlates of learning in monkeys adapting to a new dynamical environment", Proceedings of the National Academy of Sciences **97**, 5, 2259–2263, URL `http://www.pnas.org/content/97/5/2259.abstract`, 00177 (2000).

Ganguly, K. and J. M. Carmena, "Emergence of a Stable Cortical Map for Neuroprosthetic Control", PLoS Biology **7**, 7, e1000153, 00000 (2009).

Ganguly, K., D. F. Dimitrov, J. D. Wallis and J. M. Carmena, "Reversible large-scale modification of cortical networks during neuroprosthetic control", Nat Neurosci **14**, 5, 662–667, URL `http://dx.doi.org/10.1038/nn.2797`, 00058 (2011).

Georgopoulos, A., A. Schwartz and R. Kettner, "Neuronal population coding of movement direction", Science **233**, 4771, 1416–1419, 01854 (1986).

Ghahramani, Z., "The EM Algorithm for Mixtures of Factor Analyzers", URL `http://www.gatsby.ucl.ac.uk/~zoubin/software.html` (1996).

Goffe, W. L., G. D. Ferrier and J. Rogers, "Global optimization of statistical functions with simulated annealing", Journal of Econometrics **60**, 65–99 (1994).

Golub, M. D., S. M. Chase and B. M. Yu, "Learning an Internal Dynamics Model from Control Demonstration", JMLR workshop and conference proceedings pp. 606–614, URL `http://www.ncbi.nlm.nih.gov/pmc/articles/PMC3929129/` (2013).

Hatsopoulos, N., J. Joshi and J. G. O'Leary, "Decoding Continuous and Discrete Motor Behaviors Using Motor and Premotor Cortical Ensembles", Journal of Neurophysiology **92**, 2, 1165–1174, URL http://jn.physiology.org/content/92/2/1165.abstract, 00152 (2004).

Hatsopoulos, N., J. Mukand, G. Polykoff, G. Friehs and J. Donoghue, "Cortically controlled brain-machine interface", Engineering in Medicine and Biology Society, 2005. IEEE-EMBS 2005. 27th Annual International Conference of the pp. 7660–7663, 00007 (2005).

He, J. and D. J. Weber, "Adaptation in cortical control of amr movement", in "Proceedings of the IFAC Congress", (Barcelona, Spain, 2002).

Hikosaka, O., H. Nakahara, M. K. Rand, K. Sakai, X. Lu, K. Nakamura, S. Miyachi and K. Doya, "Parallel neural networks for learning sequential procedures", Trends in Neurosciences **22**, 10, 464–471, URL http://www.sciencedirect.com/science/article/pii/S0166223699014393 (1999).

Hikosaka, O., K. Nakamura, K. Sakai and H. Nakahara, "Central mechanisms of motor skill learning", Current opinion in neurobiology **12**, 2, 217–222, 00436 (2002).

Hochberg, L. R., D. Bacher, B. Jarosiewicz, N. Y. Masse, J. D. Simeral, J. Vogel, S. Haddadin, J. Liu, S. S. Cash, P. van der Smagt and J. P. Donoghue, "Reach and grasp by people with tetraplegia using a neurally controlled robotic arm", Nature **485**, 7398, 372–375, URL http://dx.doi.org/10.1038/nature11076, 00325 (2012).

Hochberg, L. R., M. D. Serruya, G. M. Friehs, J. A. Mukand, M. Saleh, A. H. Caplan, A. Branner, D. Chen, R. D. Penn and J. P. Donoghue, "Neuronal ensemble control of prosthetic devices by a human with tetraplegia", Nature **442**, 7099, 164–171, URL http://dx.doi.org/10.1038/nature04970, 01813 (2006).

Ingber, L., "Simulated annealing: Practice versus theory", Mathematical and Computer Modelling **18**, 11, 29–57, URL http://www.sciencedirect.com/science/article/pii/089571779390204C (1993).

Ishii, S., W. Yoshida and J. Yoshimoto, "Control of exploitation-exploration meta-parameter in reinforcement learning", Neural Networks **15**, 4-6, 665–687 (2002).

Jarosiewicz, B., S. M. Chase, G. W. Fraser, M. Velliste, R. E. Kass and A. B. Schwartz, "Functional network reorganization during learning in a brain-computer interface paradigm", PNAS **105**, 49, 19486 – 19491, 00109 (2008).

Jueptner, M., C. Frith, D. Brooks, R. Frackowiak and R. Passingham, "Anatomy of motor learning. II. Subcortical structures and learning by trial and error", Journal of neurophysiology **77**, 3, 1325–1337, 00407 (1997).

Kaufman, M. T., M. M. Churchland, S. I. Ryu and K. V. Shenoy, "Cortical activity in the null space: permitting preparation without movement", Nat Neurosci **17**, 3, 440–448, URL http://dx.doi.org/10.1038/nn.3643 (2014).

Kilicarslan, A., S. Prasad, R. Grossman and J. Contreras-Vidal, "High accuracy decoding of user intentions using EEG to control a lower-body exoskeleton", in "Engineering in Medicine and Biology Society (EMBC), 2013 35th Annual International Conference of the IEEE", pp. 5606–5609 (2013).

Kleim, J. A., S. Barbay and R. J. Nudo, "Functional Reorganization of the Rat Motor Cortex Following Motor Skill Learning", J of Neurophysiology **80**, 6, 3321–3325, URL `http://jn.physiology.org/content/80/6/3321.full`, 00484 (1998).

Kleim, J. A., T. M. Hogg, P. M. VandenBerg, N. R. Cooper, R. Bruneau and M. Remple, "Cortical Synaptogenesis and Motor Map Reorganization Occur during Late, But Not Early, Phase of Motor Skill Learning", The Journal of Neuroscience **24**, 3, 628–633, URL `http://www.jneurosci.org/content/24/3/628.abstract`, 00337 (2004).

Knyazev, A. and M. Argentati, "Principal Angles between Subspaces in an A-Based Scalar Product: Algorithms and Perturbation Estimates", SIAM Journal of Scientific Computing **23**, 6, 2008–2040, URL `http://epubs.siam.org/doi/abs/10.1137/S1064827500377332` (2002).

Koralek, A., R. Costa and J. Carmena, "Temporally Precise Cell-Specific Coherence Develops in Corticostriatal Networks during Learning", Neuron **79**, 5, 865–872, URL `http://www.sciencedirect.com/science/article/pii/S0896627313005631` (2013).

Koralek, A. C., X. Jin, J. D. Long, R. M. Costa and J. M. Carmena, "Corticostriatal plasticity is necessary for learning intentional neuroprosthetic skills.", Nature **483**, 331–335, URL `http://www.nature.com/nature/journal/v483/n7389/full/nature10845.html`, 00059 (2012).

Koralek, A. C., J. D. Long and R. M. Costa, "Corticostriatal dynamics during learning and performance of a neuroprosthetic task", in "Engineering in Medicine and Biology Society", (IEEE, Buenos Aires, 2010), URL `http://ieeexplore.ieee.org.ezproxy1.lib.asu.edu/xpls/icp.jsp?arnumber=5626632`.

Koyama, S., S. Chase, A. Whitford, M. Velliste, A. Schwartz and R. Kass, "Comparison of brain-computer interface decoding algorithms in open-loop and closed-loop control", Journal of Computational Neuroscience **29**, 1-2, 73–87, URL `http://dx.doi.org/10.1007/s10827-009-0196-9`, 00060 (2010).

Krakauer, J. W., "Motor learning and consolidation: the case of visuomotor rotation", in "Progress in Motor Control", pp. 405–421 (Springer, 2009), 00070.

Krakauer, J. W., M.-F. Ghilardi and C. Ghez, "Independent learning of internal models for kinematic and dynamic control of reaching", Nature neuroscience **2**, 11, 1026–1031, 00519 (1999).

Krakauer, J. W., Z. M. Pine, M.-F. Ghilardi and C. Ghez, "Learning of visuomotor transformations for vectorial planning of reaching trajectories", J of Neuroscience **20**, 23, 8916–8924, 00400 (2000).

Latash, M. L., J. P. Scholz and G. Schoner, "Motor Control Strategies Revealed in the Structure of Motor Variability", Exerc. Sport Sci. Rev. **30**, 1, 26–31 (2002).

Manjarrez, E., P. Linares, B. De la Torre Valdovinos, I. Mendez-Balbuena, A. Flores and R. Gutierrez, "Stochastic resonance in the brain elicted by optogenetic noise-photostimulation", in "Society for Neuroscience Conference", Poster session (Chicago, Il., 2015).

Manjarrez, E., I. Mendez, L. Martinez, A. Flores and C. R. Mirasso, "Effects of auditory noise on the psychophysical detection of visual signals: Cross-model stochastic resonance", Neuroscience Letters **415**, 231–236 (2007).

McAndrew, R., J. Lingo VanGilder, S. Naufel and S. Helms Tillery, "Individualized recording chambers for non-human primate neurophysiology", Journal of Neuroscience Methods **207**, 1, 86–90, URL `http://www.sciencedirect.com/science/article/pii/S0165027012001094`, 00002 (2012).

McDonnell, M. D. and L. M. Ward, "The benefits of noise in neural systems: bridging theory and experiment", Nat Rev Neurosci **12**, 7, 415–426, URL `http://dx.doi.org/10.1038/nrn3061` (2011).

McLachlan, G. J. and T. Krishnan, "Extensions of the EM Algorithm", in "The EM Algorithm and Exentesions", vol. 382, pp. 197–199 (John Wiley & Sons, 2007).

Medina, L. E., M. A. Lebedev, J. E. O'Doherty and M. A. L. Nicoleilis, "Stochastic Facilitation of Artificial Tactile Sensation in Primates", J of Neuroscience **32**, 41, 14271–14275 (2012).

Moran, D. W. and A. B. Schwartz, "Motor Cortical Representation of Speed and Direction During Reaching", Journal of Neurophysiology **82**, 5, 2676–2692, URL `http://jn.physiology.org/content/82/5/2676.abstract`, 00470 (1999).

Mosier, K. M., R. A. Scheidt, S. Acosta and F. A. Mussa-Ivaldi, "Remapping Hand Movements in a Novel Geometrical Environment", Journal of Neurophysiology **94**, 6, 4362–4372, URL `http://jn.physiology.org/content/94/6/4362.abstract`, 00055 (2005).

Naselaris, T., H. Merchant, B. Amirikian and A. Georgopoulos, "Large-Scale Organization of Preferred Directions in the Motor Cortex. II. Analysis of Local Distributions", Journal of Neurophysiology **96**, 6, 3237–3247, URL `http://jn.physiology.org/content/96/6/3237.abstract`, 00019 (2006).

Nawrot, M., A. Aertsen and S. Rotter, "Single-trial estimation of neuronal firing rates: From single-neuron spike trains to population activity", Journal of Neuroscience Methods **94**, 1, 81–92, URL `http://www.sciencedirect.com/science/article/pii/S0165027099001272`, 00099 (1999).

Nudo, R. J., G. W. Milliken, W. M. Jenkins and M. M. Merzenich, "Use-dependent alterations of movement representations in primary motor cortex of adult squirrel monkeys", J of Neuroscience **16**, 2, 785–807, URL `http://www.jneurosci.org.ezproxy1.lib.asu.edu/content/16/2/785.short`, 00976 (1996).

Okun, M., N. Steinmetz, L. Cossell, F. Iacaruso, H. Ko, P. Barto, T. Moore, S. Hofer, T. Mrsic-Flogel, M. Carandini and K. Harris, "Diverse Coupling of neurons to populations in sensory cortex", Nature **521**, 511–515 (2015).

Orsborn, A., H. Moorman, S. Overduin, M. Shanechi, D. Dimitrov and J. Carmena, "Closed-Loop Decoder Adaptation Shapes Neural Plasticity for Skillful Neuroprosthetic Control", Neuron **82**, 6, 1380–1393, URL `http://www.sciencedirect.com/science/article/pii/S0896627314003638`, 00000 (2014).

Pascual-Leone, A., J. Grafman and M. Hallet, "Modulation of Cortical Motor Output Maps During Development of Implicit and Explicit Knowledge", Science **263**, 5151, 1287–1289, URL `http://www.jstor.org/stable/2883476`, 00494 (1994).

Paz, R., T. Boraud, C. Natan, H. Bergman and E. Vaadia, "Preparatory activity in motor cortex reflects learning of local visuomotor skills", Nat Neurosci **6**, 8, 882–890, URL `http://dx.doi.org/10.1038/nn1097`, 00124 (2003).

Paz, R., C. Nathan, T. Boraud, H. Bergman and E. Vaadia, "Acquisition and generalization of visuomotor transformations by nonhuman primates", Experimental Brain Research **161**, 2, 209–219 (2005).

Paz, R. and E. Vaadia, "Learning-induced improvement in encoding and decoding of specific movement directions by neurons in the primary motor cortex", PLoS Biology **2**, 2, E45, 00056 (2004).

Plautz, E. J., G. W. Milliken and R. J. Nudo, "Effects of Repetitive Motor Training on Movement Representations in Adult Squirrel Monkeys: Role of Use versus Learning", Neurobiology of Learning and Memory **74**, 1, 27–55, URL `http://www.sciencedirect.com/science/article/pii/S1074742799939345`, 00401 (2000).

Ranganathan, R., J. Wieser, K. M. Mosier and F. A. Mussa-Ivaldi, "Learning Redundant Motor Tasks with and without Overlapping Dimensions: Facilitation and Interference Effects", Journal of Neuroscience **34**, 24, 8289–8299 (2014).

Rokni, U., A. G. Richardson and E. Bizzi, "Motor learning with unstable neural representations", Neuron **54**, 4, 653–666 (2007).

Royer, A. S. and B. He, "Goal selection versus process control in a brain-computer interface based on sensorimotor rhythms", Journal of Neural Engineering **6**, 1, 016005, URL `http://stacks.iop.org/1741-2552/6/i=1/a=016005` (2009).

Rubin, D. B. and D. T. Thayer, "EM Algorithms for ML Factor Analysis", Psychometrika **47**, 1, 69–76 (1982).

Rutenbar, R., "Simulated annealing algorithms: an overview", Circuits and Devices Magazine, IEEE **5**, 1, 19–26 (1989).

Ryu, S. I., G. Santhanam, B. M. Yu and K. V. Shenoy, "High speed neural prosthetic icon positioning", in "Soc. for Neurosci. Abstr", (2004), 00007.

Sadtler, P. T., K. M. Quick, M. D. Golub, S. M. Chase, S. I. Ryu, E. C. Tyler-Kabara, M. Y. Byron and A. P. Batista, "Neural constraints on learning", Nature **512**, 7515, 423–426, 00003 (2014).

Sakurai, Y., "Brain-machine interfaces can accelerate clarification of the principal mysteries and real plasticity of the brain", Frontiers in Systems Neuroscience **8**, 00140, 00000 (2014).

Salinas, E. and T. J. Sejnowski, "Correlated neuronal activity and the flow of neural information", Nat Rev Neurosci **2**, 8, 539–550, URL `http://dx.doi.org/10.1038/35086012`, 00694 (2001).

Santhanam, G., B. M. Yu, V. Gilja and S. I. Ryu, "A factor-analysis decoder for high-performance neural prostheses", in "Acoustics, Speech and Signal Processing", pp. 5208–5211 (IEEE, Las Vegas, NV, 2008).

Schmidt, E., M. Bak, J. McIntosh and J. Thomas, "Operant conditioning of firing patterns in monkey cortical neurons", Experimental Neurology **54**, 3, 467–477, URL `http://www.sciencedirect.com/science/article/pii/0014488677902503`, 00033 (1977).

Schollhorn, W., G. Mayer-Kress, K. Newell and M. Michelbrink, "Time scales of adaptive behavior and motor learning in the presence of stochastic perturbations", Third European Workshop on Human Movement Science **28**, 3, 319–333, URL `http://www.sciencedirect.com/science/article/pii/S0167945708000869` (2009).

Scholz, J. P. and G. Schoner, "The uncontrolled manifold concept: identifying control variables for a functional task", Experimental Brain Research **126**, 3, 289–306, URL `http://dx.doi.org/10.1007/s002210050738`, 00665 (1999).

Schweighofer, N. and K. Doya, "Meta-learning in Reinforcement Learning", Neural Networs **16**, 1, 5–9 (2003).

Scott, S. H., "Optimal feedback control and the neural basis of volitional motor control", Nat Rev Neurosci **5**, 7, 532–546, URL `http://dx.doi.org/10.1038/nrn1427`, 00315 (2004).

Semechko, A., "ExactMinBoundSphere3d", URL `http://www.mathworks.com/matlabcentral/fileexchange/48725-exact-minimum-bounding-spheres-circles/content/MinBoundSphere&Circle/ExactMinBoundSphere3D.m` (2014).

Serruya, M. D., N. G. Hatsopoulos, L. Paninski, M. R. Fellows and J. P. Donoghue, "Brain-machine interface: Instant neural control of a movement signal", Nature **416**, 6877, 141–142, URL `http://dx.doi.org/10.1038/416141a`, 01057 (2002).

Shadmehr, R. and F. A. Mussa-Ivaldi, "Adaptive representation of dynamics during learning of a motor task", J of Neuroscience **14**, 5, 3208–3224, URL `http://www.jneurosci.org.ezproxy1.lib.asu.edu/content/14/5/3208.short`, 01579 (1994).

Shadmehr, R., M. Smith and J. W. Krakauer, "Error correction, sensory prediction, and adaptation in motor control", Annual Reviews of Neuroscience **33**, 89–108 (2010).

Shenoy, K. V., D. Meeker, S. Cao, S. A. Kureshi, B. Pesaran, C. A. Buneo, A. P. Batista, P. P. Mitra, J. W. Burdick and R. A. Andersen, "Neural prosthetic control signals from plan activity", Neuroreport **14**, 4, 591–596, 00193 (2003).

Shmuelof, L. and J. W. Krakauer, "Are We Ready for a Natural History of Motor Learning?", Neuron **72**, 3, 469–476, URL `http://www.ncbi.nlm.nih.gov/pmc/articles/PMC3389513/` (2011).

So, K., K. Ganguly, J. Jimenez, M. C. Gastpar and J. M. Carmena, "Redundant information encoding in primary motor cortex during natural and prosthetic motor control", Journal of computational neuroscience **32**, 3, 555–561 (2012a).

So, K., A. C. Koralek, K. Ganguly, M. C. Gastpar and J. M. Carmena, "Assessing functional connectivity of neural ensembles using directed information", Journal of Neural Engineering **9**, 2, 026004, URL `http://stacks.iop.org/1741-2552/9/i=2/a=026004` (2012b).

Srinivasan, L. and E. Brown, "A State-Space Framework for Movement Control to Dynamic Goals Through Brain-Driven Interfaces", Biomedical Engineering, IEEE Transactions on **54**, 3, 526–535, 00017 (2007).

Suminski, A. J., D. C. Tkach, A. H. Fagg and N. G. Hatsopoulos, "Incorporating Feedback from Multiple Sensory Modalities Enhances Brain-Machine Interface Control", Journal of Neuroscience **30**, 50, 16777–16787 (2010).

Tanaka, H., T. J. Sejnowski and J. W. Krakauer, "Adaptation to Visuomotor Rotation Through Interaction Between Posterior Parietal and Motor Cortical Areas", Journal of Neurophysiology **102**, 5, 2921–2932, URL `http://jn.physiology.org/content/102/5/2921.abstract`, 00050 (2009).

Taylor, D. M., S. I. Helms Tillery and A. B. Schwartz, "Direct Cortical Control of 3d Neuroprosthetic Devices", Science **296**, 5574, 1829 – 1832, URL `http://www.sciencemag.org/content/296/5574/1829.full`, 01262 (2002).

Tkach, D., J. Reimer and N. G. Hatsopoulos, "Congruent Activity during Action and Action Observation in Motor Cortex", The Journal of Neuroscience **27**, 48, 13241–13250, URL `http://www.jneurosci.org/content/27/48/13241.abstract`, 00127 (2007).

Tong, C. and J. R. Flanagan, "Task-Specific Internal Models for Kinematic Transformations", Journal of Neurophysiology **90**, 2, 578–585, URL `http://jn.physiology.org/content/90/2/578.abstract`, 00049 (2003).

Vaadia, E., I. Haalman, M. Abeles, H. Bergman, Y. Prut, H. Slovin and A. Aertsen, "Dynamics of neuronal interactions in monkey cortex in relation to behavioral events", Letters to Nature **373**, 9, 515–518, 00000 (1995).

Velliste, M., S. Perel, M. C. Spalding, A. S. Whitford and A. B. Schwartz, "Cortical control of a prosthetic arm for self-feeding", Nature **453**, 7198, 1098–1101, URL http://dx.doi.org/10.1038/nature06996, 00801 (2008).

Wahnoun, R., S. Helms Tillery and J. He, "Selection and parameterization of cortical neurons for neuroprosthetic control", Journal of Neural Engineering **3**, 2, 162, URL http://stacks.iop.org/1741-2552/3/i=2/a=010, 00061 (2006).

Wander, J. D., T. Blakely, K. J. Miller, K. E. Weaver, L. A. Johnson, J. D. Olson, E. E. Fetz, R. P. Rao and J. G. Ojemann, "Distributed cortical adaptation during learning of a brain-computer interface task", Proceedings of the National Academy of Sciences **110**, 26, 10818–10823, 00000 (2013).

Wessberg, J., C. R. Stambaugh, J. D. Kralik, P. D. Beck, M. Laubach, J. K. Chapin, J. Kim, S. J. Biggs, M. A. Srinivasan and M. A. L. Nicolelis, "Real-time prediction of hand trajectory by ensembles of cortical neurons in primates", Nature **408**, 6810, 361–365, URL http://dx.doi.org/10.1038/35042582, 01139 (2000).

Wolpert, D., Z. Ghahramani and M. Jordan, "An internal model for sensorimotor integration", Science **269**, 5232, 1880–1882, URL http://www.sciencemag.org/content/269/5232/1880.abstract, 01716 (1995).

Wolpert, D. M., J. Diedrichsen and R. J. Flanagan, "Principles of sensorimotor learning", Nature Reviews Neuroscience **12**, 739–751, 00167 (2011).

Wright, T., "Factors Affecting the Cost of Airplanes", Journal of the Aeronautical Sciences (Institute of the Aeronautical Sciences) **3**, 4, 122–128, URL http://arc.aiaa.org/doi/abs/10.2514/8.155, 00000 (1936).

Wu, W., M. Black, Y. Gao, E. Bienenstock, M. Serruya, A. Shaikhouni and J. Donoghue, "Neural Decoding of Cursor Motion using a Kalman Filter", vol. 15, p. 133 (MIT Press, Cambridge, MA, 2003).

Wu, W. and N. G. Hatsopoulos, "Coordinate system representations of movement direction in the premotor cortex", Experimental brain research **176**, 4, 652–657, 00020 (2007).

Yu, B., J. Cunningham, G. Santhanam, S. Ryu, K. Shenoy and M. Sahani, "Gaussian-Process Factor Analysis for Low-Dimensional Single-Trial Analysis of Neural Population Activity", J of Neurophysiology **102**, 3, 2008–2008, 00000 (2009).

Yu, B. M., "GPFA", URL http://users.ece.cmu.edu/~byronyu/software/gpfa0203.tgz (2013).

Yuan, Y., H. Mao and J. Si, "Cortical neural responses to previous trial outcome during learning of a directional choice task", J of Neurophysiology **113**, 1963–1976 (2014).

Zar, J., *Biostatistical Analysis*, Prentice-Hall international editions (Prentice Hall, 1996), 00009.

APPENDIX A

ANIMAL PROTOCOL APPROVAL

Institutional Animal Care and Use Committee (IACUC)
Office of Research Integrity and Assurance
Arizona State University
660 South Mill Avenue, Suite 315
Tempe, Arizona 85287-6111
Phone: (480) 965-4387 *FAX:* (480) 965-7772

Animal Protocol Review

ASU Protocol Number: **12-1206R**
Protocol Title: **Sensory Representations and Learning in Skilled Motor Tasks**
Principal Investigator: **Stephen Helms Tillery**
Date of Action: **07/28/2011**

The animal protocol review was considered by the Committee and the following decisions were made:

- ☐ The original protocol was APPROVED as presented.
- ☒ The revised protocol was APPROVED as presented.
- ☐ The protocol was APPROVED with RESTRICTIONS or CHANGES as noted below. The project can only be pursued, subject to your acceptance of these restriction or changes. If you are not agreeable, contact the IACUC Chairperson immediately.
- ☐ The Committee requests CLARIFICATIONS or CHANGES in the protocol as described in the attached memorandum. The protocol will be considered when these issues are clarified and the revised protocol is submitted.
- ☐ The protocol was approved, subject to the approval of a WAIVER of provisions of NIH policy as noted below. Waivers require written approval from the granting agencies.
- ☐ The protocol was DISAPPROVED for reasons outlined in the attached memorandum.
- ☐ The Committee requests you to contact _____ to discuss this proposal.
- ☐ A copy of this correspondence has been sent to the Vice President for Research.
- ☐ Amendment was approved as presented.

RESTRICTIONS, CHANGES OR WAIVER REQUIREMENTS:
Total # of Animals: **24** **Pain Level:** **D** **Species:** **Macaca Mulatta**
Sponsor: **NIH, NSF, NIH/NINDS, ABRC**
Proposal #: **5R01-NS063372, CNS-0932389, R01-NS050256, 911**
Approval Period: **08/01/2011 – 07/31/2014**

Signature: J Murphy
IACUC Chair or Designee

Date: 8/1/11

Original: Principal Investigator
Cc: IACUC Office
IACUC Chair

APPENDIX B

ADDITIONAL RESULTS FIGURES

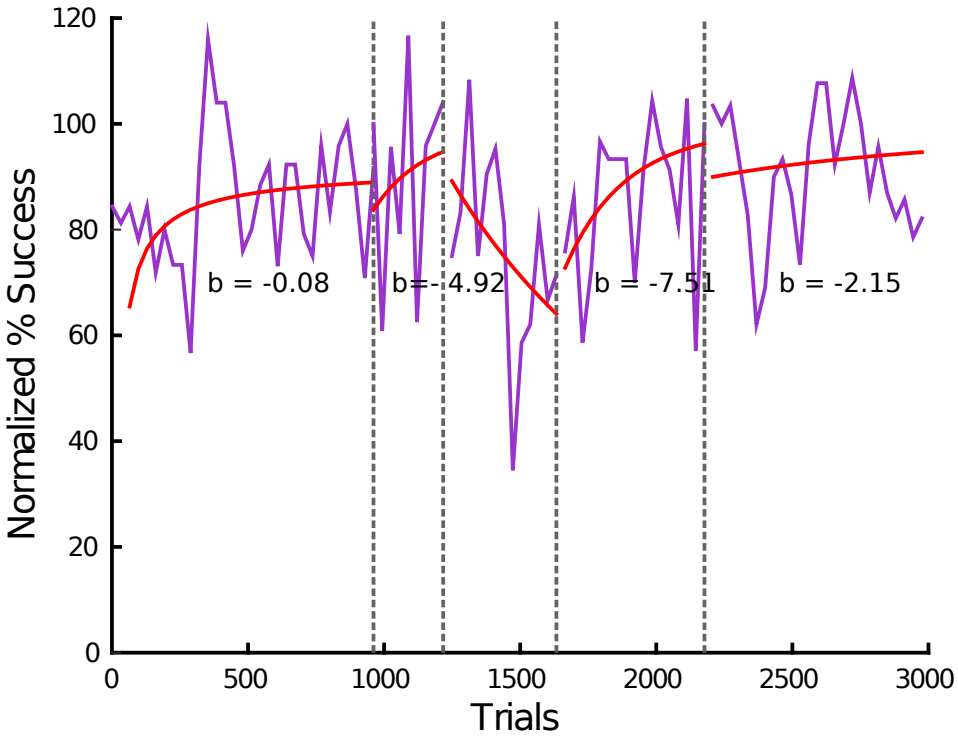

Figure B.1: Success Rate (Target Hits) during VMR Task for Subject O. Dashed lines show when there was a shift in calibration preferred directions. Red traces show the fit to the modified learning curve ($y = 100 - a * x^b$). Text shows the estimated b coefficients for each section. More negative values describe a faster learning rate. Panels that do not have b-coefficient value, did not have a good fit to the model.

Behavioral data

Success rate and time to targets

Figures B.1 through B.4 show the target hit rate and average time to targets, from successful trials, for both subject during the VMR task. Red traces show the model fit for the modified power learning curve ($y = 100 - ax^b$)) for the success rate, and the classic power curve ($y = ax^b$) for the times to target. Data are normalized according to the average target hits or time to target during the unperturbed baseline trials in each session. Similarly, Fig. B.5 shows the target hit rate for DeCorr trials of subject O, the complete data for Subject M was shown in chapter 2. Figures B.6 and B.7 show the average time to targets for subjects O and M, respectively, with their corresponding power learning curve fits.

Movement errors

Figures B.8 and B.9 show examples of movement shifts in VMR and DeCorr trials respectively, for both subjects. Solid lines show the average trajectories during unperturbed baseline control, and the dashes line represent the average of the perturbed

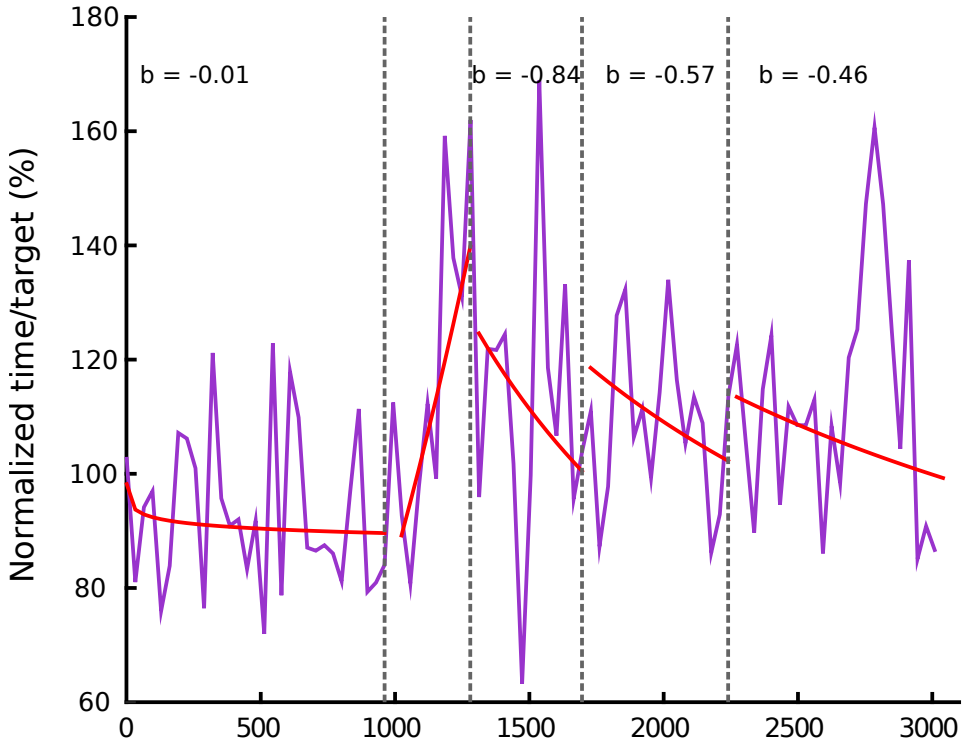

Figure B.2: Average Time to Target during VMR Trials for Subject O. Dashed lines show when there was a shift in calibration preferred directions. Red traces show power learning curve fit ($y = a * x^b$). Text shows the estimated b coefficients for each section. More negative values describe a faster learning rate. Panels that do not have b-coefficient value, did not have a good fit to the model.

trajectories. The trajectories are projected in the screen display plane, which was the plane of the visumotor rotations (reference axis going into the screen).

Average firing rates

Figures B.10 and B.11 show average firing rates during VMR trials for both subjects, respectively. The firing activity is plotted against task performance (successful target hits per block). Each color represents a different neural unit, where the same color corresponds to the same neural unit when comparing baseline and perturbed trials. Similarly, Figs. B.12 and B.13 show the average firing rates during DeCorr trials for both subjects, respectively.

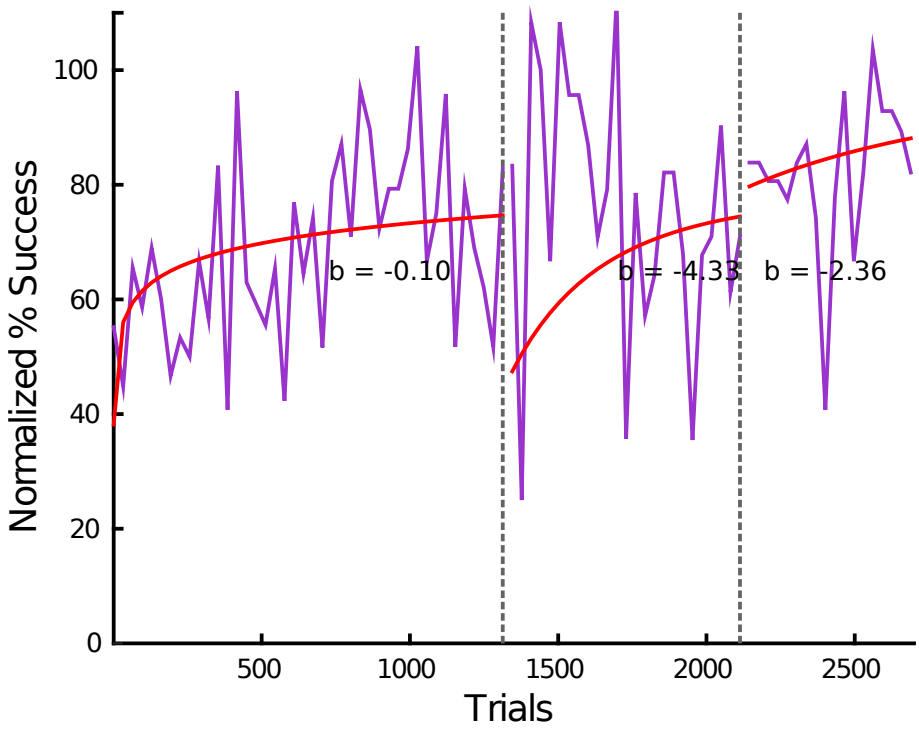

Figure B.3: Success Rate (Target Hits) during VMR Task for Subject M. Same format as in Fig. B.1.

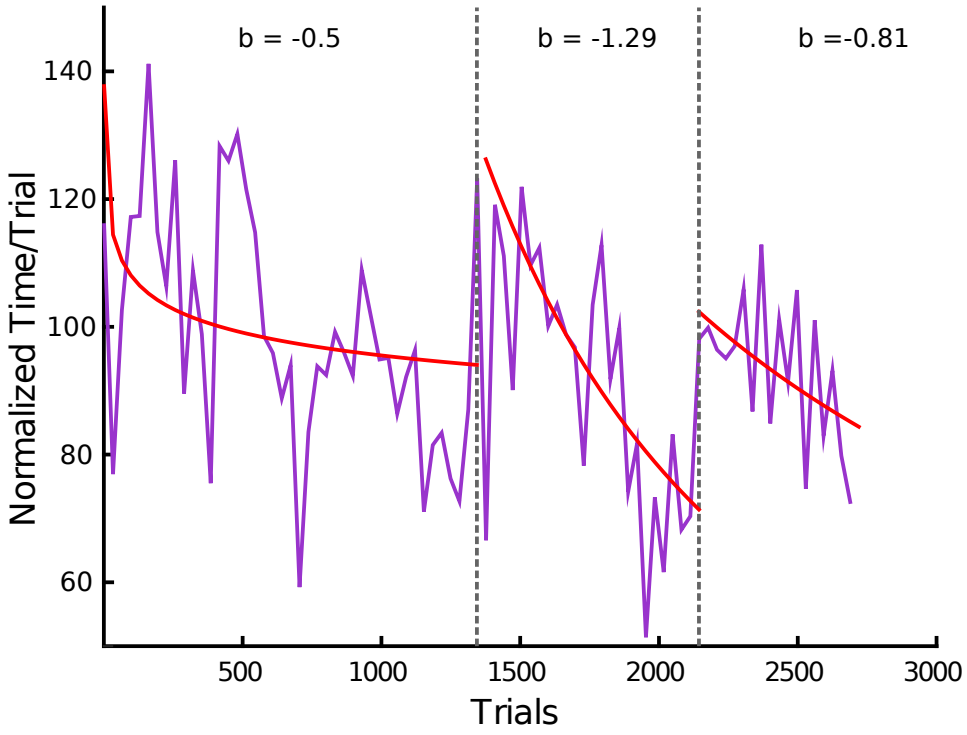

Figure B.4: Average Time to Target for Subject M for VMR trials. Same format as in Fig. B.2.

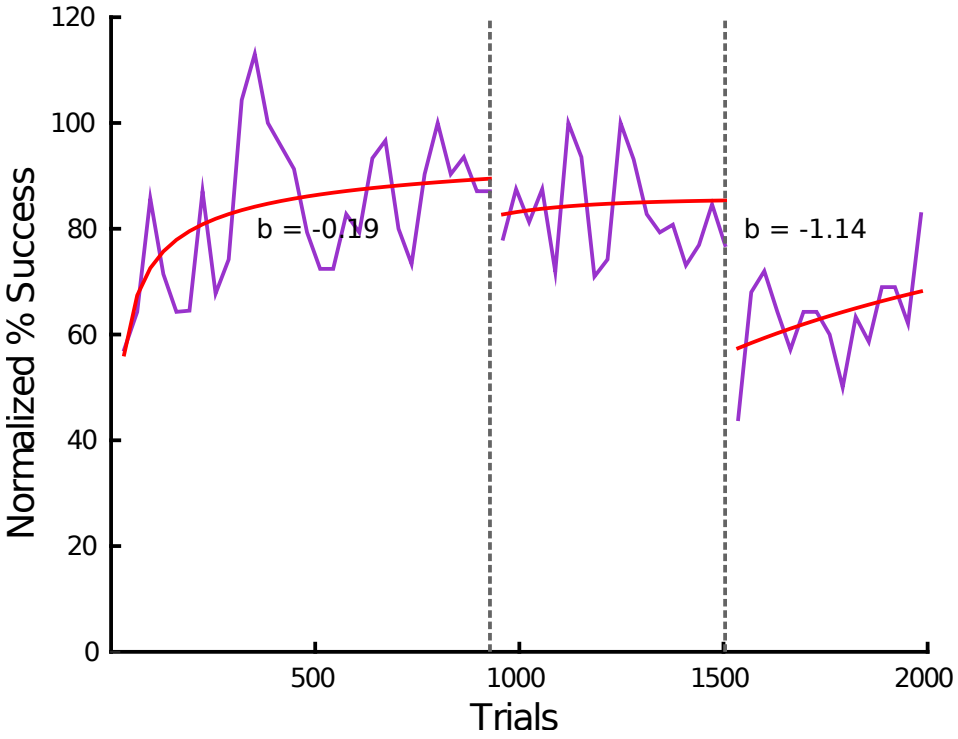

Figure B.5: Success rate (target hits) during DeCorr task for Subject O. Same format as in Fig. B.1

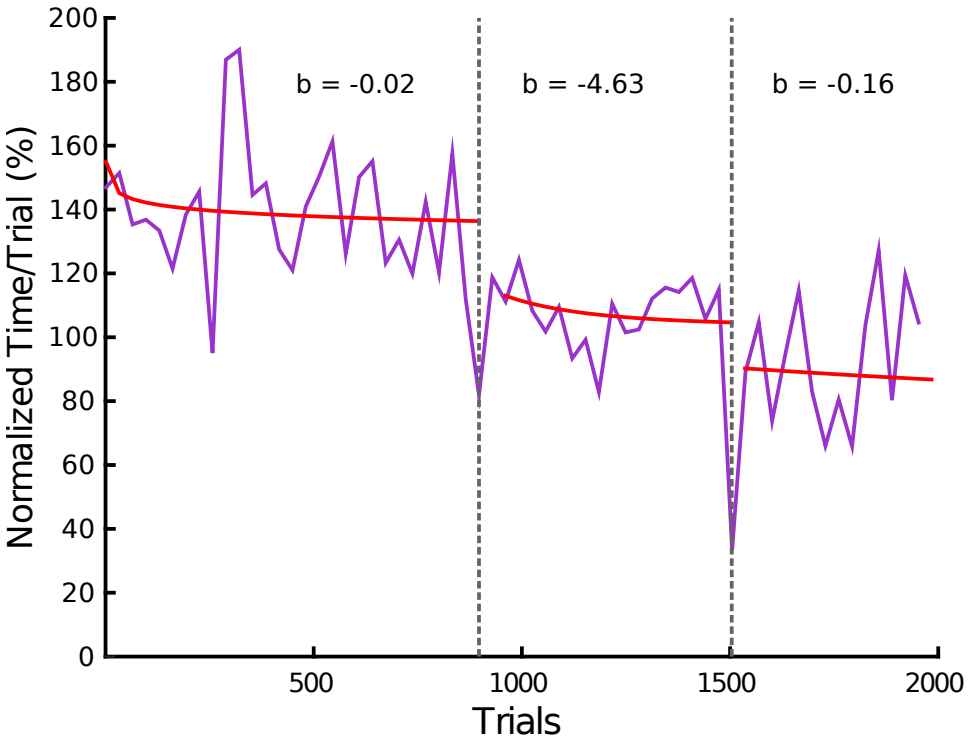

Figure B.6: Average Time to Target for DeCorr trials for Subject O. Same format as in Fig. B.2

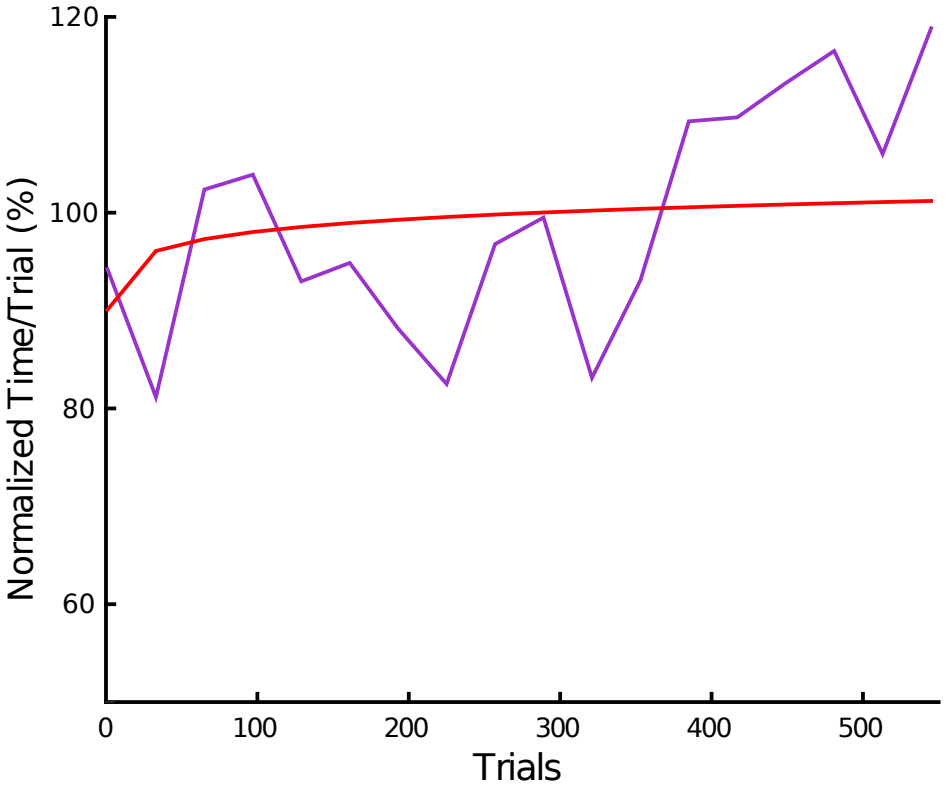

Figure B.7: Average Time to Target for DeCorr trials for Subject M. Same format as in Fig. B.2, the data did not follow a decreasing trend.

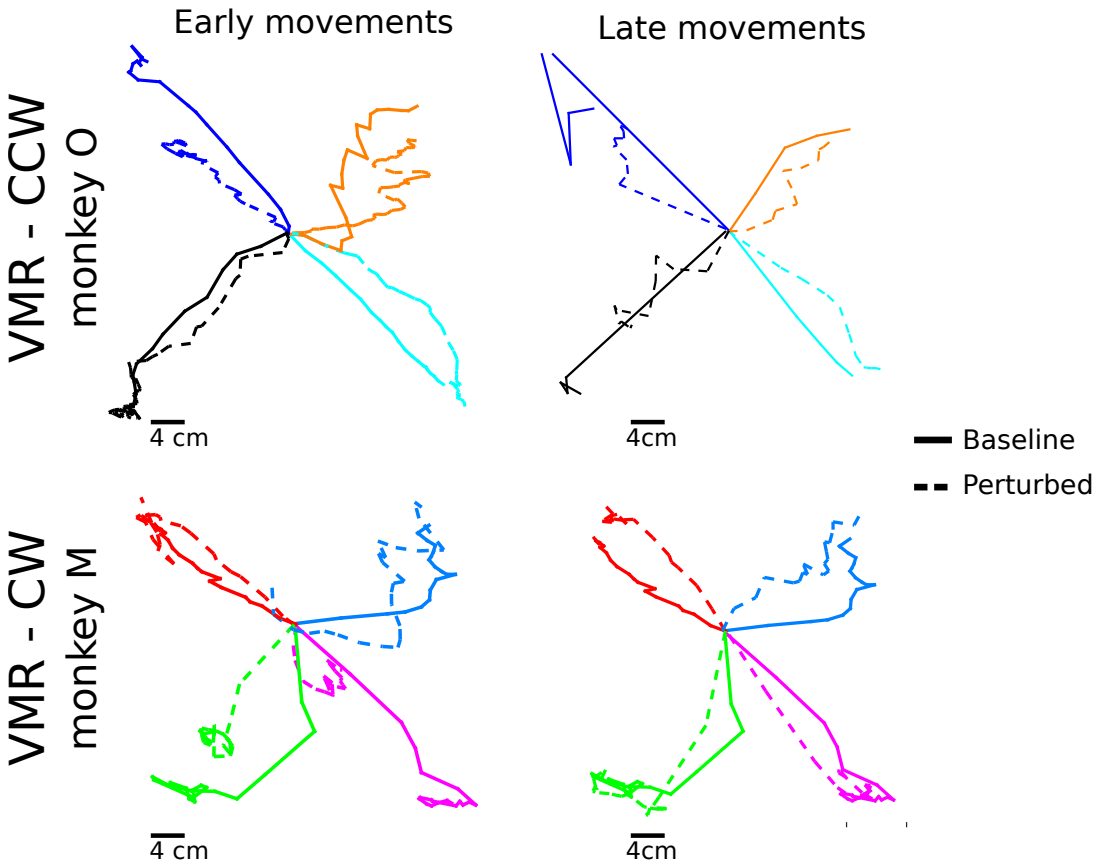

Figure B.8: Early and Late Movement Errors during VMR Trials for Both Subjects. Different colors depict separate target locations. Solid lines show the average unperturbed baseline trajectories, and dashed lines the average of four first (or last) successful trajectories.

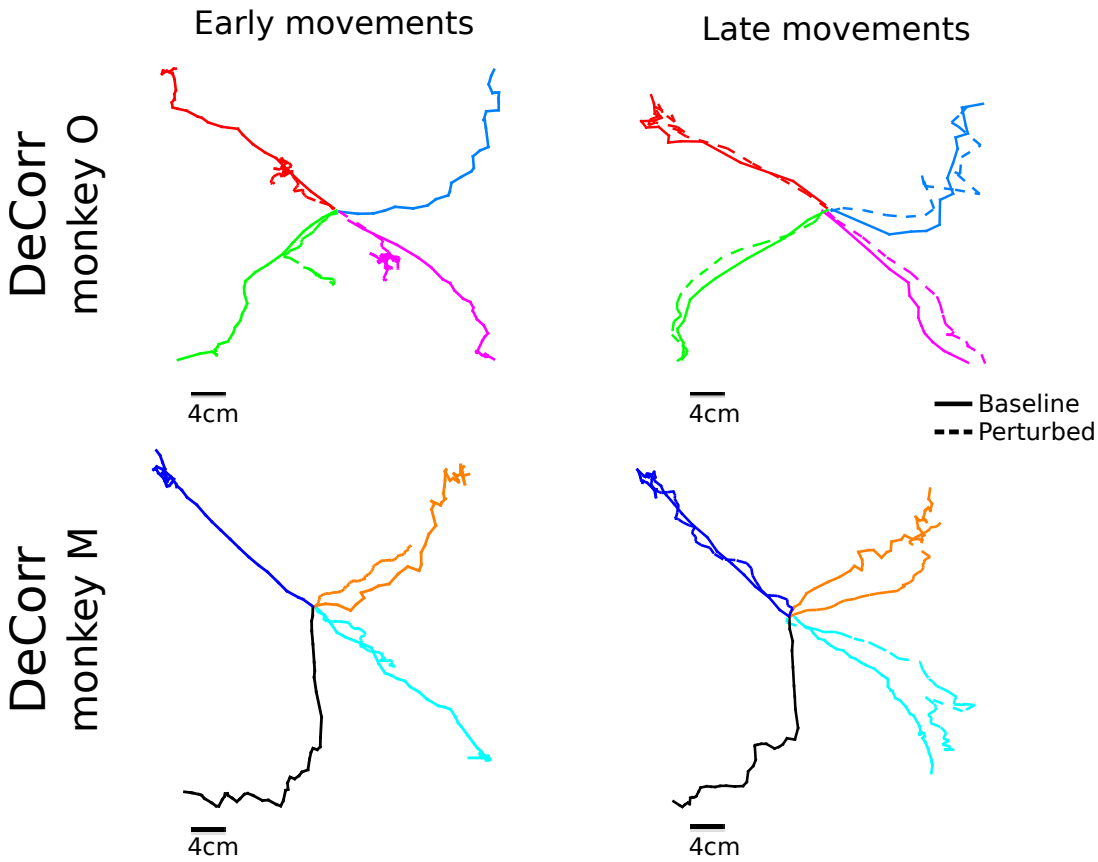

Figure B.9: Early and Late Movement Errors during DeCorr Trials for Both Subjects. Different colors depict separate target locations. Solid lines show the average unperturbed baseline trajectories, and dashed lines the average of four first (or last) successful trajectories.

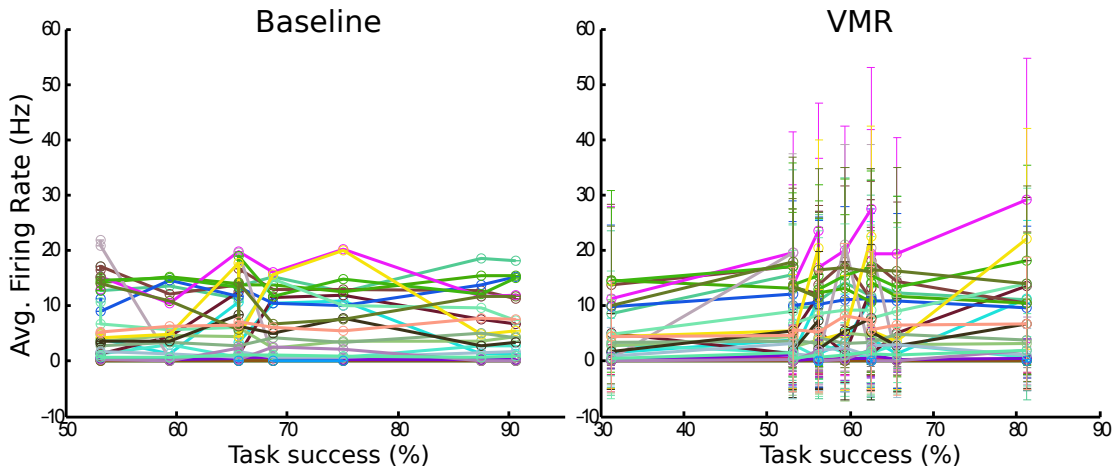

Figure B.10: Average Firing Activity in VMR Trials for Subject O. Mean firing rates vs. task success (percentage target hits per block), the error bars display one standard deviation. Left panel shows the activity during the unperturbed baseline trials, and right panels shows the activity for the same neural units during VMR trials.

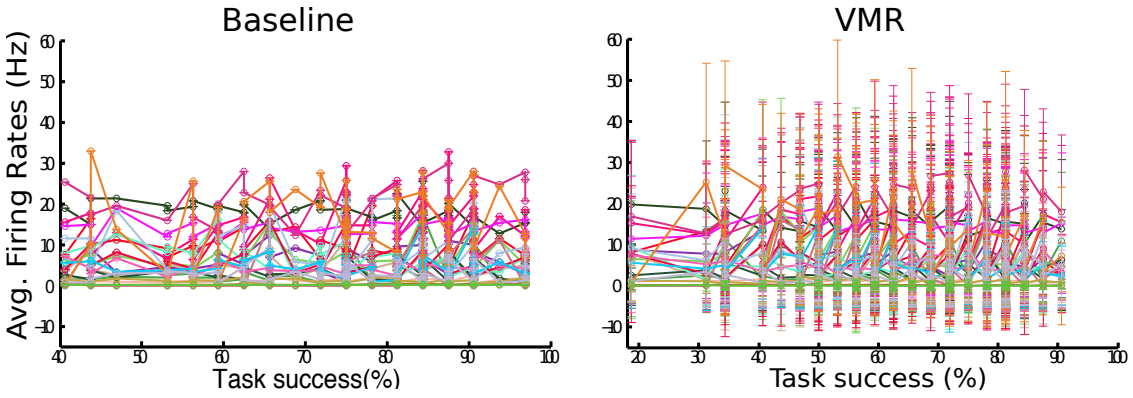

Figure B.11: Average Firing Activity in VMR Trials for Subject M. Mean firing rates vs. task success (percentage target hits per block), the error bars display one standard deviation. Left panel shows the activity during the unperturbed baseline trials, and right panels shows the activity for the same neural units during VMR trials.

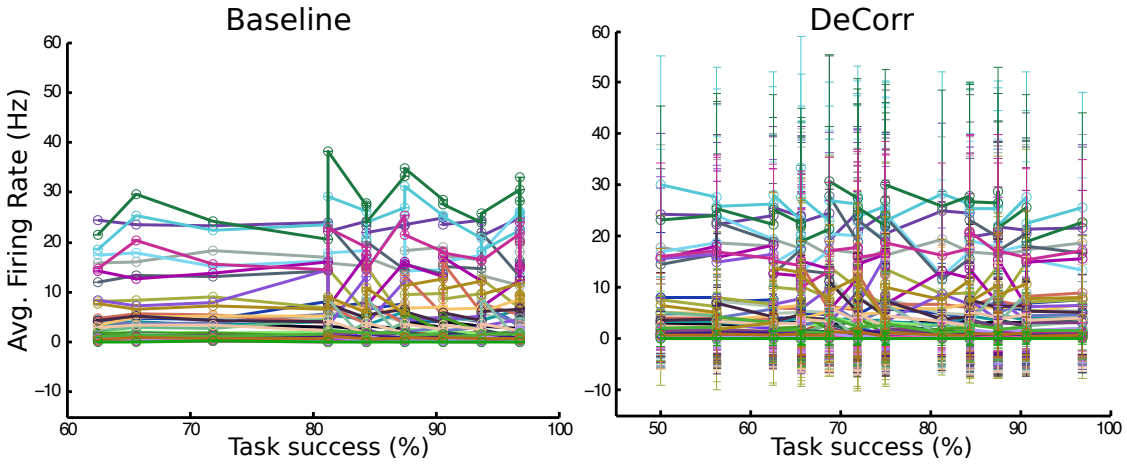

Figure B.12: Average Firing Activity in DeCorr Trials for Subject O. Mean firing rates vs. task success (percentage target hits/block). Same format as Fig. B.10.

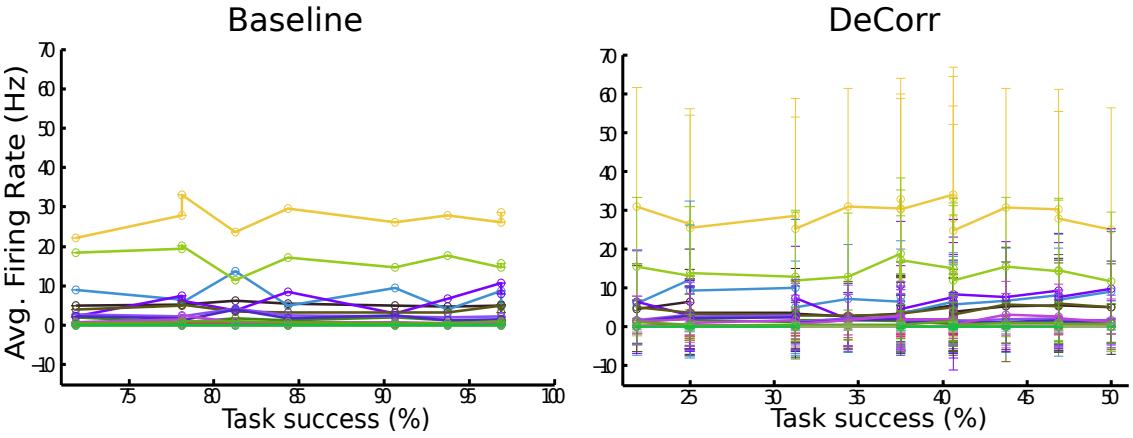

Figure B.13: Average Firing Activity in DeCorr Trials for Subject M. Mean firing rates vs. task success (percentage target hits/block). Same format as Fig. B.10

APPENDIX C

MAXIMUM LIKELIHOOD FACTOR ANALYSIS

Application of EM Algorithm to Factor Analysis

The following derivations and extensions of the expectation maximization (EM) algorithm and factor analysis reduction were based on those developed by Dempster *et al.* (1977); Rubin and Thayer (1982); McLachlan and Krishnan (2007).

Factor analysis (FA) is a statistical tool to estimate unobservable variables (Z) which are independent from the observed variables (Y), and identically distributed. Following (C.1)

$$\left(Y_1^T, Z_1^T\right)^T, ..., \left(Y_n^T, Z_n^T\right)^T, \tag{C.1}$$

where n is the total number of observations. The unobservable variables are also assumed to be independent and identically distributed, as stated in (3.2). The model used for the FA is shown in (C.2):

$$Y_j = \mu + \Lambda Z_j + e_j \quad (j = 1, ..., n), \tag{C.2}$$

where Y_j is p-dimensional, Z_j is q-dimensional, and $q < p$. The μ represents the mean of the observed variables, which can be estimated by the mean vector of the sample, Λ is a $p \times q$ matrix that has the parameters of factor loadings, and e_j are the measurement errors which follow $N(0, D)$, where $D = \text{diag}\left(\sigma_1^2, ...\sigma_{\text{p}}^2\right)$, and σ_i^2 are the uniqueness (McLachlan and Krishnan, 2007) or variance which is not shared with any other variable.

The variables Y_j can be taken as conditionally on the Z_j, as stated in (3.1), but they can also be taken as unconditionally distributed, independent and identically distributed given (C.3)

$$Y \sim N\left(\mu, \Lambda\Lambda^T + D\right), \tag{C.3}$$

where the values of variable Λ and the diagonal of D will conform the parameter vector Θ. The observed data vector $y = \left(y_1^T, ..., y_n^T\right)^T$ the maximum likelihood of the given the parameters Θ from the incomplete data set, that is the y observations, is described in (C.4):

$$\log L(\Theta) = -\frac{1}{2} n \left\{ \log\left|\Lambda\Lambda^T + D\right| + \sum_{j=1}^{m} (y_j - \bar{y})^T \left(\Lambda\Lambda^T + D\right)^{-1} (y_j - \bar{y}) \right\}, \tag{C.4}$$

which describes the log-likelihood function of a Gaussian distribution. If we consider that the "complete" data set (unobservable and observable variables) will be described by $x = \left(x_1^T, ..., x_m^T\right)^T$, where each $x_j = \left(y_j^T, z_j^T\right)^T$ for $j = (1, ..., m)$. Our "missing" data or unobservable factors will be then described by $z = \left(z_1^T, ...z_m^T\right)^T$. Then we can describe the complete data set log-likelihood as in (C.5):

$$\log L_c(\Theta) = -\frac{1}{2} n \log|D| - \frac{1}{2} \sum_{j=1}^{m} \left\{ (y_j - Bz_j)^T D^{-1} (y_j - Bz_j) + z_j^T z_j \right\}. \tag{C.5}$$

This complete log-likelihood will then belong to the exponential family, and will have sufficient statistics described by C_{yy}, C_{yz} and C_{zz} as shown in (C.6)-(C.8).

$$C_{yy} = \frac{1}{n}\sum_{j=1}^{n}\left(y_j - \bar{y}\right)\left(y_j - \bar{y}\right)^T; \tag{C.6}$$

$$C_{yz} = \frac{1}{m}\sum_{j=1}^{m}\left(y_j - \bar{y}\right)z_j^T; \tag{C.7}$$

and

$$C_{zz} = \frac{1}{m}\sum_{j=1}^{m} z_j z_j^T. \tag{C.8}$$

We can get the conditional expectation of these sufficient statistics, given the observations of y. We then start the EM algorithm (see 3.2.2) giving the expected values (C.9)-(C.11), where each k represents a different iteration in the algorithm.

$$E_{\Theta^{(k)}}\left(C_{yy} \mid y\right) = C_{yy}; \tag{C.9}$$

$$E_{\Theta^{(k)}}\left(C_{yz} \mid y\right) = C_{yy}\gamma^T; \tag{C.10}$$

and

$$E_{\Theta^{(k)}}\left(C_{zz} \mid y\right) = \gamma^{(k)^T} C_{yy}\gamma^{(k)} + n\Delta^{(k)}, \tag{C.11}$$

where

$$\gamma^{(k)} = \left\{D^{(k)} + B^{(k)}B^{(k)^T}\right\}^{-1} B^{(k)}, \tag{C.12}$$

and

$$\Delta^{(k)} = I_q - B^{(k)^T}\left(D^{(k)} + B^{(k)}B^{(k)^T}\right)B^{(k)}. \tag{C.13}$$

Equations (C.12) and (C.13) represent the regression coefficients and the residual covariance of the unobservable variables z on the observed measurements y, respectively (McLachlan and Krishnan, 2007).

Finally, we can estimate the parameters Λ and D with the M-step equations (C.14) and (C.15).

$$\Lambda^{(k+1)} = \left(\gamma^T C_{yy}\gamma + \Delta\right)^{-1}\gamma^T C_{yy}, \tag{C.14}$$

and

$$D^{(k+1)} = \operatorname{diag}\left\{\mathrm{C_{yy}} - \mathrm{C_{yy}}\gamma\left(\gamma^{\mathrm{T}}\mathrm{C_{yy}}\gamma + \Delta\right)^{-1}\gamma^{\mathrm{T}}\mathrm{C_{yy}}\right\}. \tag{C.15}$$

We can compute the log-likelihood function given the $\gamma^{(k)}$ and $\Delta^{(k)}$ estimates from the E-step. These steps (E- and M-) are repeated iteratively until the difference between the log-likelihood is equal or smaller than $1e^{-8}$.